

Galaxy rotation curves in multi-fractional spacetimes

Gianluca Calcagni,^a Gabriele U. Variaschi^b

^aInstituto de Estructura de la Materia, CSIC, Serrano 121, 28006 Madrid, Spain

^bDepartment of Physics, Loyola Marymount University, 1 LMU Drive, Los Angeles, CA 90045, USA

E-mail: g.calcagni@csic.es, Gabriele.Variaschi@lmu.edu

Abstract. Multi-fractional theories with integer-order derivatives are simple models of gravitational and matter fields living in spacetimes with variable Hausdorff and spectral dimension, originally proposed as descriptions of spacetimes arising in quantum gravity. In this paper, we pose the question of whether they can serve as an alternative to dark matter. We give a preliminary positive answer. We find the Poisson equation and the Newtonian potential of the multi-fractional theories with integer-order derivatives starting from their covariant modified Einstein's equations. We show that neither the theory T_v with weighted derivatives in the extreme fractional limit nor the theory T_q with q -derivatives fit the rotation curve of any of the galaxies NGC7814, NGC6503 and NGC3741 in the SPARC catalogue. The rotation curve of all three galaxies can be explained by purely geometric effects in the theory T_v with weighted derivatives with small fractional corrections when the fractional exponent takes the special value $\alpha = 4/3$, but only at large radii.

Contents

1	Introduction	1
2	Rotation curves in general relativity and SPARC data	3
2.1	General relativity: equations of motion	3
2.2	General relativity: Poisson equation and Newton's potential	3
2.2.1	General relativity: Poisson equation	4
2.2.2	General relativity: Newton's potential	5
2.3	General relativity: thin-disk exponential-density rotation curve	6
2.4	General relativity: data-based rotation curve	7
3	Spacetime measure in multi-fractional theories	10
4	Theory T_1 with ordinary derivatives	12
4.1	T_1 : equations of motion	12
4.2	T_1 : Poisson equation and Newton's potential	13
4.2.1	T_1 : Poisson equation in Cartesian coordinates	13
4.2.2	T_1 : Poisson equation in spherical coordinates	13
4.2.3	T_1 : Poisson equation in cylindrical coordinates	15
4.2.4	T_1 : Newton's potential	16
5	Theory T_v with weighted derivatives	17
5.1	T_v : equations of motion	17
5.2	T_v : Poisson equation and Newton's potential	19
5.2.1	T_v : Poisson equation in Cartesian coordinates	19
5.2.2	T_v : Poisson equation in spherical coordinates	19
5.2.3	T_v : Newton's potential	20
5.3	T_v : thin-disk exponential-density rotation curve	23
5.3.1	T_v : extreme fractional limit	23
5.3.2	T_v : small fractional corrections	24
5.4	T_v : data-based rotation curve	25
5.4.1	T_v : extreme fractional limit	25
5.4.2	T_v : small fractional corrections	26
6	Theory T_q with q-derivatives	27
6.1	T_q : equations of motion	27
6.2	T_q : Poisson equation and Newton's potential	30
6.2.1	T_q : Poisson equation in Cartesian coordinates	30
6.2.2	T_q : Poisson equation in spherical coordinates	30
6.2.3	T_q : Newton's potential	31
6.3	T_q : thin-disk exponential-density rotation curve	32
6.4	T_q : data-based rotation curve	34
7	Conclusions	34
A	Circular velocity in the theory T_v	36

B	Multipole expansion of inverse-power potentials	36
C	Useful formulæ	38
	C.1 Angular integrals of Gegenbauer polynomials	38
	C.2 Radial integrals	39
D	Galaxy potential in the theory T_v with exponential matter density	40
	D.1 Calculation of eqs. (5.46) and (5.47)	40
	D.2 Calculation of eqs. (5.49c) and (5.49d)	41
E	Thick-disk data-based galaxy potential and gravitational field in T_v	42
	E.1 Extreme fractional limit	42
	E.1.1 $\alpha \neq 2/3$	42
	E.1.2 $\alpha = 2/3$	45
	E.1.3 Comparison with data	47
	E.2 Small fractional corrections	47
	E.2.1 $\alpha \neq 4/3$	47
	E.2.2 $\alpha = 4/3$	54

1 Introduction

Quantum gravity is a subject of research and debate at multiple levels. Often, the discussion is centered on whether a consistent theory of quantum gravity exists, which is no longer an issue because it has already been solved in several independent ways [1–3]. On the other hand, paradoxically, the big question of whether it can be tested by observations is sometimes dismissed on the grounds that quantum-gravity effects should always be confined to Planck scales, which is true only in the very specific and limited case of perturbative corrections to the action in the form of higher-order curvature operators (e.g., [4] and references therein).

To answer to the above question, it may be useful to concentrate to features commonly shared by all or most quantum-gravity scenarios. One such feature is dimensional flow, the change of spacetime dimension with the probed scale. By “spacetime dimension” one may indicate different concepts, usually limited to the Hausdorff dimension d_H (the scaling of spacetime volumes with respect to the linear length) and the spectral dimension d_s (the scaling of the dispersion relation of a particle with respect to the momentum). While there is great variation in the details of dimensional flow, such as the numerical values of the dimensions and the scales at which transitions from one value to another take place, the phenomenon *per se* occurs in all known theories of quantum gravity [5–10].

One of the attempts to better understand dimensional flow has taken the straightforward route to implement this feature explicitly at the level of the action. The ensuing class of theories is generically called multi-scale spacetimes [11] and a particular realization of multi-scale geometries goes under the name of multi-fractional spacetimes [12, 13]. In these scenarios, the measure of the action is factorized in the spacetime coordinates for simplicity and, under very mild assumptions, acquires a universal parametric form [8]. The Hausdorff dimension d_H is determined by the scaling of this measure. The spectral dimension d_s , however, depends on the kinetic term of the fields in the action and there is no unique way to fix this. Depending on the symmetries of the Lagrangian, one can realize different kinetic terms with the same anomalous scaling. According to the classification of [12, 13],

if the kinetic term is made of ordinary partial derivatives ∂_μ , the theory is called multi-fractional theory with ordinary derivatives, labelled as T_1 in short. If, instead, one uses ordinary derivatives decorated with measure weights, one realizes the theory T_v with weighted derivatives (if the weights are balanced on the left and on the right of each derivative) or the theory T_q with q -derivatives (if the weight is only on the left). Finally, if the kinetic term is made of fractional differential operators, one has several other possibilities, collectively labelled as T_γ and called multi-fractional theories with fractional operators.

Although multi-fractional theories have been explored in many aspects ranging from particle physics to cosmology, there are several important gaps in our knowledge about whether and how dimensional flow can leave an observable imprint. The example we choose in this paper is the problem of dark matter. When the gravitational theory changes, it may be possible to get an alternative to particle-like dark matter and explain the rotation curve of galaxies, the matter and galaxy distribution and the content of the universe in terms of a modified dynamics and new degrees of freedom [14]. The cases of $f(R)$ gravity [15] and models of modified Newtonian dynamics (MOND) [16–18] are well documented. Recently, the idea of invoking anomalous dimensions to realize dark-matter galactic observations has been retaken, implicitly, in Newtonian dynamics with a fractional Laplacian [19, 20] and, explicitly, in Newtonian fractional-dimension gravity (NFDG) [21–23]. A covariant version of NFDG was shown to essentially match with the multi-fractional theory T_1 [24], so that one may wonder whether multi-fractional theories can directly say anything interesting about the dark-matter problem.

In this work, we will use astrophysical data from the Spitzer Photometry & Accurate Rotation Curves (SPARC) database, a catalogue of the rotation curves of 175 galaxies [25, 26]. In particular, here we take the three prototypical galaxies presented in [25]: the bulge-dominated spiral NGC7814, the disk-dominated spiral NGC6503 and the gas-dominated dwarf NGC3741, which were used as main examples of the empirical radial acceleration relation in MOND-like models [25] and were also studied in the recent NFDG model [23]. An explanation of the rotation curves of these and other galaxies would be the first step for a purely geometric alternative to dark matter, while we will leave outside subjects such as galaxy clusters, the Bullet cluster, gravitational lensing, and so on.

The plan of the paper is as follows. Section 2 is a review of the SPARC observational results for the galaxies NGC7814, NGC6503 and NGC3741 and of the rotation curves predicted by general relativity, obtained both from a theoretical approximation of the baryonic matter distribution (an exponentially damped energy area density distributed in a thin disk) and from the energy density actually observed. Those familiar with the details can skip this section but we recommend its reading because it serves as a parallel of the ingredients, calculations and strategies employed in the multi-fractional cases.

In section 3, we review the spacetime measure used in multi-fractional theories. The Poisson equation and Newton’s potential of the theory T_1 are derived for the first time in section 4. The Poisson equation, Newton’s potential, the theoretical galaxy rotation curves and the observational rotation curves compared with SPARC data for the theories T_v and T_q are discussed in sections 5 and 6, respectively. Section 7 is devoted to conclusions, where we also sketch some preliminary results about the Bullet cluster. The circular velocity for the theory T_v is derived in Appendix A. Appendix B contains some technical material about the multipole expansion of inverse-power potentials. Some useful integration formulæ are collected in Appendix C. Appendix D contains the calculations of the thin-disk approximation with exponential matter density for the theory T_v , while Appendix E contains the expressions

of the thick-disk data-based galactic potential and gravitational field for the theory T_ν .

2 Rotation curves in general relativity and SPARC data

2.1 General relativity: equations of motion

We work in a D -dimensional spacetime with signature $(-, +, \dots, +)$ and indicate with $d = D - 1$ the number of spatial directions. For the physical application of the model to galaxy rotation curves, we will eventually set $D = 4$ and $d = 3$.

Via the standard Levi-Civita connection and curvature tensors,

$$\Gamma_{\mu\nu}^\rho := \frac{1}{2}g^{\rho\sigma} (\partial_\mu g_{\nu\sigma} + \partial_\nu g_{\mu\sigma} - \partial_\sigma g_{\mu\nu}), \quad (2.1a)$$

$$\text{Riemann tensor: } R_{\mu\sigma\nu}^\rho := \partial_\sigma \Gamma_{\mu\nu}^\rho - \partial_\nu \Gamma_{\mu\sigma}^\rho + \Gamma_{\mu\nu}^\tau \Gamma_{\sigma\tau}^\rho - \Gamma_{\mu\sigma}^\tau \Gamma_{\nu\tau}^\rho, \quad (2.1b)$$

$$\text{Ricci tensor: } R_{\mu\nu} := R_{\mu\rho\nu}^\rho, \quad (2.1c)$$

$$\text{Ricci scalar: } R := g^{\mu\nu} R_{\mu\nu}, \quad (2.1d)$$

$$\text{Einstein tensor: } G_{\mu\nu} := R_{\mu\nu} - \frac{1}{2}g_{\mu\nu}R. \quad (2.1e)$$

the action of general relativity is

$$S = \frac{1}{2\kappa^2} \int d^D x \sqrt{|g|} R + S_m, \quad (2.2)$$

where $\kappa^2 = 8\pi G$ is proportional to Newton's constant G , g is the determinant of the metric and S_m is the baryonic matter action.

The Einstein equations are

$$\kappa^2 T_{\mu\nu} = G_{\mu\nu}, \quad (2.3)$$

where the energy-momentum tensor is

$$T_{\mu\nu} := -\frac{2}{\sqrt{|g|}} \frac{\delta S_m}{\delta g^{\mu\nu}}. \quad (2.4)$$

For later purposes, we recast the equations of motion (2.3) in a more convenient form. Taking their trace,

$$\kappa^2 T = -\frac{D-2}{2}R, \quad (2.5)$$

and replacing R back into (2.3), we get

$$\kappa^2 S_{\mu\nu} = R_{\mu\nu}, \quad S_{\mu\nu} := T_{\mu\nu} - \frac{1}{D-2}g_{\mu\nu}T, \quad T = T_\sigma^\sigma. \quad (2.6)$$

2.2 General relativity: Poisson equation and Newton's potential

To find the gravitational potential in a static matter configuration, we expand the metric into Minkowski background $\eta_{\mu\nu}$ and a perturbation $h_{\mu\nu}$,

$$g_{\mu\nu} = \eta_{\mu\nu} + h_{\mu\nu}. \quad (2.7)$$

In a weak static field with non-relativistic matter, the component

$$h_{00} = -2\Phi \quad (2.8)$$

is proportional to Newton's potential $\Phi(\mathbf{x})$. In the absence of matter, to get the equation of motion for Φ it would be sufficient to linearize the modified Einstein equations in $h_{\mu\nu}$ and then take the 00 component. Expanding the Levi-Civita connection and the curvature terms, a textbook exercise shows that

$$\delta^{(1)}\Gamma_{\mu\nu}^{\sigma} = \frac{1}{2}(\partial_{\mu}h_{\nu}^{\sigma} + \partial_{\nu}h_{\mu}^{\sigma} - \partial^{\sigma}h_{\mu\nu}), \quad (2.9)$$

$$\delta^{(1)}R_{\mu\nu} = -\frac{1}{2}\square h_{\mu\nu} + \partial^{\sigma}\partial_{(\mu}h_{\nu)\sigma} - \frac{1}{2}\partial_{(\mu}\partial_{\nu)}h, \quad (2.10)$$

$$\delta^{(1)}R = -\square h + \partial^{\sigma}\partial^{\tau}h_{\sigma\tau}, \quad (2.11)$$

$$\delta^{(1)}G_{\mu\nu} = -\frac{1}{2}\square h_{\mu\nu} + \partial^{\sigma}\partial_{(\mu}h_{\nu)\sigma} - \frac{1}{2}\eta_{\mu\nu}\partial^{\sigma}\partial^{\tau}h_{\sigma\tau} + \frac{1}{2}[\eta_{\mu\nu}\square - \partial_{(\mu}\partial_{\nu)}]h. \quad (2.12)$$

Also, for any two scalars A and B

$$\begin{aligned} A\delta^{(1)}\square B &= -Ah^{\mu\nu}\partial_{\mu}\partial_{\nu}B + A\delta^{(1)}\nabla_{\mu}\partial^{\mu}B = -Ah^{\mu\nu}\partial_{\mu}\partial_{\nu}B + A\delta^{(1)}\Gamma_{\mu\sigma}^{\mu}\partial^{\sigma}B \\ &= -Ah^{\mu\nu}\partial_{\mu}\partial_{\nu}B, \end{aligned} \quad (2.13)$$

$$\begin{aligned} A\delta^{(1)}(\nabla_{\mu}\nabla_{\nu})B &= A\delta^{(1)}\nabla_{\mu}\partial_{\nu}B = -A\delta^{(1)}\Gamma_{\mu\nu}^{\sigma}\partial_{\sigma}B \\ &= -\frac{1}{2}A(\partial_{\mu}h_{\nu}^{\sigma} + \partial_{\nu}h_{\mu}^{\sigma} - \partial^{\sigma}h_{\mu\nu})\partial_{\sigma}B, \end{aligned} \quad (2.14)$$

where in the last expression we used the definition of covariant derivative on a covariant vector, $\nabla_{\mu}A_{\nu} := \partial_{\mu}A_{\nu} - \Gamma_{\mu\nu}^{\sigma}A_{\sigma}$.

In any covariant, D -dimensional, torsion-free theory expanded around Minkowski background, it is possible to choose the transverse-traceless gauge $\partial^{\mu}h_{\mu\nu} = 0 = h_{\mu}^{\mu}$ [27], so that $\delta^{(1)}R = 0$ and $\delta^{(1)}G_{\mu\nu} = \delta^{(1)}R_{\mu\nu} = -\frac{1}{2}\square h_{\mu\nu}$. We will not use the transverse-traceless gauge.

2.2.1 General relativity: Poisson equation

In the presence of matter, it would be inconsistent to equate $\delta^{(1)}G_{00}$ to the matter energy density $\rho = T_{00}$ because one should also perturb the energy-momentum tensor at the linear order in the metric.¹ One way to account for that contribution is to extract the trace part $T = T_{\mu}^{\mu}$ of the energy-momentum tensor, which is the reason why we recast (2.3) as (2.6).

Taking the 00 component of the Einstein equations (2.6) for a static configuration $h_{00} = -2\Phi(\mathbf{x})$, on the left-hand side we get $S_{00} \simeq [(D-3)/(D-2)]\rho$, where $\rho = T_{00}$ is the matter energy density and we ignored the pressure part in the trace, since we are in a non-relativistic regime. Expanding the right-hand side of (2.6) at linear order,

$$\frac{d-2}{d-1}\kappa^2\rho = \nabla^2\Phi, \quad (2.15)$$

where $d = D - 1$ and ∇^2 is the spatial flat Laplacian. In spherical coordinates,

$$\nabla^2 = \frac{1}{r^{d-1}}\partial_r\left(r^{d-1}\partial_r\cdot\right) + \frac{1}{r^2}\nabla_{S^{d-1}}^2 = \partial_r^2 + \frac{d-1}{r}\partial_r + \frac{1}{r^2}\nabla_{S^{d-1}}^2, \quad (2.16)$$

¹In general relativity, the energy-momentum tensor for non-relativistic matter is such that $|T_{ij}| \ll |T_{00}|$, which implies $|G_{ij}| \ll |G_{00}|$, i.e., $R_{ij} \simeq g_{ij}R/2$. In turn, in the weak-field approximation (2.7) this implies $R \simeq \eta^{\mu\nu}R_{\mu\nu} = -R_{00} + \sum_i R_{ii} \simeq -R_{00} + (D-1)R/2$, that is, $R \simeq 2R_{00}/(D-3)$. Therefore, $\delta^{(1)}G_{\mu\nu}$ does not include all the contributions of the gravitational field in the Einstein equations.

where $\nabla_{S^{d-1}}^2$ is the spherical Laplacian. The Poisson equation (2.15) then reads

$$\frac{d-2}{d-1}\kappa^2\rho = \left[\partial_r^2 + \frac{d-1}{r}\partial_r + \frac{1}{r^2}\nabla_{S^{d-1}} \right] \Phi. \quad (2.17)$$

Using instead cylindrical coordinates, one defines a radial, an azimuth and elevation variables $x_1 = R \cos \varphi$, $x_2 = R \sin \varphi$, $x_i = Z_i$, where $i = 3, \dots, d$:

$$\nabla^2 = \frac{1}{R}\partial_R(R\partial_R\cdot) + \frac{1}{R^2}\partial_\varphi^2 + \nabla_{(i)}^2 = \partial_R^2 + \frac{1}{R}\partial_R + \frac{1}{R^2}\partial_\varphi^2 + \nabla_{(i)}^2, \quad (2.18)$$

where $\nabla_{(i)}^2$ is the Laplacian in Cartesian coordinates x_i , $i = 3, \dots, d$. The Poisson equation is then

$$\frac{d-2}{d-1}\kappa^2\rho = \left[\partial_R^2 + \frac{1}{R}\partial_R + \frac{1}{R^2}\partial_\varphi^2 + \nabla_{(i)}^2 \right] \Phi. \quad (2.19)$$

2.2.2 General relativity: Newton's potential

The solution of the Poisson equation (2.17) for a radial potential $\Phi(r)$ and a pointwise source $\rho = m\delta^d(\mathbf{x})$ of mass m is found with standard techniques. We have

$$\frac{d-2}{d-1}\kappa^2 m\delta^d(\mathbf{x}) = \mathcal{C}\Phi := \left(\partial_r^2 + \frac{d-1}{r}\partial_r \right) \Phi(r) \quad (2.20)$$

$$= \frac{1}{r^{d-1}}\partial_r \left(r^{d-1}\partial_r\Phi \right). \quad (2.21)$$

Everywhere except at $r = 0$, the solution is

$$\Phi(r) = C_+ r^{-c_+} + C_-, \quad c_+ = d - 2. \quad (2.22)$$

We can redefine the potential by a shift, thus setting $C_- = 0$ from now on. The normalization constant C_+ can be found by looking at the solution at $r = 0$. First, recall that the radial Dirac distribution $\delta(r)$ is related to $\delta^d(\mathbf{x})$ by

$$\int dr \delta(r) = 1 = \int d^d\mathbf{x} \delta^d(\mathbf{x}) = \frac{2\pi^{\frac{d}{2}}}{\Gamma(\frac{d}{2})} \int dr r^{d-1} \delta^d(\mathbf{x}), \quad (2.23)$$

so that for a test function f

$$\begin{aligned} \int d^d\mathbf{x} (\mathcal{C}\Phi) f &= \lim_{\epsilon \rightarrow 0} \frac{2\pi^{\frac{d}{2}}}{\Gamma(\frac{d}{2})} \int_\epsilon^{+\infty} dr r^{d-1} (\mathcal{C}\Phi) f \\ &\stackrel{(2.21)}{=} \lim_{\epsilon \rightarrow 0} \frac{2\pi^{\frac{d}{2}}}{\Gamma(\frac{d}{2})} \int_\epsilon^{+\infty} dr \left[\partial_r \left(r^{d-1}\partial_r\Phi \right) \right] f \\ &= - \lim_{\epsilon \rightarrow 0} \frac{2\pi^{\frac{d}{2}}}{\Gamma(\frac{d}{2})} \int_\epsilon^{+\infty} dr \left(r^{d-1}\partial_r\Phi \right) \partial_r f \\ &= \lim_{\epsilon \rightarrow 0} \frac{2\pi^{\frac{d}{2}}}{\Gamma(\frac{d}{2})} C_+(d-2) \int_\epsilon^{+\infty} dr \partial_r f \\ &= - \frac{2\pi^{\frac{d}{2}}}{\Gamma(\frac{d}{2})} C_+(d-2) f(0) \end{aligned}$$

$$\stackrel{(2.20)}{=} \frac{d-2}{d-1} 8\pi Gm \int d^d \mathbf{x} \delta^d(\mathbf{x}) f(\mathbf{x}) = \frac{d-2}{d-1} 8\pi Gm f(0),$$

thus fixing the constant C_+ and the solution (2.22):

$$\Phi(r) = \Phi_0(r) := -\frac{4\Gamma\left(\frac{d}{2}\right)}{(d-1)\pi^{\frac{d}{2}-1}} \frac{Gm}{r^{d-2}}. \quad (2.24)$$

In $d = 3$ spatial dimensions, this reduces to the standard Newtonian potential

$$\Phi(r) = \Phi_0(r) = -\frac{Gm}{r}. \quad (2.25)$$

Here and in the following, a subscript 0 denotes a quantity (potential, gravitational field, rotation velocity) in general relativity.

2.3 General relativity: thin-disk exponential-density rotation curve

Call

$$\Phi(r) = m\mathcal{G}(\mathbf{x} - \mathbf{x}') \quad (2.26)$$

the solution of the Poisson equation with pointwise source with mass m , where we factorized the mass dependence. The gravitational potential of a galaxy can be obtained taking an infinitesimal mass $dm = \rho d\mathcal{V}$ and integrating \mathcal{G} over the volume \mathcal{V} of the galaxy. In general relativity in three spatial dimensions, the potential of the matter distribution is

$$\Phi_0^{\text{galaxy}}(\mathbf{x}) = \int_{\mathcal{V}} d^3 \mathbf{x}' \rho(\mathbf{x}') \mathcal{G}(\mathbf{x} - \mathbf{x}'), \quad (2.27)$$

which is calculated as follows [14]. Assume that the galaxy has cylindrical symmetry, and that the spherical bulge component is negligible. In cylindrical coordinates, the integration volume is

$$\int_{\mathcal{V}} d^3 \mathbf{x}' = \int_0^{+\infty} dR' R' \int_0^{2\pi} d\phi' \int_{-\infty}^{+\infty} dZ'. \quad (2.28)$$

The Green's function is eq. (2.25), $\mathcal{G} = -G/|\mathbf{x} - \mathbf{x}'|$. Using eq. (B.4):

$$\frac{1}{|\mathbf{x} - \mathbf{x}'|} = \sum_{m=-\infty}^{+\infty} \int_0^{+\infty} dy e^{im(\phi-\phi')-|Z-Z'|y} J_m(Ry) J_m(R'y), \quad (2.29)$$

where J_m is the Bessel function of the first kind. Assuming that the galaxy completely lies on the $Z = 0$ plane, the matter energy distribution only depends on the coordinates R' and Z' and, in fact, it is symmetric under a reflection $Z' \rightarrow -Z'$. Therefore, $\rho(\mathbf{x}') = \rho(R', |Z'|)$ and

$$\begin{aligned} \Phi_0^{\text{disk}}(R) &= -G \int_0^{+\infty} dR' R' \int_0^{2\pi} d\phi' \int_{-\infty}^{+\infty} dZ' \rho(R', |Z'|) \\ &\quad \times \sum_{m=-\infty}^{+\infty} \int_0^{+\infty} dy e^{im(\phi-\phi')-|Z-Z'|y} J_m(Ry) J_m(R'y) \\ &= -2\pi G \int_0^{+\infty} dy J_0(Ry) \int_0^{+\infty} dR' R' J_0(R'y) \int_{-\infty}^{+\infty} dZ' e^{-|Z'|y} \rho(R', |Z'|), \end{aligned} \quad (2.30)$$

where only the zero mode $m = 0$ gives a non-zero angular integral. The gravitational field in the $Z = 0$ plane and in the radial direction is

$$g_0^{\text{disk}}(R) = -\frac{d\Phi_0^{\text{disk}}(R)}{dR}, \quad (2.31)$$

while the circular velocity is

$$v_{\text{circ},0}^{\text{disk}} = \sqrt{|R g_0^{\text{disk}}(R)|}. \quad (2.32)$$

At this point, we can decide whether to employ an analytic model of the galaxy or to use real data. In this sub-section, we study the analytic model, later showing how it deviates from the actual prediction for real galaxies.

In the thin-disk approximation, one assumes that the galaxy has a total mass M , is dominated by the disk component with characteristic scale length R_0 and that the disk is infinitely thin. Then, one can take the matter distribution

$$\rho(R', Z') = \frac{M}{2\pi R_0^2} e^{-\frac{R'}{R_0}} \delta(Z'), \quad (2.33)$$

so that

$$\begin{aligned} \Phi_0^{\text{disk}}(R) &= -\frac{GM}{R_0^2} \int_0^{+\infty} dy J_0(Ry) \int_0^{+\infty} dR' R' J_0(R'y) e^{-\frac{R'}{R_0}} \int_{-\infty}^{+\infty} dZ' e^{-|Z'|y} \delta(Z') \\ &= -\frac{GM}{R_0^2} \int_0^{+\infty} dy J_0(Ry) \int_0^{+\infty} dR' R' J_0(R'y) e^{-\frac{R'}{R_0}} \\ &= -GM \int_0^{+\infty} dy \frac{J_0(Ry)}{(1 + R_0^2 y^2)^{\frac{3}{2}}} \\ &= -\frac{GM}{R_0} \frac{R}{2R_0} \left[I_0\left(\frac{R}{2R_0}\right) K_1\left(\frac{R}{2R_0}\right) - I_1\left(\frac{R}{2R_0}\right) K_0\left(\frac{R}{2R_0}\right) \right], \end{aligned} \quad (2.34)$$

where I_m and K_m are the modified Bessel functions of the first and second kind, respectively. The gravitational field $g_0(R)$ can be calculated using the relations

$$I'_0(z) = I_1(z), \quad I'_1(z) = I_0(z) - \frac{I_1(z)}{z}, \quad K'_0(z) = -K_1(z), \quad K'_1(z) = -K_0(z) - \frac{K_1(z)}{z}, \quad (2.35)$$

so that the circular velocity is

$$v_{\text{circ},0}^{\text{disk}} = \frac{R}{2R_0} \sqrt{\frac{2GM}{R_0} \left| I_1\left(\frac{R}{2R_0}\right) K_1\left(\frac{R}{2R_0}\right) - I_0\left(\frac{R}{2R_0}\right) K_0\left(\frac{R}{2R_0}\right) \right|}. \quad (2.36)$$

2.4 General relativity: data-based rotation curve

In this subsection, we take the route of calculating eq. (2.30) with actual surface-luminosity data. We also lift the thin-disk approximation by taking a thick-disk profile [28]

$$\rho(R', |Z'|) = \Sigma^{\text{disk}}(R') \frac{e^{-\frac{|Z'|}{h_Z}}}{2h_Z}, \quad (2.37)$$

where $\Sigma^{\text{disk}}(R')$ is the surface matter distribution of the disk and h_Z is the vertical scale height, related to the radial scale R_0 by [26, 29]

$$h_Z = 0.196 \left(\frac{R_0}{\text{kpc}} \right)^{0.663} \text{ kpc}. \quad (2.38)$$

Other thick-disk profiles are possible [14, 29] but (2.37) will be sufficient for our aim. Since

$$\int_{-\infty}^{+\infty} dZ' e^{-|Z'|y} \frac{e^{-\frac{|Z'|}{h_Z}}}{2h_Z} = \int_0^{+\infty} dZ' \frac{e^{-\frac{1+h_Z y}{h_Z} Z'}}{h_Z} = \frac{1}{1+h_Z y}, \quad (2.39)$$

then eq. (2.30) becomes

$$\Phi_0^{\text{disk}}(R) = -2\pi G \int_0^{+\infty} dy \frac{J_0(Ry)}{1+h_Z y} \int_0^{+\infty} dR' R' J_0(R'y) \Sigma^{\text{disk}}(R'). \quad (2.40)$$

The thin-disk limit corresponds to $h_Z \rightarrow 0$.

So far, we computed only the disk component but the total surface distribution of baryonic matter is made of three contributions: one from the disk, one from the gas (including helium) and one from the bulge of the galaxy. Each of these contributions is measured separately from its surface luminosity Σ_L and it is converted to a mass distribution via an appropriate mass-to-light ratio [23]. The gas contribution is axisymmetric just like the disk component, so that its potential $\Phi_0^{\text{gas}}(R)$ and circular velocity $v_{\text{circ},0}^{\text{gas}}$ are given by eqs. (2.30) and (2.32) with $\Sigma^{\text{disk}}(R')$ replaced by $\Sigma^{\text{gas}}(R')$. Additionally, we have [23]

$$\Sigma(R') = \Sigma^{\text{disk}}(R') + \Sigma^{\text{gas}}(R'), \quad (2.41a)$$

$$\Sigma^{\text{disk}}(R') = 0.50 \Sigma_L^{\text{disk}}(R') \frac{M_\odot}{L_\odot}, \quad (2.41b)$$

$$\Sigma^{\text{gas}}(R') = 1.33 \Sigma_L^{\text{gas}}(R') \frac{M_\odot}{L_\odot}, \quad (2.41c)$$

$$\Sigma^{\text{bulge}}(R') = 0.70 \Sigma_L^{\text{bulge}}(R') \frac{M_\odot}{L_\odot}, \quad (2.41d)$$

where the surface luminosities Σ_L are available from the SPARC database [26].

The bulge component requires some extra work because it has spherical instead of axial symmetry. Going back to eq. (2.27), instead of expression (2.30) in cylindrical coordinates we have, in three spatial dimensions, the volume element

$$\int_{\mathcal{V}} d^3 \mathbf{x}' = \int_0^{+\infty} dr' r'^2 \int_0^\pi d\theta' \sin \theta' \int_0^{2\pi} d\varphi' \quad (2.42)$$

and

$$\begin{aligned} \Phi_0^{\text{bulge}}(r) &= -G \int_0^\pi d\theta' \sin \theta' \int_0^{2\pi} d\varphi' \int_0^{+\infty} dr' r'^2 \frac{\rho^{\text{bulge}}(r')}{|\mathbf{x} - \mathbf{x}'|} \\ &= -2\pi G \sum_{n=0}^{+\infty} \int_0^\pi d\theta' \sin \theta' P_n(\cos \theta') \int_0^{+\infty} dr' r'^2 \frac{r_{<}^n}{r_{>}^{n+1}} \rho^{\text{bulge}}(r') \\ &= -4\pi G \int_0^{+\infty} dr' \frac{r'^2}{r_{>}} \rho^{\text{bulge}}(r') \end{aligned}$$

$$= -\frac{4\pi G}{r} \int_0^r dr' r'^2 \rho^{\text{bulge}}(r') - 4\pi G \int_r^{+\infty} dr' r' \rho^{\text{bulge}}(r'), \quad (2.43)$$

where we used eq. (B.10) with $\cos \gamma = \cos \theta'$, $r_>$ (respectively, $r_<$) is the largest (smallest) between r and r' , the $n = 0$ mode is the only one giving a non-zero contribution and

$$\rho^{\text{bulge}}(r') = 0.70 \rho_L^{\text{bulge}}(r') \frac{M_\odot}{L_\odot}. \quad (2.44)$$

To get the luminosity volume density $\rho_L^{\text{bulge}}(r')$, one converts the observed surface luminosity $\Sigma_L^{\text{bulge}}(R')$ via the formula [30]

$$\rho_L^{\text{bulge}}(r') = -\frac{1}{\pi} \int_{r'}^{+\infty} \frac{dR'}{\sqrt{R'^2 - r'^2}} \frac{d\Sigma_L^{\text{bulge}}}{dR'}. \quad (2.45)$$

In the SPARC database, each surface luminosity distribution Σ_L is given in L_\odot/pc^2 , solar luminosity per (parsec)². To convert Σ_L into kg/pc^2 units and ρ^{bulge} into kg/pc^3 units, one further multiplies eqs. (2.41) and (2.44) by a conversion factor $1.989 \times 10^{30} (\text{kg}/M_\odot)$. The total baryonic mass M of the galaxy can be obtained from integrating the total area energy density $\Sigma^{\text{disk}} + \Sigma^{\text{gas}} + \Sigma^{\text{bulge}}$ over the disk or, equivalently, the area disk+gas density Σ over the disk and the volume density ρ^{bulge} over the bulge,

$$\begin{aligned} M &= 2\pi \int_0^{+\infty} dR' R' [\Sigma(R') + \Sigma^{\text{bulge}}(R')] \\ &= 2\pi \int_0^{+\infty} dR' R' \Sigma(R') + 4\pi \int_0^{+\infty} dr' r'^2 \rho^{\text{bulge}}(r'). \end{aligned} \quad (2.46)$$

In this expression as well as in eqs. (2.40) and (2.43), the upper extremum of the integrals in R' and r' is actually taken to be a finite value R_{max} , much larger than R_0 and slightly larger than the radial coordinate of the last data point.

The total potential is

$$\Phi_0^{\text{galaxy}} = \Phi_0^{\text{disk}} + \Phi_0^{\text{gas}} + \Phi_0^{\text{bulge}}, \quad (2.47)$$

while the gravitational fields are

$$\begin{aligned} g_0^{\text{disk,gas}}(R) &= -\frac{d\Phi_0^{\text{disk,gas}}}{dR} \\ &= -2\pi G \int_0^{+\infty} dy y \frac{J_1(Ry)}{1 + h_{zy}} \int_0^{+\infty} dR' R' J_0(R'y) \Sigma^{\text{disk,gas}}(R'), \end{aligned} \quad (2.48)$$

$$\begin{aligned} g_0^{\text{bulge}}(R) &= -\left. \frac{d\Phi_0^{\text{bulge}}}{dr} \right|_{r=R} \\ &= -\frac{4\pi G}{R^2} \int_0^R dr' r'^2 \rho^{\text{bulge}}(r'), \end{aligned} \quad (2.49)$$

where we used $dJ_0(Ry)/dR = -y J_1(Ry)$. Finally, the total rotation velocity is

$$v_{\text{circ},0}(R) = \sqrt{R \left| g_0^{\text{disk}}(R) + g_0^{\text{gas}}(R) + g_0^{\text{bulge}}(R) \right|}. \quad (2.50)$$

The three galaxies selected in [25] have different properties.

- NGC7814 is a bulge-dominated spiral galaxy 14.4 Mpc away with all three components, a radial scale $R_0 = 2.54$ kpc and a total baryonic mass $M = 8.26 \times 10^{40}$ kg. In this case, we set $R_{\max} = 20$ kpc.
- NGC6503 is a disk-dominated dwarf spiral galaxy 6.3 Mpc away with two components (a thick disk and gas) and a negligible bulge ($\Sigma_{\text{bulge}}^L = 0$), a radial scale $R_0 = 2.16$ kpc and a total baryonic mass $M = 1.72 \times 10^{40}$ kg. In this case, we set $R_{\max} = 24$ kpc.
- NGC3741 is a gas-dominated irregular spiral galaxy 3.2 Mpc away with two components (a thick disk and gas) and a negligible bulge ($\Sigma_{\text{bulge}}^L = 0$), a radial scale $R_0 = 0.20$ kpc and a total baryonic mass $M = 5.06 \times 10^{38}$ kg. In this case, we set $R_{\max} = 7.5$ kpc.

The rotation curve (2.50) is shown in Fig. 1 together with the thin-disk expression (2.36) with exponentially decaying matter distribution. As is well known, the Newtonian limit of general relativity fails to reproduce the observed rotation curve of galaxies. The point here is that, when testing a theory where the matter component is purely baryonic, it is important to use the full matter distribution obtained by data rather than assuming a specific radial profile such as (2.33). As one can appreciate, using the actual baryonic matter density profile with a thick-disk assumption changes the rotation curve considerably, especially at small radii. The main change stems from the use of the actual profile $\Sigma(R')$, since the exponential *Ansatz* (2.33) deviates from the actual matter density at small radii. On the other hand, one can check that the effect of approximating the disk from thick to thin is comparatively smaller and it would amount to an increase in the peak of the curve [23].

3 Spacetime measure in multi-fractional theories

Since the spacetime measure is the same for all the theories we will consider in the following, we recall its main aspects.

Any continuous spacetime with a varying Hausdorff dimension admits an integration measure of a universal parametric form, where the choice of parameter values strongly depends on the specific theory [8, 12]. Here we consider factorizable measure weights,

$$d^D q(x) := \prod_{\mu=0}^d dq_{\mu}(x^{\mu}) = d^D x v(x) = d^D x \prod_{\mu=0}^d v_{\mu}(x^{\mu}), \quad (3.1)$$

where $v_{\mu}(x^{\mu}) := \partial_{\mu} q_{\mu}(x^{\mu})$ is a function of the Cartesian coordinate along the direction μ and of some fundamental scales of geometry ℓ_l , $l = 1, 2, \dots$. This measure breaks Lorentz invariance and recovers it only at certain scales where $q_{\mu}(x^{\mu}) \rightarrow x^{\mu}$ and $v(x) \rightarrow 1$. In the most general factorizable case, the profiles $q_{\mu}(x^{\mu})$ are an infinite superposition of complex powers, $q_{\mu}(x^{\mu}) = \sum_l \gamma_l |x^{\mu}/\ell_l^{\mu}|^{\alpha_l + i\omega_l}$ for all μ , where $\alpha_l, \omega_l \in \mathbb{R}$ and $\gamma_l \in \mathbb{C}$ are dimensionless constants and $\ell_l^{\mu} \in \mathbb{R}$ are fundamental length or time scales of the geometry. However, reality of the measure constrains the parameters γ_l and ω_l of this sum to combine into a real-valued expression, a generalized polynomial deformed by logarithmic oscillations.

In most applications ranging from classical mechanics to quantum field theory, factorizable measures are much more manageable [31, 32] than measures preserving, say, only spatial rotation [7, 33]. However, as a first approximation in spherically or axially symmetric configurations one can rewrite (3.1) in terms of the radial coordinate r (spherical radius) or R (cylinder radius). Also, in this paper we consider only static configurations and we

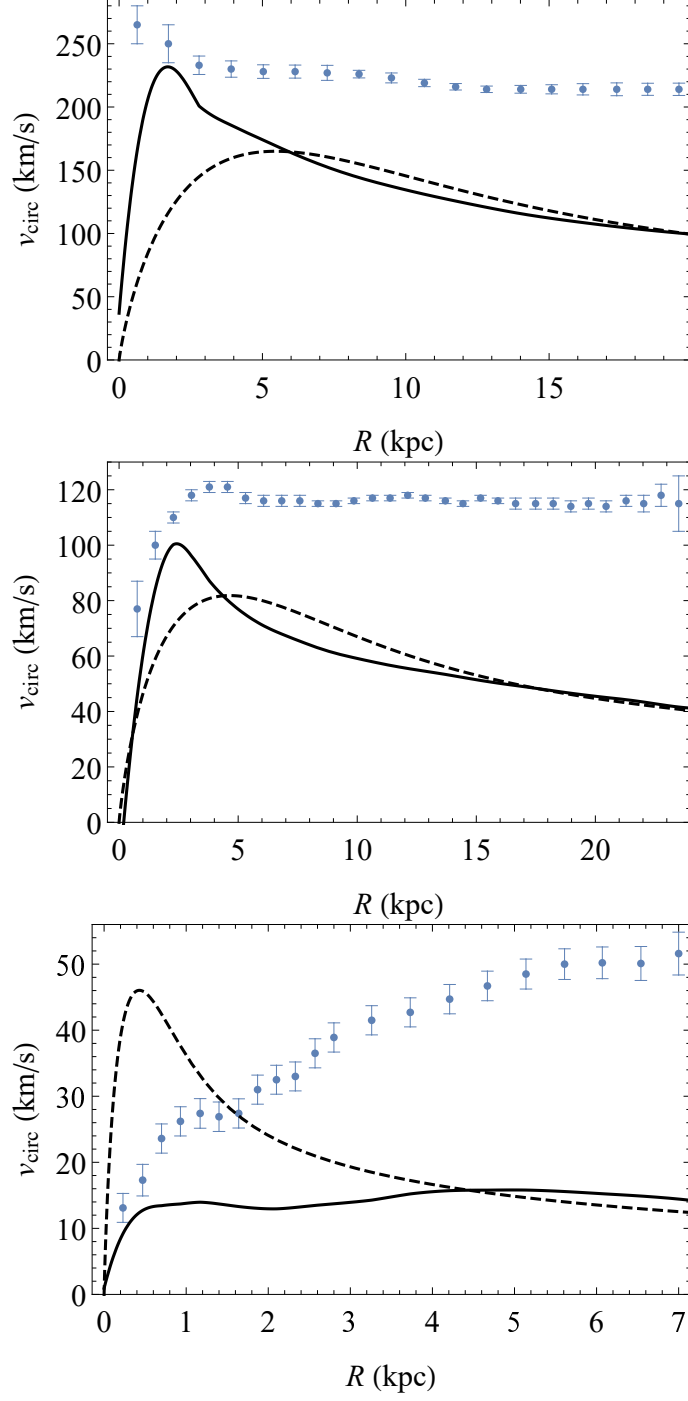


Figure 1. SPARC data points for the rotation curves of NGC7814 (top panel), NGC6503 (middle panel) and NGC3741 (bottom panel) compared with the prediction of general relativity using the observed baryonic mass distribution (solid curve) or the exponentially decaying thin-disk profile (2.33) (dashed curve).

can ignore the time-dependent part of the measure or, equivalently, set $v_0(x^0) = v_0(t) = 1$.

Lastly, only one fundamental scale $\ell_1 \equiv \ell_*$ is necessary to get dimensional flow, which is the simplest configuration giving rise to non-trivial effects. For a spherical or axially symmetric configuration, we can dub this scale r_* or R_* .

In this setting, the universal scaling found in [8, 12] takes the following form for a one-dimensional measure $q(r)$, using the spherical radius r as an example (the same expression would hold for R , under some approximation we will discuss later):

$$q(r) = r + \frac{r_*}{\alpha} \left| \frac{r}{r_*} \right|^\alpha F(r), \quad (3.2a)$$

$$F(r) = A_0 + \sum_{n=1}^{+\infty} \tilde{F}_n(r), \quad (3.2b)$$

$$\tilde{F}_n(r) = A_n \cos\left(n\omega \ln \frac{r}{r_*}\right) + B_n \sin\left(n\omega \ln \frac{r}{r_*}\right), \quad (3.2c)$$

where $r > 0$, $\alpha \in \mathbb{R}$ is a fractional exponent proportional to the Hausdorff dimension of spacetime, $0 < A_n, B_n < 1$ are constant amplitudes and $\omega = 2\pi\alpha/\ln N$ is a frequency taking values on the discrete set $N = 2, 3, \dots$. The constant A_0 can take the values 1 or 0, depending on whether one includes the zero mode or not, respectively. We will always set $A_0 = 1$.

The measure weight $v(r)$ is simply

$$v(r) = \partial_r q(r). \quad (3.3)$$

The log-oscillating part of the measure enjoys discrete scale invariance,

$$F\left(e^{\frac{2\pi}{\omega}} r\right) = F(r), \quad e^{\frac{2\pi}{\omega}} = N^{\frac{1}{\alpha}}, \quad (3.4)$$

a property typical of fractals and multi-fractals. Averaging out the oscillations [12, 31], $\langle F \rangle = 1$ and one finds a simple power-law behaviour capturing the scaling of geometry across an infrared (IR) to ultraviolet (UV) divide set by r_* :

$$\langle q(r) \rangle = r + \frac{r_*}{\alpha} \left| \frac{r}{r_*} \right|^\alpha. \quad (3.5)$$

This averaging is useful in many applications of multi-fractional theories because it removes a modulation of the measure which does not add much to the main geometric effect. We will adopt (3.5) in most of the paper. However, in certain cases log oscillations do play an important physical role [34, 35] and we will include them whenever the main effect we want to find (a flattening of the rotation curve of galaxies) is not captured by geometries with the power law (3.5).

The exact, full form of the measure in Cartesian coordinates with many fundamental scales as well as the exact form of the amplitudes A_n and B_n can be found in [8, 12, 13].

4 Theory T_1 with ordinary derivatives

4.1 T_1 : equations of motion

Introducing the standard Levi-Civita connection and curvature tensors (2.1), the action of the multi-fractional theory with ordinary derivatives is [33, 36]

$$S = \frac{1}{2\kappa^2} \int d^D x v \sqrt{|g|} [R - w(v) \partial_\mu v \partial^\mu v - 2U(v)] + S_m, \quad (4.1)$$

where we included a kinetic-like term for the measure weight where w is a function of v , U is a potential-like term for the measure weight and S_m is the baryonic matter action. There is no dark-matter component in this and the other multi-fractional theories. The prefactor 2 in front of U is just a convenient notation following [13]. While in general it could be assumed that $w = 0$ because it is not required by any symmetry consideration [36], the Poisson equation will actually be independent of w .

The modified Einstein equations of the theory are [36]

$$\kappa^2 T_{\mu\nu}^v = G_{\mu\nu} + U g_{\mu\nu} + g_{\mu\nu} \frac{\square v}{v} - \frac{\nabla_\mu \nabla_\nu v}{v} + w \left(\frac{1}{2} g_{\mu\nu} \partial_\sigma v \partial^\sigma v - \partial_\mu v \partial_\nu v \right), \quad (4.2)$$

where the energy-momentum tensor of matter fields is

$$T_{\mu\nu}^v := - \frac{2}{\sqrt{|g|} v} \frac{\delta S_m}{\delta g^{\mu\nu}}. \quad (4.3)$$

Notice the extra weight factor compared with (2.4). In general, the term U cannot be set to zero before checking the consistency of the background solutions, but in this case we will do so later because we can always reabsorb it in a suitable choice of the matter energy-momentum tensor.

Taking the trace of (4.2),

$$\kappa^2 T^v = - \frac{D-2}{2} R + DU + (D-1) \frac{\square v}{v} + \frac{D-2}{2} w \partial_\sigma v \partial^\sigma v, \quad (4.4)$$

and replacing R back into (4.2), we get

$$\kappa^2 S_{\mu\nu}^v = R_{\mu\nu} - \frac{1}{D-2} g_{\mu\nu} \frac{\square v}{v} - \frac{\nabla_\mu \nabla_\nu v}{v} - w \partial_\mu v \partial_\nu v, \quad (4.5)$$

$$S_{\mu\nu}^v := \tilde{T}_{\mu\nu}^v - \frac{1}{D-2} g_{\mu\nu} \tilde{T}^v, \quad \tilde{T}_{\mu\nu}^v := T_{\mu\nu}^v - \frac{U}{\kappa^2} g_{\mu\nu}. \quad (4.6)$$

4.2 T_1 : Poisson equation and Newton's potential

4.2.1 T_1 : Poisson equation in Cartesian coordinates

After expanding the metric as in eq. (2.7) and taking the 00 component of the modified Einstein equations (4.5) with $U = 0$ for a static configuration $h_{00} = -2\Phi(\mathbf{x})$, on the left-hand side we get $S_{00}^v \simeq [(D-3)/(D-2)]\rho$, where $\rho = T_{00}^v$ is the non-relativistic matter energy density and we ignored pressure. Expanding the right-hand side of (4.5) at linear order,

$$\frac{d-2}{d-1} \kappa^2 \rho = \left(\nabla^2 + \frac{\partial^i v}{v} \partial_i + \frac{2}{d-1} \frac{\nabla^2 v}{v} \right) \Phi - \frac{1}{d-1} h^{ij} \frac{\partial_i \partial_j v}{v}, \quad (4.7)$$

where ∇^2 is the spatial flat Laplacian. Here we assumed that the time-dependent part of the measure weight v is constant at the scales where the weak-field, static, non-relativistic approximation holds.

4.2.2 T_1 : Poisson equation in spherical coordinates

On Minkowski background in spherical coordinates, we can symmetry reduce the measure weight to a radial or an axisymmetric configuration, where only the radial part has an anomalous scaling:

$$v = v(r) = 1 + \left| \frac{r}{r_*} \right|^{d(\alpha-1)}, \quad (4.8)$$

where we leave $\alpha \in \mathbb{R}$ generic and we ignore logarithmic oscillations. Different choices that included the angular part would not lead to very different physics, since the difference between (4.8) and a profile $v(r)v(\theta)\dots$ or $v(r,\theta,\dots)$ would be negligible across galactic distances. The power of r in eq. (4.8) has been chosen in order to maintain a spatial Hausdorff dimension

$$d_{\text{H}}^{\text{space}} \simeq d\alpha \quad (4.9)$$

at scales where fractional effects are maximal ($r \ll r_*$ or $r \gg r_*$, depending on whether $\alpha < 1$ or $\alpha > 1$). In fact, in spherical coordinates the spatial volume element is $d^d x = dr r^{d-1} d\Omega_{d-2}$, where $d\Omega_{d-2}$ is the angular volume element. Therefore, the multi-fractional measure anomalous only in the radial direction in spherical coordinates is of the form

$$d^d x v(\mathbf{x}) = dr r^{d-1} v(r) d\Omega_{d-2}, \quad (4.10)$$

where $v(r)$ is the profile (4.8). In the fractional regime, the radial measure scales as $dr r^{d-1} \times v(r) \simeq dr r^{d\alpha-1}$.

Using (4.8), one can check that

$$\frac{\partial_r v}{v} = \frac{d(\alpha-1)}{r} \mathcal{A}(r), \quad (4.11)$$

$$\frac{\nabla^2 v}{v} = \frac{1}{v} \frac{1}{r^{d-1}} \partial_r \left(r^{d-1} \partial_r v \right) = \frac{d(\alpha-1)(d\alpha-2)}{r^2} \mathcal{A}(r), \quad (4.12)$$

where

$$\mathcal{A}(r) := \frac{|r/r_*|^{d(\alpha-1)}}{1 + |r/r_*|^{d(\alpha-1)}}. \quad (4.13)$$

Since the background-metric rr -component in spherical coordinates is $\eta^{rr} = 1$, eq. (4.7) becomes

$$\begin{aligned} \frac{d-2}{d-1} \kappa^2 \rho = & \left[\partial_r^2 + \frac{d-1+d(\alpha-1)\mathcal{A}(r)}{r} \partial_r + \frac{1}{r^2} \nabla_{S^{d-1}} \right. \\ & \left. + \frac{2d(\alpha-1)(d\alpha-2)\mathcal{A}(r)}{d-1} \frac{\mathcal{A}(r)}{r^2} \right] \Phi - \frac{d(\alpha-1)(d\alpha-d-1)\mathcal{A}(r)}{(d-1)r^2} h^{rr}. \end{aligned} \quad (4.14)$$

At this point, we recall that the condition $h_{\mu}^{\mu} = 0$ is dictated by the fact that $g_{\mu}^{\mu} = D = \eta_{\mu}^{\mu}$. Choosing a gauge where $h_{\theta\theta} = 0 = h_{\phi\phi}$, this implies that $0 = h_{00}\eta^{00} + h_{rr}\eta^{rr} = -h_{00} + h_{rr}$, so that $h^{rr} = h_{rr} = -2\Phi$. Thus,

$$\boxed{\frac{d-2}{d-1} \kappa^2 \rho = \left[\partial_r^2 + \frac{d-1+d(\alpha-1)\mathcal{A}(r)}{r} \partial_r + \frac{1}{r^2} \nabla_{S^{d-1}} + \frac{2d(\alpha-1)(2d\alpha-d-3)\mathcal{A}(r)}{(d-1)r^2} \right] \Phi.} \quad (4.15)$$

In the general-relativity or Newtonian limit $\mathcal{A} \rightarrow 0$, one gets the ordinary Poisson equation (2.17), while in the fractional limit $\mathcal{A} \rightarrow 1$ we obtain

$$\frac{d-2}{d-1} \kappa^2 \rho \simeq \left[\partial_r^2 + \frac{d\alpha-1}{r} \partial_r + \frac{1}{r^2} \nabla_{S^{d-1}} + \frac{2d(\alpha-1)(2d\alpha-d-3)}{(d-1)r^2} \right] \Phi. \quad (4.16)$$

4.2.3 T_1 : Poisson equation in cylindrical coordinates

In cylindrical coordinates, we take a measure weight which is non-trivial only in the radial direction because we expect multi-fractional effects to depend on the distance from the center of the galaxy, not on the direction one is looking at. Since in cylindrical coordinates the spatial volume element is $d^d x = R dR d\varphi \prod_i dZ_i$, the multi-fractional measure anomalous only in the radial direction in cylindrical coordinates is

$$d^d x v(\mathbf{x}) = dR R v(R) d\varphi \prod_i dZ_i, \quad (4.17)$$

where

$$v(R) = 1 + \left| \frac{R}{R_*} \right|^{d(\alpha-1)}. \quad (4.18)$$

Again, the power in v has been chosen to keep the spatial Hausdorff dimension equal to (4.9), to compare it with the other models.

Notice that the weight (4.18) is not exactly equivalent to a coordinate transformation of eq. (4.8) from spherical to cylindrical coordinates, since the system is not coordinate invariant except in the general-relativity limit $v \sim 1$. Furthermore, this theory in particular is not invariant under any modified version of coordinate invariance, contrary to T_v and T_q . Therefore, eq. (4.18) has to be taken as an *Ansatz* or approximation of the effects we expect to find in a spacetime with a certain matter distribution. Since such effects usually depend on the distance from the observer [37, 38], it is natural to confine the weight $v \neq 1$ to the radial direction both in spherical coordinates (modeling globular galaxies or the bulge of spiral galaxies) and in cylindrical coordinates (modeling the disk of spiral galaxies).

From (4.18),

$$\frac{\partial_R v}{v} = \frac{d(\alpha-1)}{R} \mathcal{A}(R), \quad (4.19)$$

$$\frac{\nabla^2 v}{v} = \frac{1}{v} \frac{1}{R} \partial_R (R \partial_R v) = \frac{d^2(\alpha-1)^2}{R^2} \mathcal{A}(R), \quad (4.20)$$

where \mathcal{A} is the same expression as before but with r and r_* replaced by R and R_* , so that using (2.18)

$$\begin{aligned} \frac{d-2}{d-1} \kappa^2 \rho = & \left[\partial_R^2 + \frac{1+d(\alpha-1)\mathcal{A}(R)}{R} \partial_R + \frac{1}{R^2} \partial_\varphi^2 + \nabla_i^2 \right. \\ & \left. + \frac{2d^2(\alpha-1)^2 \mathcal{A}(R)}{d-1 R^2} \right] \Phi - \frac{d(\alpha-1)(d\alpha-d-1)\mathcal{A}(R)}{(d-1)R^2} h^{RR}. \end{aligned} \quad (4.21)$$

As in the case in spherical coordinates, we can set $h^{RR} = -2\Phi$, leading to

$$\boxed{\frac{d-2}{d-1} \kappa^2 \rho = \left[\partial_R^2 + \frac{1+d(\alpha-1)\mathcal{A}(R)}{R} \partial_R + \frac{1}{R^2} \partial_\varphi^2 + \nabla_i^2 + \frac{2d(\alpha-1)(2d\alpha-2d-1)\mathcal{A}(R)}{(d-1)R^2} \right] \Phi.} \quad (4.22)$$

In the general-relativity or Newtonian limit $\mathcal{A} \rightarrow 0$, one gets the ordinary Poisson equation (2.19) in cylindrical coordinates, while in the fractional limit $\mathcal{A} \rightarrow 1$ this expression is approximated to

$$\frac{d-2}{d-1} \kappa^2 \rho \simeq \left[\partial_R^2 + \frac{d(\alpha-1)+1}{R} \partial_R + \frac{1}{R^2} \partial_\varphi^2 + \nabla_{(i)}^2 + \frac{2d(\alpha-1)(2d\alpha-2d-1)}{(d-1)R^2} \right] \Phi. \quad (4.23)$$

4.2.4 T_1 : Newton's potential

The Poisson equation is more difficult to solve with respect to the other two theories we will discuss below. The reason is that, although its solution is the combination of two power laws (possibly reducible to only one), the $1/r^2$ term never vanishes in $d = 3$ dimensions, unless $\alpha = 1$. This implies a difficulty when solving the Poisson equation in the sense of distributions at the point $r = 0$. Here we limit the discussion to the solution in spherical coordinates for $r \neq 0$ and $d = 3$. Taking a pointwise source $\rho = m\delta^3(\mathbf{x})/v$ of mass m ,

$$\frac{\kappa^2 m}{2} \delta^3(\mathbf{x}) \simeq v \left[\partial_r^2 + \frac{3\alpha - 1}{r} \partial_r + \frac{18(\alpha - 1)^2}{r^2} \right] \Phi(r). \quad (4.24)$$

For $r \neq 0$ the radial solution of eq. (4.24) is

$$\Phi(r) = C_1 r^{\frac{2-3\alpha-a}{2}} + C_2 r^{\frac{2-3\alpha+a}{2}}, \quad a := \sqrt{3(44 - 21\alpha)\alpha - 68}. \quad (4.25)$$

When a is purely imaginary, which happens for

$$\alpha < \frac{2(11 - \sqrt{2})}{21} \approx 0.91 \quad \text{or} \quad \alpha > \frac{2(11 + \sqrt{2})}{21} \approx 1.18, \quad (4.26)$$

one can make the potential real provided $C_1 = (c_1 - c_2)r_*^{a/2}/2$ and $C_2 = (c_1 + c_2)r_*^{-a/2}/2$, where $c_{1,2}$ are real. In this case,

$$\Phi(r) = \frac{1}{r^{\frac{3\alpha}{2}-1}} \left[c_1 \cos\left(\frac{|a|}{2} \ln \frac{r}{r_*}\right) + c_2 \sin\left(\frac{|a|}{2} \ln \frac{r}{r_*}\right) \right]. \quad (4.27)$$

The coefficients $c_{1,2}$ should be determined via techniques of the theory of distributions by considering the point $r = 0$, but we will not do it here. We only notice that this solution wildly oscillates near the origin when $\alpha > 2/3$ and may have other undesirable properties when applied to physical problems, such as a vanishing circular velocity at large radii. Therefore, we allow (4.27) only for

$$\alpha \leq \frac{2}{3}. \quad (4.28)$$

In this range of values, the fractional limit corresponds to short scales. When $\alpha = 2/3$, the potential undergoes infinitely many oscillations as it approaches the origin but it remains bounded. When $\alpha < 2/3$, these oscillations are progressively damped and $\Phi(0) = 0$. This suggests that the singularity of Newton's potential, and perhaps other classical singularities met in general relativity, may be resolved in this theory.

The alternative is to consider the profile (4.25) with real a , i.e., in the interval

$$0.91 \approx \frac{2(11 - \sqrt{2})}{21} < \alpha < \frac{2(11 + \sqrt{2})}{21} \approx 1.18. \quad (4.29)$$

In particular, when $\alpha = 1$, $a = 1$, $\Phi(r) = C_2 + C_1/r$ and one can set $C_2 = 0$ by a shift.

In this paper, we will not study in detail the predictions of this theory about the rotation curve of galaxies, since we have not solved the Poisson equation completely. However, in order to get a flat curve in the fractional limit the potential in that range of scales should be approximately constant. This suggests the following special value of α that could fit data well:

$$\alpha = \frac{2}{3}. \quad (4.30)$$

In fact, for the oscillating solution (4.27) we have just seen that (4.30) makes the potential bounded. On the other hand, in the solution (4.25) neither of the two power laws becomes a constant for any $\alpha \neq 1$. This strongly indicates that data fitting should be carried out with the rotation curve stemming from (4.27), once the coefficients c_1 and c_2 were determined.

We will meet the special value (4.30) again in the theory T_v , described in the next section.

5 Theory T_v with weighted derivatives

5.1 T_v : equations of motion

Let ${}_\beta\mathcal{D}_\mu$ be a weighted derivative of order β , i.e., an ordinary derivative with weight factors inserted to the left and to the right:

$${}_\beta\mathcal{D}_\mu := \frac{1}{v^\beta} \partial_\mu (v^\beta \cdot). \quad (5.1)$$

On rank-0 and rank-1 tensors, $\beta = 1/2$ [36, 39]:

$$\mathcal{D}_\mu := \frac{1}{\sqrt{v}} \partial_\mu (\sqrt{v} \cdot), \quad (5.2)$$

while on rank-2 tensors [36]

$$\check{\mathcal{D}}_\mu := {}_\beta\mathcal{D}_\mu, \quad \beta = \frac{2}{D-2}. \quad (5.3)$$

In $D = 4$ dimensions, $\check{\mathcal{D}}_\mu = {}_1\mathcal{D}_\mu$. The Levi-Civita connection and the curvature tensors are defined with this differential structure:

$${}^v\Gamma_{\mu\nu}^\rho := \frac{1}{2} g^{\rho\sigma} (\check{\mathcal{D}}_\mu g_{\nu\sigma} + \check{\mathcal{D}}_\nu g_{\mu\sigma} - \check{\mathcal{D}}_\sigma g_{\mu\nu}), \quad (5.4)$$

$$\mathcal{R}^\rho_{\mu\sigma\nu} := \partial_\sigma {}^v\Gamma_{\mu\nu}^\rho - \partial_\nu {}^v\Gamma_{\mu\sigma}^\rho + {}^v\Gamma_{\mu\nu}^\tau {}^v\Gamma_{\sigma\tau}^\rho - {}^v\Gamma_{\mu\sigma}^\tau {}^v\Gamma_{\nu\tau}^\rho, \quad (5.5)$$

$$\mathcal{R}_{\mu\nu} := \mathcal{R}^\rho_{\mu\rho\nu}, \quad \mathcal{R} := g^{\mu\nu} \mathcal{R}_{\mu\nu}. \quad (5.6)$$

The action in the physical frame is [36]

$$\begin{aligned} S &= \frac{1}{2\kappa^2} \int d^D x v \sqrt{|g|} [\mathcal{R} - w(v) \mathcal{D}_\mu v \mathcal{D}^\mu v - 2U(v)] + S_m \\ &= \frac{1}{2\kappa^2} \int d^D x \sqrt{|g|} e^{\frac{D-2}{2}\varphi} [R - \Omega' \partial_\mu \varphi \partial^\mu \varphi - 2U] + S_m, \end{aligned} \quad (5.7)$$

where U is a function of the weight v and

$$\varphi := \frac{2}{D-2} \ln v, \quad (5.8)$$

$$\Omega' := \frac{(\Omega - D + 1)(D - 2)}{4}, \quad \Omega := \frac{9(D - 2)w}{4} e^{(D-2)\varphi} = \frac{9(D - 2)w}{4} v^2. \quad (5.9)$$

In the second line of eq. (5.7), we reexpressed the action in terms of the ordinary Ricci scalar and the scalar-looking quantity φ . One can map the theory to a frame

$$\bar{g}_{\mu\nu} = e^\varphi g_{\mu\nu}, \quad (5.10)$$

where the curvature decouples from the measure weight. It is not difficult to show that

$$\square = e^\varphi \left(\bar{\square} - \frac{D-2}{2} \bar{\partial}_\mu \varphi \bar{\partial}^\mu \right), \quad (5.11)$$

$$\sqrt{|\bar{g}|} = e^{\frac{D}{2}\varphi} \sqrt{|g|}, \quad (5.12)$$

$$\bar{R}_{\mu\nu} = R_{\mu\nu} - \frac{1}{2} g_{\mu\nu} \square \varphi + \frac{D-2}{4} (\partial_\mu \varphi \partial_\nu \varphi - g_{\mu\nu} \partial_\sigma \varphi \partial^\sigma \varphi - 2 \nabla_\mu \nabla_\nu \varphi), \quad (5.13)$$

$$e^\varphi \bar{R} = R - (D-1) \square \varphi - \frac{(D-1)(D-2)}{4} \partial_\mu \varphi \partial^\mu \varphi, \quad (5.14)$$

so that the action in the \bar{g} frame is²

$$S = \frac{1}{2\kappa^2} \int d^D x \sqrt{|\bar{g}|} \left[\bar{R} - \frac{(D-2)\Omega}{4} \bar{\partial}_\mu \varphi \bar{\partial}^\mu \varphi - 2e^{-\varphi} U \right], \quad (5.15)$$

where the bar on top of ∂_μ is pleonastic. Although this looks like an ordinary conformal transformation from the Jordan to the Einstein frame, in fact it is not, since φ is not a scalar field but a fixed coordinate profile establishing that rulers and clocks measure scale-dependent events in the original frame without bars, sometimes called fractional frame. By definition, the fractional frame (corresponding to the Jordan frame) is the physical frame and one should revert to it when comparing observables with data [36].

The equations of motion from (5.15) are

$$\kappa^2 \bar{T}_{\mu\nu} = \bar{G}_{\mu\nu} + e^{-\varphi} U \bar{g}_{\mu\nu} - \frac{(D-2)\Omega}{4} \left(\bar{\partial}_\mu \varphi \bar{\partial}_\nu \varphi + \frac{1}{2} \bar{g}_{\mu\nu} \bar{\partial}_\sigma \varphi \bar{\partial}^\sigma \varphi \right), \quad (5.16)$$

where

$$\bar{T}_{\mu\nu} := -\frac{2}{\sqrt{|\bar{g}|}} \frac{\delta S_m}{\delta \bar{g}^{\mu\nu}} = e^{-\frac{D-2}{2}\varphi} v T_{\mu\nu}^v = T_{\mu\nu}^v. \quad (5.17)$$

Taking the trace of (5.16),

$$\kappa^2 \bar{T} = -\frac{D-2}{2} \bar{R} + e^{-\varphi} D U - \frac{(D-2)(D+2)\Omega}{8} \bar{\partial}_\sigma \varphi \bar{\partial}^\sigma \varphi, \quad (5.18)$$

we rewrite (5.16) as

$$\kappa^2 \bar{S}_{\mu\nu} = \bar{R}_{\mu\nu} + \frac{\Omega}{2} \left(\bar{g}_{\mu\nu} \bar{\partial}_\sigma \varphi \bar{\partial}^\sigma \varphi - \frac{D-2}{2} \bar{\partial}_\mu \varphi \bar{\partial}_\nu \varphi \right), \quad (5.19)$$

$$\bar{S}_{\mu\nu} := \tilde{T}_{\mu\nu} - \frac{1}{D-2} \bar{g}_{\mu\nu} \tilde{T}, \quad \tilde{T}_{\mu\nu} := \bar{T}_{\mu\nu} - e^{-\varphi} U \bar{g}_{\mu\nu}. \quad (5.20)$$

Using (5.13), we get

$$\begin{aligned} \kappa^2 S_{\mu\nu}^v &= R_{\mu\nu} + \frac{(D-2)(1-\Omega)}{4} \partial_\mu \varphi \partial_\nu \varphi - \frac{D-2-2\Omega}{4} g_{\mu\nu} \partial_\sigma \varphi \partial^\sigma \varphi \\ &\quad - \frac{1}{2} g_{\mu\nu} \square \varphi - \frac{D-2}{2} \nabla_\mu \nabla_\nu \varphi, \end{aligned} \quad (5.21)$$

where $S_{\mu\nu}^v$ is defined in (4.6).

²This expression corrects a typo in the published version of [36, eq. (5.28)]. The arXiv version is correct.

We can repeat the same calculation in the fractional frame. Since from (5.13) and (5.14)

$$\bar{G}_{\mu\nu} = G_{\mu\nu} + \frac{D-2}{2} \left(\frac{1}{2} \partial_\mu \varphi \partial_\nu \varphi + \frac{D-3}{4} g_{\mu\nu} \partial_\sigma \varphi \partial^\sigma \varphi + g_{\mu\nu} \square \varphi - \nabla_\mu \nabla_\nu \varphi \right), \quad (5.22)$$

in the physical frame the modified Einstein equations (5.16) become

$$\begin{aligned} \kappa^2 T_{\mu\nu}^v &= G_{\mu\nu} + U g_{\mu\nu} + \frac{(D-2)(1-\Omega)}{4} \partial_\mu \varphi \partial_\nu \varphi + \frac{(D-2)(D-3-\Omega)}{8} g_{\mu\nu} \partial_\sigma \varphi \partial^\sigma \varphi \\ &\quad + \frac{D-2}{2} (g_{\mu\nu} \square \varphi - \nabla_\mu \nabla_\nu \varphi). \end{aligned} \quad (5.23)$$

The trace equation is

$$\begin{aligned} \kappa^2 T^v &= -\frac{D-2}{2} R + DU + \frac{(D-2)[2(1-\Omega) + D(D-3-\Omega)]}{8} \partial_\sigma \varphi \partial^\sigma \varphi \\ &\quad + \frac{(D-2)(D-1)}{2} \square \varphi, \end{aligned} \quad (5.24)$$

which, combined with (5.23), gives (5.21).

5.2 T_v : Poisson equation and Newton's potential

To get the Poisson equation for the perturbation h_{00} , we can either calculate it directly from (5.21) or via the expression (5.19) in the integer frame. Equation (5.16) looks deceptively simple but one should bear in mind that perturbing around Minkowski spacetime in the fractional frame implies an integer-frame background which is only conformally equivalent to Minkowski. Consequently, the background operators in the perturbed equation for \bar{h}_{00} should be further expanded to make v -terms explicit. We choose the easiest route and work directly in the fractional frame.

5.2.1 T_v : Poisson equation in Cartesian coordinates

Plugging (2.7) into (5.21) and expanding, we get

$$\begin{aligned} \frac{d-2}{d-1} \kappa^2 \rho &= \left[\nabla^2 + \frac{d-1}{2} \partial^i \varphi \partial_i + \frac{d-1-2\Omega}{2} \partial_i \varphi \partial^i \varphi + \nabla^2 \varphi \right] \Phi \\ &\quad + \frac{1}{2} h^{ij} \left(\frac{d-1-2\Omega}{2} \partial_i \varphi \partial_j \varphi - \partial_i \partial_j \varphi \right). \end{aligned} \quad (5.25)$$

5.2.2 T_v : Poisson equation in spherical coordinates

In spherical coordinates,

$$\partial_i \varphi = \partial_r \varphi = \frac{2}{d-1} \frac{\partial_r v}{v} = \frac{2d(\alpha-1)\mathcal{A}(r)}{(d-1)r}, \quad (5.26)$$

$$\nabla^2 \varphi = \frac{2d(\alpha-1)}{d-1} \frac{[d\alpha-2-d(\alpha-1)\mathcal{A}(r)]\mathcal{A}(r)}{r^2}, \quad (5.27)$$

and

$$\frac{d-2}{d-1} \kappa^2 \rho = \left\{ \partial_r^2 + \frac{d-1+d(\alpha-1)\mathcal{A}(r)}{r} \partial_r + \frac{1}{r^2} \nabla_{S^{d-1}}^2 \right.$$

$$\begin{aligned}
& + \frac{2d(\alpha-1)[(d-1)(d\alpha-2) - 2d\Omega(\alpha-1)\mathcal{A}(r)]\mathcal{A}(r)}{(d-1)^2 r^2} \Big\} \Phi \\
& + \frac{[2d(d-1-\Omega)(\alpha-1)\mathcal{A}(r) - (d-1)(d\alpha-d-1)]d(\alpha-1)\mathcal{A}(r)}{(d-1)^2 r^2} h^{rr}, \quad (5.28)
\end{aligned}$$

where \mathcal{A} is given in (4.13). We can eliminate the h^{rr} term either by choosing

$$\Omega = \frac{(d-1)[d+1-d\alpha+2d(\alpha-1)\mathcal{A}(r)]}{2d(\alpha-1)\mathcal{A}(r)}$$

or, as we did in the theory T_1 , by fixing the gauge so that $h^{rr} = -2\Phi$. The result is exactly the same in both procedures and the Poisson equation in spherical coordinates reads

$$\boxed{\frac{d-2}{d-1}\kappa^2\rho = \left\{ \partial_r^2 + \frac{d-1+d(\alpha-1)\mathcal{A}(r)}{r}\partial_r + \frac{1}{r^2}\nabla_{S^{d-1}}^2 + \frac{2d(\alpha-1)[2d\alpha-d-3-2d(\alpha-1)\mathcal{A}(r)]\mathcal{A}(r)}{(d-1)r^2} \right\} \Phi.} \quad (5.29)$$

5.2.3 T_v : Newton's potential

Extreme fractional limit. The asymptotic solution of the Poisson equation (5.29) for a radial potential $\Phi(r)$ and a pointwise source $\rho = m\delta^d(\mathbf{x})/v$ of mass m can be found easily. In the general-relativity or Newtonian limit $\mathcal{A} \rightarrow 0$, i.e., when $\alpha < 1$ and $r \gg r_*$ or when $\alpha > 1$ and $r \ll r_*$, one gets (2.20), while in the fractional limit $\mathcal{A} \rightarrow 1$, i.e., when $\alpha < 1$ and $r \ll r_*$ or when $\alpha > 1$ and $r \gg r_*$, we have

$$\begin{aligned}
\frac{d-2}{d-1}\kappa^2 m \frac{\delta^d(\mathbf{x})}{v} & \simeq \mathcal{C}\Phi := \left[\partial_r^2 + \frac{d\alpha-1}{r}\partial_r + \frac{2d(\alpha-1)(d-3)}{(d-1)r^2} \right] \Phi \\
& = \left[\frac{1}{r^{d\alpha-1}}\partial_r \left(r^{d\alpha-1}\partial_r \cdot \right) + \frac{2d(\alpha-1)(d-3)}{(d-1)r^2} \right] \Phi. \quad (5.30)
\end{aligned}$$

Everywhere except at $r = 0$, the solution is

$$\Phi(r) = C_+ r^{-c_+} + C_- r^{-c_-}, \quad (5.31)$$

$$c_{\pm} = \frac{1}{2} \left[d\alpha - 2 \pm \sqrt{(d\alpha - 2)^2 - \frac{8d(\alpha-1)(d-3)}{d-1}} \right]. \quad (5.32)$$

When $d = 3$ or $\alpha = 1$, $c_- = 0$ and we can redefine the potential by a shift, thus setting $C_- = 0$ from now on. The normalization constant C_+ can be found by looking at the solution at $r = 0$. Using (2.23), for a test function f

$$\begin{aligned}
\int d^d \mathbf{x} v (\mathcal{C}\Phi) f & = \lim_{\epsilon \rightarrow 0} \frac{2\pi^{\frac{d}{2}}}{\Gamma(\frac{d}{2})} \int_{\epsilon}^{+\infty} dr r^{d-1} v (\mathcal{C}\Phi) f \\
& \stackrel{(5.31)}{=} \lim_{\epsilon \rightarrow 0} \frac{2\pi^{\frac{d}{2}}}{\Gamma(\frac{d}{2})} \frac{1}{r_*^{d(\alpha-1)}} \int_{\epsilon}^{+\infty} dr \left[\partial_r \left(r^{d\alpha-1} \partial_r \Phi \right) + r^{d\alpha-3} \frac{2d(\alpha-1)(d-3)}{d-1} \Phi \right] f \\
& = \lim_{\epsilon \rightarrow 0} \frac{2\pi^{\frac{d}{2}}}{\Gamma(\frac{d}{2})} \frac{1}{r_*^{d(\alpha-1)}} \int_{\epsilon}^{+\infty} dr \left[- \left(r^{d\alpha-1} \partial_r \Phi \right) \partial_r f + r^{d\alpha-3} \frac{2d(\alpha-1)(d-3)}{d-1} \Phi f \right]
\end{aligned}$$

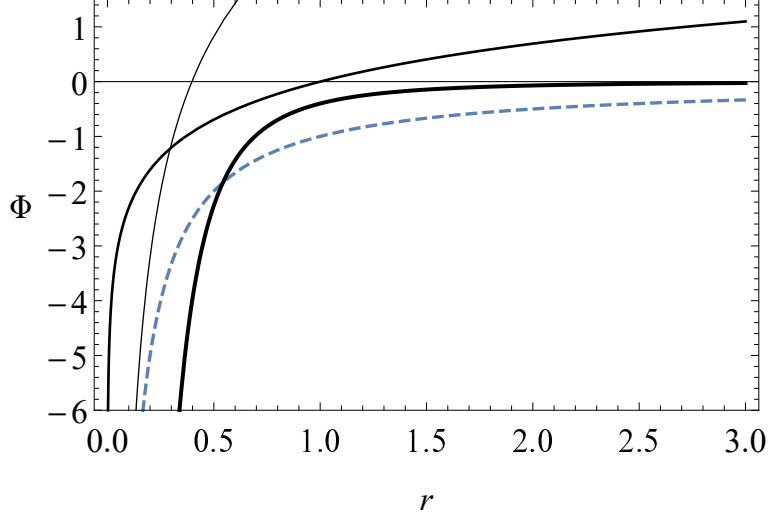


Figure 2. Gravitational potential in $d = 3$ spatial dimensions for a pointwise source in the theory with weighted derivatives with $r_* = 1$. Dashed curve: general-relativity limit (2.25) (valid for $r \ll r_*$). Solid curves of increasing thickness: approximation (5.40) with small fractional correction with $\alpha = 1.5$ (valid for $r \ll r_*$), logarithmic potential (5.35) (valid for $\alpha = 2/3$ and $r \ll r_*$) and the extreme fractional limit (5.34) with $\alpha = 1.5$ (valid for $r \gg r_*$). Here $Gm = 1$.

$$= \lim_{\epsilon \rightarrow 0} \frac{2\pi^{\frac{d}{2}}}{\Gamma(\frac{d}{2})} \frac{C_+ c_+}{r_*^{d(\alpha-1)}} \int_{\epsilon}^{+\infty} dr \left[r^{d\alpha-c_+-2} \partial_r f + r^{d\alpha-3} \frac{2d(\alpha-1)(d-3)}{d-1} \Phi f \right]. \quad (5.33)$$

We can use this expression in the general-relativistic or Newtonian limit, which is achieved by setting $\alpha = 1$. Then, the last term vanishes, $c_+ = d - 2$ and one gets (2.24). In the fractional limit, we are unable to proceed unless $d = 3$, in which case $c_+ = 3\alpha - 2$ and

$$\int d^3 \mathbf{x} v \mathcal{C} \Phi f = -4\pi \frac{C_+(3\alpha-2)}{r_*^{3(\alpha-1)}} f(0) = 4\pi Gm f(0),$$

yielding

$$\Phi(r) \simeq -\frac{1}{3\alpha-2} \frac{Gm}{r_*} \left| \frac{r_*}{r} \right|^{3\alpha-2}. \quad (5.34)$$

The asymptotic limits (2.25) and (5.34) are shown in Fig. 2.

The special value (4.30) reappears in this theory in this regime. In the limit $\alpha \rightarrow 2/3$, the potential (5.34) becomes (Fig. 2)

$$\Phi(r) \simeq \frac{Gm}{r_*} \ln \frac{r}{r_*}, \quad (5.35)$$

up to a divergent constant $\propto (3\alpha - 2)^{-1}$ that can be eliminated by a shift. This potential can be obtained directly from the Poisson equation (5.30) setting $d = 3$ and $\alpha = 2/3$ therein. The logarithmic behaviour implies that the rotation velocity

$$v_{\text{circ}}(r) = \sqrt{\left| \frac{1}{\sqrt{v}} \frac{d(\sqrt{v}\Phi)}{d \ln r} \right|} \quad (5.36)$$

tends to a constant plus a logarithm, i.e., approximately a plateau. Since values in the half-line $\alpha < 1$ correspond to an extreme fractional limit valid at $r \ll r_*$, then, if r_* was much larger than the galaxy scale and α was close to $2/3$, one could realize an almost flat rotation curve in the extreme fractional regime (5.34) in a self-consistent way.

Small fractional corrections. An intermediate form of the Newtonian potential when the fractional correction is small can be obtained by expanding the Poisson equation (5.29) for small $\mathcal{A} \simeq |r/r_*|^{d(\alpha-1)}$ with a delta source for a radial solution:

$$\begin{aligned} \frac{d-2}{d-1} \kappa^2 m \delta^d(\mathbf{x}) \left[1 - \left| \frac{r}{r_*} \right|^{d(\alpha-1)} \right] &\simeq \left(\partial_r^2 + \frac{d-1}{r} \partial_r \right) \Phi(r) \\ &+ \frac{d(\alpha-1)}{r} \left| \frac{r}{r_*} \right|^{d(\alpha-1)} \left[\partial_r + \frac{2(2d\alpha-d-3)}{(d-1)r} \right] \Phi(r). \end{aligned} \quad (5.37)$$

Splitting the potential $\Phi = \Phi_0 + \Phi_1$ into a zero-order part Φ_0 solving the ordinary Poisson equation (2.20) and a first-order part Φ_1 and dropping higher-order terms, one has to solve

$$\begin{aligned} -\frac{d-2}{d-1} \kappa^2 m \delta^d(\mathbf{x}) \left| \frac{r}{r_*} \right|^{d(\alpha-1)} &= \left(\partial_r^2 + \frac{d-1}{r} \partial_r \right) \Phi_1(r) \\ &+ \frac{d(\alpha-1)}{r} \left| \frac{r}{r_*} \right|^{d(\alpha-1)} \left[\partial_r + \frac{2(2d\alpha-d-3)}{(d-1)r} \right] \Phi_0(r) \\ &= \left(\partial_r^2 + \frac{d-1}{r} \partial_r \right) \Phi_1(r) \\ &+ \frac{4Gmd(\alpha-1)\Gamma\left(\frac{d}{2}\right)}{\pi^{\frac{d}{2}-1}} \left| \frac{r}{r_*} \right|^{d(\alpha-1)} \frac{d^2-d-4\alpha d+8}{(d-1)^2 r^d}, \end{aligned} \quad (5.38)$$

where Φ_0 is given by (2.24). The solution is

$$\Phi_1(r) = \Phi_0(r) \frac{8+d(d-1-4\alpha)}{(d-1)(2-2d+d\alpha)} \left| \frac{r}{r_*} \right|^{d(\alpha-1)},$$

so that

$$\Phi(r) \simeq \Phi_0(r) \left[1 - \frac{8+d(d-1-4\alpha)}{(d-1)(2-2d+d\alpha)} \left| \frac{r}{r_*} \right|^{d(\alpha-1)} \right]. \quad (5.39)$$

In $d = 3$ spatial dimensions (Fig. 1),

$$\Phi(r) \simeq \Phi_0(r) \left[1 - \frac{7-6\alpha}{4-3\alpha} \left| \frac{r}{r_*} \right|^{3(\alpha-1)} \right]. \quad (5.40)$$

When $\alpha \rightarrow 4/3$, the potential becomes

$$\Phi(r) \simeq -\frac{Gm}{r} + \frac{Gm}{r_*} \ln \frac{r}{r_*}, \quad (5.41)$$

up to a shiftable constant. This potential can be obtained directly from eq. (5.38) setting $d = 3$ and $\alpha = 4/3$. Therefore, since for $\alpha > 1$ the fractional correction is small when $r \ll r_*$, the rotation velocity (5.36) tends to a constant when α is close to the special value

$$\alpha = \frac{4}{3}. \quad (5.42)$$

This could provide a self-consistent explanation of galaxy rotation curves if r_* was much larger than the typical galactic size.

Curiously, the second term in (5.41) coincides with the potential (5.35) obtained in the extreme fractional regime for a different value of the fractional exponent, $\alpha = 2/3$.

5.3 T_v : thin-disk exponential-density rotation curve

Let (2.26) be the full solution of the Poisson equation with pointwise source with mass m . The multi-fractional generalization of eq. (2.27) is

$$\Phi^{\text{galaxy}}(R) = \int_{\mathcal{V}} d^3\mathbf{x}' v(\mathbf{x}') \rho(\mathbf{x}') \mathcal{G}(\mathbf{x} - \mathbf{x}'). \quad (5.43)$$

The extreme asymptotic limits of $m\mathcal{G}$ are given by eqs. (2.25) and (5.34) or (5.35), while (5.40) and (5.41) include a correction to (2.25) in the limit of small fractional correction $|r/r_*|^{3(\alpha-1)}$.

The gravitational field in the theory T_v is

$$g(R) = -\mathcal{D}_R \Phi^{\text{galaxy}}(R) = -\frac{1}{\sqrt{|v(R)|}} \frac{d}{dR} \left[\sqrt{|v(R)|} \Phi^{\text{galaxy}}(R) \right], \quad (5.44)$$

while the circular velocity is

$$v_{\text{circ}}(R) = \sqrt{|Rg(R)|}. \quad (5.45)$$

We used the derivative \mathcal{D} in eq. (5.44) because the gravitational field is a rank-1 tensor [36, 39] (we omitted the unit vector in the expression). Expression (5.45) is derived in Appendix A

5.3.1 T_v : extreme fractional limit

In this approximation, when $\alpha \neq 2/3$ one can use the potential (5.34), so that eq. (5.43) with $r_* = R_*$ becomes

$$\Phi^{\text{disk}}(R) \simeq -\frac{1}{3\alpha - 2} \frac{G}{R_*} \int_{\mathcal{V}} d^3\mathbf{x}' \left| \frac{R'}{R_*} \right|^{3(\alpha-1)} \rho(\mathbf{x}') \left(\frac{R_*}{|\mathbf{x} - \mathbf{x}'|} \right)^{3\alpha-2}, \quad (5.46)$$

while when $\alpha = 2/3$ one takes (5.35) and

$$\Phi^{\text{disk}}(R) \simeq \frac{G}{R_*} \int_{\mathcal{V}} d^3\mathbf{x}' \left| \frac{R'}{R_*} \right|^{-1} \rho(\mathbf{x}') \ln \frac{|\mathbf{x} - \mathbf{x}'|}{R_*}. \quad (5.47)$$

Both expressions are calculated in Appendix D.1 and they are given by eqs. (D.1) (approximated to (D.2)) and (D.3). The gravitational field and circular velocity are found plugging these expressions into eqs. (5.44) and (5.45), respectively. In particular,

$$g(R) = -\frac{d\Phi^{\text{galaxy}}(R)}{dR} - \frac{3(\alpha - 1)}{2R} \Phi^{\text{galaxy}}(R). \quad (5.48)$$

To explore in a preliminary way how the rotation curve is modified in this theory, we compare the thin-disk analytic approximation in the extreme fractional limit with the general-relativity result (2.36) (Fig. 3) and, for reference, the values of M and R_0 of NGC6503.

These results are not conclusive because they are not based on actual matter density data but they illustrate the possibilities of the model. As one can see in Fig. 3, depending on the value of α one can enhance the tail or lift and flatten the whole curve, although without ever forming a plateau at the peak height, even when $\alpha = 2/3$.

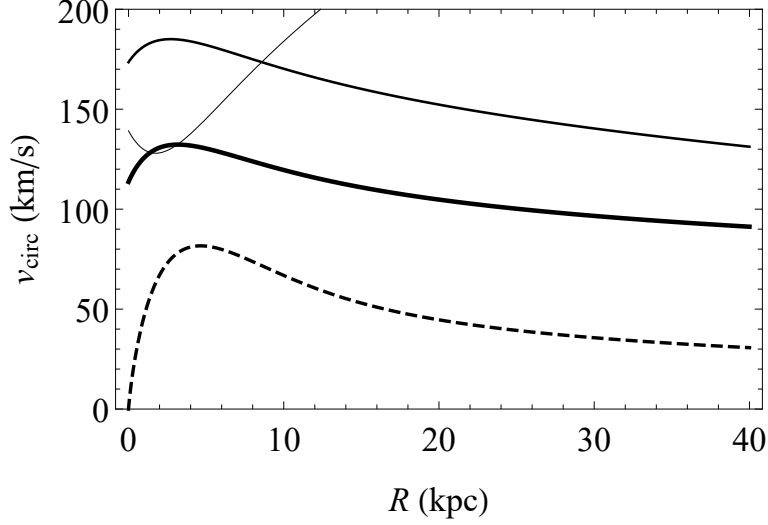


Figure 3. Rotation curve of baryonic matter in the thin-disk approximation and an exponential matter density profile in general relativity (eq. (2.36), dashed curve) and in the multi-fractional theory T_v with weighted derivatives in the extreme fractional limit ((5.45), (5.46) or (5.47), and eqs. (5.48), where $\alpha < 1$ and $R \ll R_*$) for $\alpha = 0.4$, $\alpha = 2/3$ and $\alpha = 0.8$ (solid curves of increasing thickness). Here $M = 1.72 \times 10^{40}$ kg, $R_0 = 2.16$ kpc and $R_* = 40$ kpc.

5.3.2 T_v : small fractional corrections

Expanding (5.43), for $\alpha \neq 4/3$

$$\Phi^{\text{disk}}(R) \simeq \Phi_0^{\text{disk}}(R) + \delta\Phi_1^{\text{disk}}(R) + \delta\Phi_2^{\text{disk}}(R), \quad (5.49a)$$

$$\Phi_0^{\text{disk}}(R) = -G \int_{\mathcal{V}} d^3\mathbf{x}' \frac{\rho(\mathbf{x}')}{|\mathbf{x} - \mathbf{x}'|}, \quad (5.49b)$$

$$\delta\Phi_1^{\text{disk}}(R) = -G \int_{\mathcal{V}} d^3\mathbf{x}' \left| \frac{R'}{R_*} \right|^{3(\alpha-1)} \frac{\rho(\mathbf{x}')}{|\mathbf{x} - \mathbf{x}'|}, \quad (5.49c)$$

$$\delta\Phi_2^{\text{disk}}(R) = -G \frac{7 - 6\alpha}{(3\alpha - 4)r_*^{3(\alpha-1)}} \int_{\mathcal{V}} d^3\mathbf{x}' \frac{\rho(\mathbf{x}')}{|\mathbf{x} - \mathbf{x}'|^{4-3\alpha}}. \quad (5.49d)$$

In cylindrical coordinates, the integration volume (2.28) is decorated with a measure $v(R')$. The measure weight $v(R')$ is assumed to have cylindrical symmetry because we want to test how the rotation curve of baryonic matter deviates from general-relativity in a region of space with multi-fractional measure of galactic size $\sim R_0 \ll R_*$. Within this region, one considers infinitesimal masses dm each generating a radial potential which is in turn multi-fractional.

In the thin-disk approximation, the lowest-order term Φ_0 is the standard Newtonian potential (2.34), which was calculated in section 2.3. The terms (5.49c) and (5.49d) are calculated in Appendix D.2 using some formulæ of Appendix B and C.

The gravitational field in the theory T_v is (5.44):

$$\begin{aligned} g^{\text{disk}}(R) &\simeq -\frac{d}{dR} \left[\Phi_0^{\text{disk}}(R) + \delta\Phi_1^{\text{disk}}(R) + \delta\Phi_2^{\text{disk}}(R) \right] - \Phi_0(R) \frac{1}{\sqrt{v(R)}} \frac{d}{dR} \sqrt{v(R)} \\ &\simeq -\frac{d}{dR} \left[\Phi_0^{\text{disk}}(R) + \delta\Phi_1^{\text{disk}}(R) + \delta\Phi_2^{\text{disk}}(R) \right] - \frac{3(\alpha - 1)}{2R} \left| \frac{R}{R_*} \right|^{3(\alpha-1)} \Phi_0^{\text{disk}}(R), \end{aligned} \quad (5.50)$$

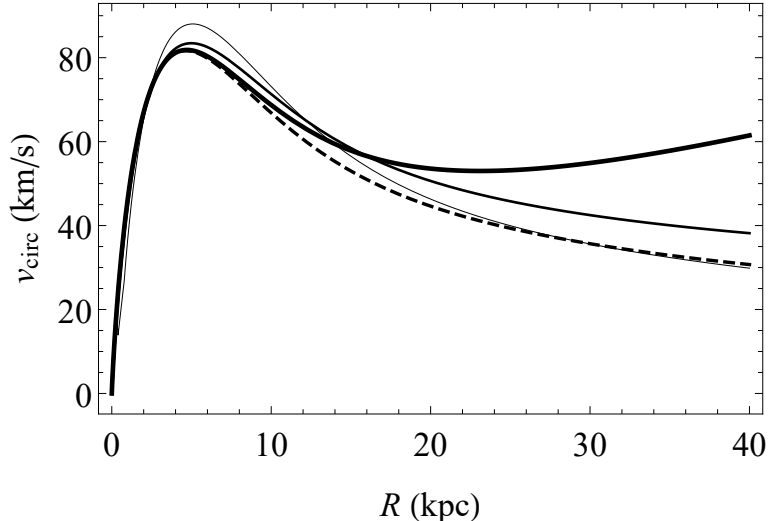


Figure 4. Rotation curve of baryonic matter in the thin-disk approximation and an exponential matter density profile in general relativity (eq. (2.36), dashed curve) and in the multi-fractional theory T_v with weighted derivatives in the limit of small corrections (eqs. (5.50) and (5.45), where $\alpha > 1$ and $R \ll R_*$) for $\alpha = 1.1$, $\alpha = 4/3$ and $\alpha = 1.9$ (solid curves of increasing thickness). Here $M = 1.72 \times 10^{40}$ kg, $R_0 = 2.16$ kpc and $R_* = 40$ kpc.

while the circular velocity to leading order in the fractional limit is (5.45) with g given by (5.50), which can be further expanded for small corrections. This model is self-consistent at all galactic scales only if $R_0 \ll R_*$ and $\alpha > 1$.

Figure 4 compares the velocity (5.45) from the gravitational field (5.50) in the thin-disk analytic approximation with small fractional corrections with the general-relativity result (2.36), using again the values of M and R_0 of NGC6503.

Depending on the value of α , one can enhance the peak or lift the damping tail, although without ever forming a plateau at the peak height, even when $\alpha = 4/3$.

5.4 T_v : data-based rotation curve

In this sub-section, we finally compare the predictions of the theory T_v with SPARC data, assuming that the only matter component is baryonic.

5.4.1 T_v : extreme fractional limit

The profiles $\Phi^{\text{disk+gas}}(R)$ and $\Phi^{\text{bulge}}(R)$ and the corresponding gravitational fields $g^{\text{disk+gas}}(R)$ and $g^{\text{bulge}}(R)$ for a thick disk and a generic matter density profile are calculated in Appendix E.1: eqs. (E.1), (E.4), (E.3) and (E.5) for $\alpha \neq 2/3$, and eqs. (E.6), (E.8), (E.7) and (E.9) for $\alpha = 2/3$. The circular velocity is

$$v_{\text{circ}}(R) = \sqrt{|Rg(R)|}, \quad g(R) = g^{\text{disk+gas}}(R) + g^{\text{bulge}}(R). \quad (5.51)$$

We checked that the n -expansion of (5.45) in Gegenbauer polynomials converges quickly for various values of α . For instance, when $\alpha = 1$ one recovers the general-relativity curve already at $n = 5$, with a good approximation already at $n = 3$.³

³The series for $\alpha = 1$ actually has a better numerical convergence than the formulæ of section 2.4 and, in fact, we used the $n_{\text{max}} = 5$ expression to plot Fig. 1.

In the cases of all three galaxies, the model in the extreme fractional regime does not fit the data (Appendix E.1.3).

5.4.2 T_v : small fractional corrections

The total potential is the sum of terms as in eq. (5.49a), extended to a gas and a bulge component:

$$\begin{aligned} \Phi^{\text{galaxy}}(R) = & \left[\Phi_0^{\text{disk+gas}}(R) + \Phi_0^{\text{bulge}}(R) \right] + \left[\delta\Phi_1^{\text{disk+gas}}(R) + \delta\Phi_1^{\text{bulge}}(R) \right] \\ & + \left[\delta\Phi_2^{\text{disk+gas}}(R) + \delta\Phi_2^{\text{bulge}}(R) \right]. \end{aligned} \quad (5.52)$$

All its components for a thick disk and a generic matter density profile are calculated in Appendix E.2: eqs. (E.10), (E.11), (E.14), (E.15), (E.18) and (E.19) for $\alpha \neq 4/3$ and eqs. (E.10), (E.11), (E.24), (E.25), (E.28) and (E.29) for $\alpha = 4/3$.

The gravitational field is the data-based version of eq. (5.50):

$$\begin{aligned} g^{\text{galaxy}}(R) = & \left[g_0^{\text{disk+gas}}(R) + g_0^{\text{bulge}}(R) \right] + \left[\delta g_1^{\text{disk+gas}}(R) + \delta g_1^{\text{bulge}}(R) \right] \\ & + \left[\delta g_2^{\text{disk+gas}}(R) + \delta g_2^{\text{bulge}}(R) \right], \end{aligned} \quad (5.53a)$$

$$g_0^{\text{disk+gas}}(R) = -\frac{d\Phi_0^{\text{disk+gas}}(R)}{dR} - \frac{3(\alpha-1)}{2R} \left| \frac{R}{R_*} \right|^{3(\alpha-1)} \Phi_0^{\text{disk+gas}}(R), \quad (5.53b)$$

$$g_0^{\text{bulge}}(R) = -\frac{d\Phi_0^{\text{bulge}}(r)}{dr} \Big|_{r=R} - \frac{3(\alpha-1)}{2R} \left| \frac{R}{R_*} \right|^{3(\alpha-1)} \Phi_0^{\text{bulge}}(R), \quad (5.53c)$$

$$\delta g_1^{\text{disk+gas}}(R) = -\frac{d\delta\Phi_1^{\text{disk+gas}}(R)}{dR}, \quad (5.53d)$$

$$\delta g_1^{\text{bulge}}(R) = -\frac{d\delta\Phi_1^{\text{bulge}}(r)}{dr} \Big|_{r=R}, \quad (5.53e)$$

$$\delta g_2^{\text{disk+gas}}(R) = -\frac{d\delta\Phi_2^{\text{disk+gas}}(R)}{dR}, \quad (5.53f)$$

$$\delta g_2^{\text{bulge}}(R) = -\frac{d\delta\Phi_2^{\text{bulge}}(r)}{dr} \Big|_{r=R}, \quad (5.53g)$$

and is reported in eqs. (E.12), (E.13), (E.16), (E.17), (E.20) and (E.21) for $\alpha \neq 4/3$, and eqs. (E.22), (E.23), (E.26), (E.27), (E.30) and (E.31) for $\alpha = 4/3$. The rotation curves of the three galaxies for some values of α and R_* are shown in Figs. 5–7. We took up to three modes in the calculation because, in this regime and for all values of α and R_* , the zero mode receives sizable corrections only from the $n = 1, 2, 3$ contributions, while higher-order modes are negligible. As one can see, although the rotation curve is lifted at some points with respect to the one in general relativity, the model is unable to fit the data when $\alpha \neq 4/3$.

When $\alpha = 4/3$, the model matches the large- R data of the three galaxies, while it fails to fit small- R data, showing that this model needs further improvement, in order to fully fit the galactic rotation data. However, it should be noted that, using the values for the R_* parameter from the bottom panels in Figs. 5–7 combined with the respective galactic masses, one obtains a MOND-like acceleration parameter $a_0 \sim GM/R_*^2 \simeq 0.72 - 2.1 \times 10^{-10} \text{ m s}^{-2}$, comparable with the actual value of the MOND acceleration $a_0 = 1.2 \times 10^{-10} \text{ m s}^{-2}$ [25].

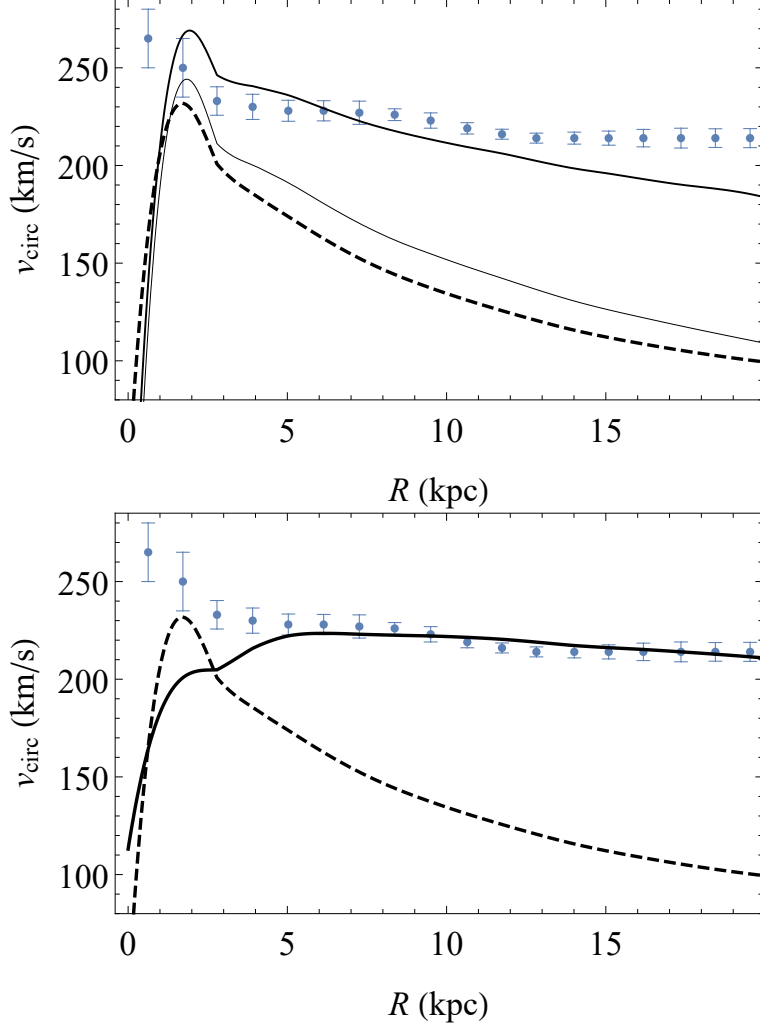


Figure 5. Comparison of the data points of NGC7814 with the $n = 3$ rotation curve of the theory T_v with weighted derivatives in the limit of weak fractional corrections with a data-based matter density profile for $\alpha = 1$ (general relativity, dashed curve), $\alpha = 1.1, 1.3$ and $R_* = 4$ kpc (top panel, increasing thickness) or $\alpha = 4/3$ and $R_* = 5.3$ kpc (bottom panel, increasing thickness).

This connection is similar to the one used by Giusti [19, 20] and Variaschi [21–23] in their fractional models.

6 Theory T_q with q -derivatives

6.1 T_q : equations of motion

The theory with q -derivatives is the simplest of the three multi-fractional scenarios with ordinary differential structure. All equations of general relativity look the same in this theory, except that coordinates x^μ are replaced by the composite coordinates (no summation over μ)

$$q(x^\mu) = \int dx^\mu v_\mu(x^\mu). \quad (6.1)$$

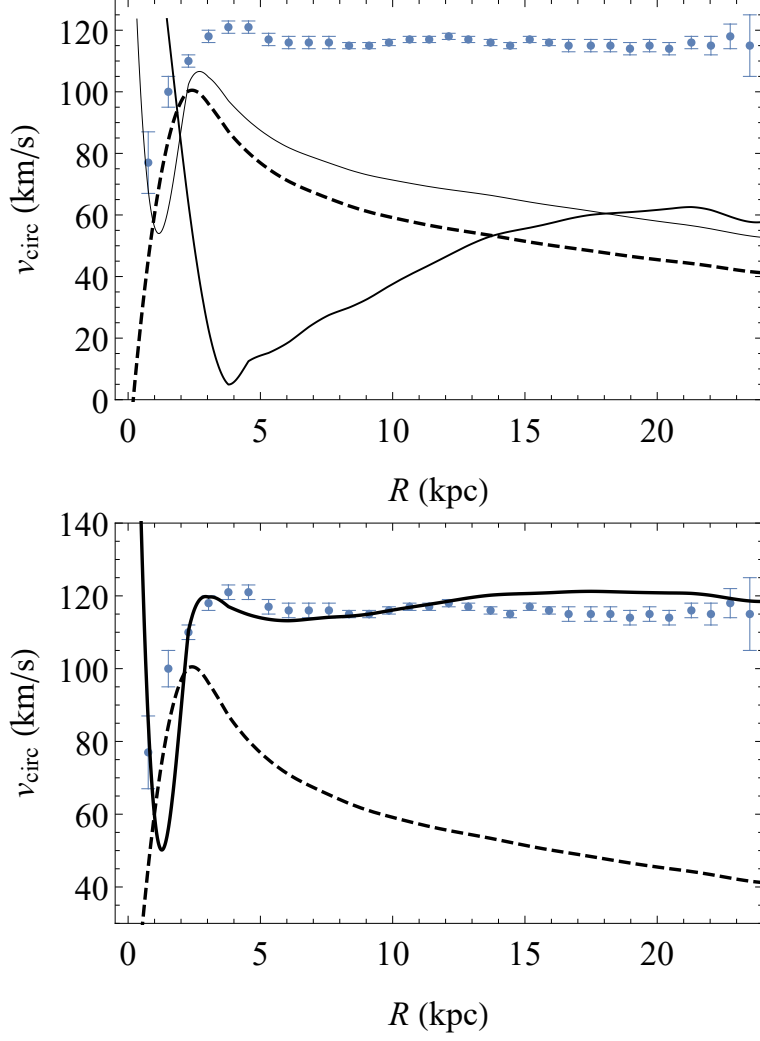


Figure 6. Comparison of the data points of NGC6503 with the $n = 3$ rotation curve of the theory T_v with weighted derivatives in the limit of weak fractional corrections with a data-based matter density profile for $\alpha = 1$ (general relativity, dashed curve), $\alpha = 1.1, 1.6$ and $R_* = 5$ kpc (top panel, increasing thickness) or $\alpha = 4/3$ and $R_* = 3.5$ kpc (bottom panel, increasing thickness).

In particular, all ordinary derivatives are replaced by the q -derivatives (no summation over μ)

$$\frac{\partial}{\partial q^\mu(x^\mu)} = \frac{1}{v_\mu(x^\mu)} \frac{\partial}{\partial x^\mu}. \quad (6.2)$$

Defining [36]

$${}^q\Gamma_{\mu\nu}^\rho := \frac{1}{2}g^{\rho\sigma} \left(\frac{1}{v_\mu} \partial_\mu g_{\nu\sigma} + \frac{1}{v_\nu} \partial_\nu g_{\mu\sigma} - \frac{1}{v_\sigma} \partial_\sigma g_{\mu\nu} \right), \quad (6.3)$$

$${}^qR_{\mu\sigma\nu}^\rho := \frac{1}{v_\sigma} \partial_\sigma {}^q\Gamma_{\mu\nu}^\rho - \frac{1}{v_\nu} \partial_\nu {}^q\Gamma_{\mu\sigma}^\rho + {}^q\Gamma_{\mu\nu}^\tau {}^q\Gamma_{\sigma\tau}^\rho - {}^q\Gamma_{\mu\sigma}^\tau {}^q\Gamma_{\nu\tau}^\rho, \quad (6.4)$$

$${}^qR_{\mu\nu} := {}^qR_{\mu\rho\nu}^\rho, \quad {}^qR := g^{\mu\nu} {}^qR_{\mu\nu}, \quad (6.5)$$

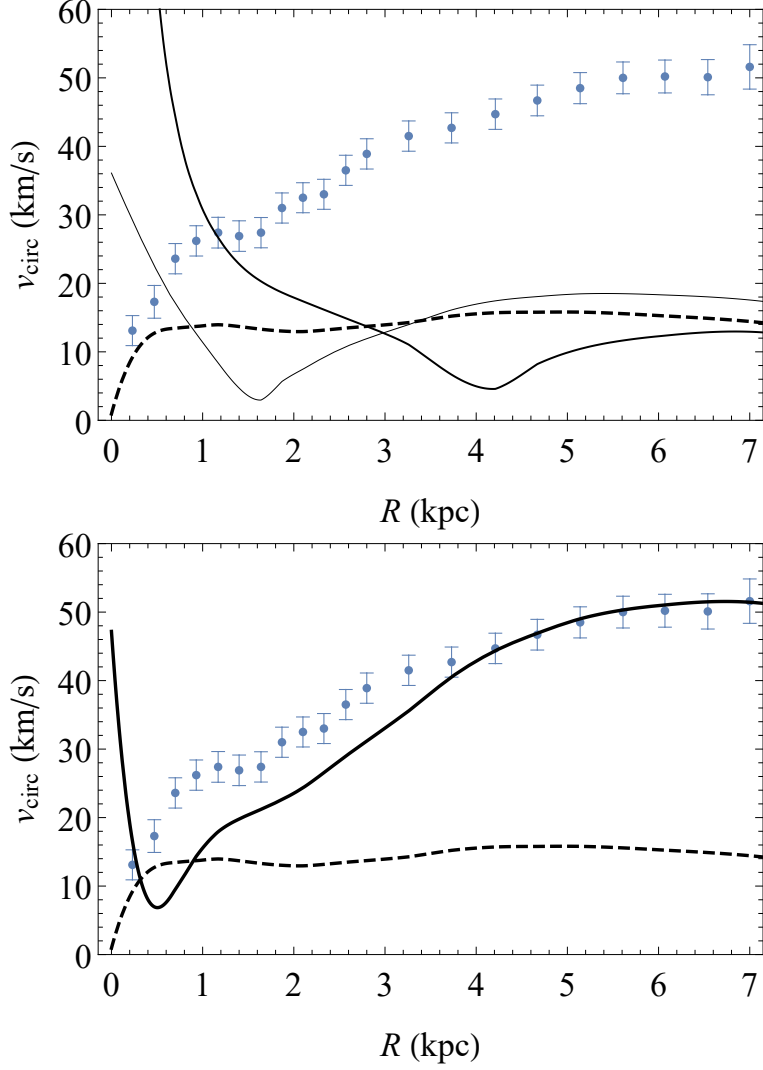


Figure 7. Comparison of the data points of NGC3741 with the $n = 3$ rotation curve of the theory T_v with weighted derivatives in the limit of weak fractional corrections with a data-based matter density profile for $\alpha = 1$ (general relativity, dashed curve), $\alpha = 1.1, 1.6$ and $R_* = 5$ kpc (top panel, increasing thickness) or $\alpha = 4/3$ and $R_* = 0.7$ kpc (bottom panel, increasing thickness).

$${}^q G_{\mu\nu} := {}^q R_{\mu\nu} - \frac{1}{2} g_{\mu\nu} {}^q R, \quad (6.6)$$

the action is

$$S = \frac{1}{2\kappa^2} \int d^D x v \sqrt{|g|} {}^q R + S_m, \quad (6.7)$$

while the modified Einstein equations are

$$\kappa^2 T_{\mu\nu} = {}^q G_{\mu\nu}, \quad T_{\mu\nu} := -\frac{2}{\sqrt{|g|}} \frac{\delta S_m}{\delta g^{\mu\nu}}. \quad (6.8)$$

Taking the trace and plugging it back,

$$\kappa^2 S_{\mu\nu} = {}^q R_{\mu\nu}, \quad S_{\mu\nu} := T_{\mu\nu} - \frac{1}{D-2} g_{\mu\nu} T. \quad (6.9)$$

6.2 T_q : Poisson equation and Newton's potential

6.2.1 T_q : Poisson equation in Cartesian coordinates

Following the standard calculation in general relativity, it is easy to see that the Poisson equation is

$$\frac{d-2}{d-1}\kappa^2\rho = {}^q\nabla^2\Phi, \quad (6.10)$$

where the Laplacian is made of q -derivatives (6.2).

6.2.2 T_q : Poisson equation in spherical coordinates

When passing from Cartesian to spherical coordinates, we have to translate the anomalous scaling of the $q_i(x^i)$ into an anomalous scaling which, again, we take only in the radial direction. To understand the form of the effective coordinate $q(r)$, consider a $d = 2$ problem with isotropic coordinates $q_i = q$:

$$q^2(x) + q^2(y) =: \mathcal{Q}^2(r). \quad (6.11)$$

Writing $q(x) = x + Ax^\alpha$, $q(y) = y + Ay^\alpha$ and $\mathcal{Q}(r) = r + Br^\beta$ for constant A and B , we have

$$q^2(x) + q^2(y) = x^2 + y^2 + A^2(x^{2\alpha} + y^{2\alpha}) + O(xy^\alpha, yx^\alpha) =: r^2 + B^2r^{2\beta} + 2Br^{\beta+1}. \quad (6.12)$$

Since, by definition of the theory, the rulers of observers in the fractional frame follow standard geometry, we equate $x^2 + y^2 \simeq r^2$ to give r the same geometric meaning as usual. Then, from

$$\begin{aligned} r^{2\beta} &= (x^2 + y^2)^\beta \\ &= x^{2\beta} + \sum_{n=1}^{+\infty} \frac{\Gamma(\beta+1)}{n!\Gamma(\beta-n+1)} x^{2(\beta-n)} y^{2n} \\ &= y^{2\beta} + \sum_{n=1}^{+\infty} \frac{\Gamma(\beta+1)}{n!\Gamma(\beta-n+1)} y^{2(\beta-n)} x^{2n} \\ &= \frac{1}{2} \left\{ x^{2\beta} + y^{2\beta} + \sum_{n=1}^{+\infty} \frac{\Gamma(\beta+1)}{n!\Gamma(\beta-n+1)} [x^{2(\beta-n)} y^{2n} + y^{2(\beta-n)} x^{2n}] \right\} \\ &= \frac{1}{2} (x^{2\beta} + y^{2\beta}) + (\text{mixed terms}), \end{aligned} \quad (6.13)$$

we can realize the correspondence (6.12) approximately provided $\alpha = \beta$ and $A^2 = B^2/2$. Generalizing to d dimensions, $B = \sqrt{d}A$, but we can always reabsorb the factor \sqrt{d} into the scale r_* , so that the averaged expression (3.5),

$$q(r) = r + \frac{r_*}{\alpha} \left| \frac{r}{r_*} \right|^\alpha, \quad (6.14)$$

approximates $\mathcal{Q}(r)$ up to mixed coordinate terms, while the radial derivative of (6.14) is a measure weight slightly different from (4.8),

$$\tilde{v}(r) = \partial_r q(r) = 1 + \left| \frac{r}{r_*} \right|^{\alpha-1}. \quad (6.15)$$

The same radial composite coordinate (6.14) can be obtained directly in the fractional frame using an exact procedure [37]. Whichever route one takes to arrive at eq. (6.14), the scaling of the radial measure is then $dq(r) q^{d-1}(r) \simeq dr \tilde{v}(r) [r\tilde{v}(r)]^{d-1} = dr r^{d-1} \tilde{v}^d(r)$, which is the same as the scaling of the radial measure $dr r^{d-1} v(r)$ defined from eq. (4.8).

Of course, one could define the theory with an exact profile $q(r)$ and trace back its anomalous scaling to Cartesian coordinates, i.e., take (6.11) as a definition of the left-hand side ($:=$) instead of the right-hand side ($=:$). However, Cartesian coordinates are usually the starting point to construct this Lorentz-breaking theory.

Therefore, we get

$$\frac{d-2}{d-1} \kappa^2 \rho = \left[\partial_{q(r)}^2 + \frac{d-1}{q(r)} \partial_{q(r)} + \frac{1}{q^2(r)} \nabla_{S^{d-1}} \right] \Phi \quad (6.16)$$

$$= \frac{1}{\tilde{v}^2} \left\{ \partial_r^2 + \left[(d-1) \frac{\tilde{v}}{q} - \frac{\partial_r \tilde{v}}{\tilde{v}} \right] \partial_r + \frac{\tilde{v}^2}{q^2} \nabla_{S^{d-1}}^2 \right\} \Phi. \quad (6.17)$$

When $\alpha < 1$ and $r \ll r_*$, or when $\alpha > 1$ and $r \gg r_*$, $q \simeq r\tilde{v}/\alpha$ and this expression is approximated to

$$\frac{d-2}{d-1} \kappa^2 \tilde{v}^2 \rho \simeq \left[\partial_r^2 + \frac{(d-2)\alpha + 1}{r} \partial_r + \frac{\alpha^2}{r^2} \nabla_{S^{d-1}}^2 \right] \Phi. \quad (6.18)$$

6.2.3 T_q : Newton's potential

The solution of the Poisson equation for a radial potential and a pointwise source of mass m is more easily found from (6.16) rather than (6.17). Treating q as a coordinate, the equation to solve is

$$\left[\partial_q^2 + \frac{d-1}{q} \partial_q \right] \Phi(\mathbf{x}, \mathbf{x}') = \frac{d-2}{d-1} \kappa^2 m \delta^d[q(\mathbf{x}) - q(\mathbf{x}')], \quad (6.19)$$

where $\delta^d[q(\mathbf{x}) - q(\mathbf{x}')] = \delta[q(x^1) - q(x'^1)] \cdots \delta[q(x^d) - q(x'^d)]$. The solution is found as in the previous section. Setting $\mathbf{x}' = 0$,

$$\Phi(r) = -\frac{4\Gamma\left(\frac{d}{2}\right)}{(d-1)\pi^{\frac{d}{2}-1}} \frac{Gm}{[Q(r)]^{d-2}} \simeq -\frac{4\Gamma\left(\frac{d}{2}\right)}{(d-1)\pi^{\frac{d}{2}-1}} \frac{Gm}{[q(r)]^{d-2}}. \quad (6.20)$$

In $D = d + 1 = 4$ dimensions (Fig. 8),

$$\Phi(r) = -\frac{Gm}{q(r)}, \quad (6.21)$$

which reduces to the standard Newtonian potential (2.25) in the general-relativity limit, while in the fractional limit we obtain

$$\Phi(r) \simeq -\alpha \frac{Gm}{r} \left(\frac{r_*}{r} \right)^{\alpha-1}. \quad (6.22)$$

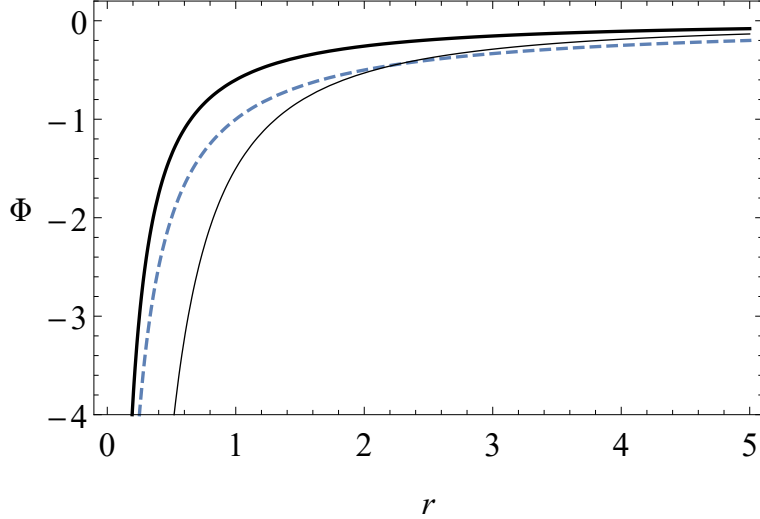


Figure 8. Gravitational potential in $d = 3$ spatial dimensions for a pointwise source in the theory with q -derivatives with $\alpha > 1$ ($\alpha = 1.5$ in this example) and $r_* = 1$, in the general-relativity limit (2.25) ($r \ll r_*$, dashed curve), in the fractional limit (6.22) ($r \gg r_*$, solid thin curve) and for the exact expression (6.21) (solid thick curve). Here $Gm = 1$.

6.3 T_q : thin-disk exponential-density rotation curve

To get an extended matter configuration, as before one can consider (6.20) for an infinitesimal mass $dm = \rho d\mathcal{V}$ and then integrate over the q -volume \mathcal{V} of the source. Restoring $\mathbf{x}' \neq 0$ and changing integration variable $q(\mathbf{x}') \rightarrow z'$,

$$\begin{aligned} \Phi^{\text{disk}}(\mathbf{x}) &= -\frac{4G\Gamma\left(\frac{d}{2}\right)}{(d-1)\pi^{\frac{d}{2}-1}} \int_{\mathcal{V}} \frac{d^d q(\mathbf{x}') \rho[q(\mathbf{x}')] }{|q(\mathbf{x}) - q(\mathbf{x}')|^{d-2}} \\ &= -\frac{4G\Gamma\left(\frac{d}{2}\right)}{(d-1)\pi^{\frac{d}{2}-1}} \int_{\mathcal{V}} \frac{d^d z' \rho(z')}{|q(\mathbf{x}) - z'|^{d-2}}. \end{aligned} \quad (6.23)$$

This is the standard expression in ordinary gravity except for the q -dependence in the denominator. In $d = 3$ dimensions,

$$\Phi^{\text{disk}}(\mathbf{x}) = -G \int_{\mathcal{V}} \frac{d^3 z' \rho(z')}{|q(\mathbf{x}) - z'|}. \quad (6.24)$$

This is the starting point to build a model of a galaxy (or its bulge) and its rotation curve. The calculation is identical to the standard one reported in section 5.3 [14], the only difference being the replacement $R \rightarrow \mathcal{Q}(R)$ in eq. (B.4),

$$\frac{1}{|q(\mathbf{x}) - z'|} = \sum_{m=-\infty}^{+\infty} \int_0^{+\infty} dy e^{im(\phi-\phi')-|z-z'|y} J_m[\mathcal{Q}(R)y] J_m(R'y), \quad (6.25)$$

and, at the last step in the derivation, the approximation $\mathcal{Q}(R) \simeq q(R)$:

$$\Phi^{\text{disk}}(R) \simeq -\frac{GM}{R_0} \frac{q(R)}{2R_0} \left\{ I_0 \left[\frac{q(R)}{2R_0} \right] K_1 \left[\frac{q(R)}{2R_0} \right] - I_1 \left[\frac{q(R)}{2R_0} \right] K_0 \left[\frac{q(R)}{2R_0} \right] \right\}. \quad (6.26)$$

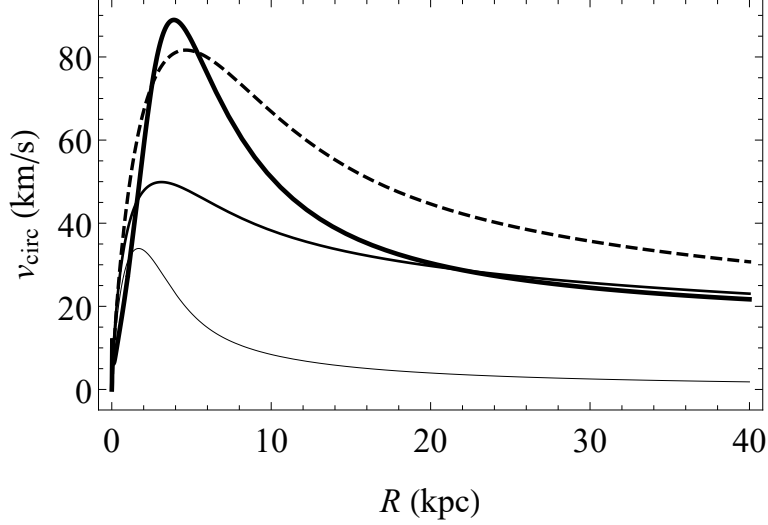


Figure 9. Rotation curve of baryonic matter in the thin-disk approximation and an exponential matter density profile (2.33) in general relativity (eq. (2.36), dashed curve) and in the multi-fractional theory T_q with q -derivatives (eq. (6.28)) for $\alpha = 1.5$ and $A = 0 = B$, $\alpha = 0.5$ and $A = 0 = B$, and $\alpha = 0.5$ and 5 harmonics all with amplitudes $A = 0.2$, $B = 0$ and parameter $N = 10^{10}$ (solid curves of increasing thickness). Here $M = 1.72 \times 10^{40}$ kg, $R_0 = 2.16$ kpc and $R_* = 40$ kpc.

The gravitational field in the $Z = 0$ plane and in the radial direction is $g(R) = -d\Phi(R)/dq(R)$. The circular velocity with respect to q -coordinates is $v_{q,\text{circ}} = \sqrt{|q(R)g(R)|}$, whose expression is (2.36) with R replaced by $q(R)$. Noting that the physical circular velocity is [11]

$$v_{\text{circ}} = v_{q,\text{circ}} \frac{dR}{dq(R)} = \frac{v_{q,\text{circ}}}{v(R)}, \quad (6.27)$$

we get

$$v_{\text{circ}} = \frac{1}{v(R)} \frac{q(R)}{2R_0} \sqrt{\frac{2GM}{R_0} \left| I_1 \left[\frac{q(R)}{2R_0} \right] K_1 \left[\frac{q(R)}{2R_0} \right] - I_0 \left[\frac{q(R)}{2R_0} \right] K_0 \left[\frac{q(R)}{2R_0} \right] \right|}. \quad (6.28)$$

It is easy to check that this function never “improves” its counterpart (2.36) from general relativity for any value and sign of the fractional exponent α , since it always decays at large R instead of reaching a plateau (Fig. 9). The reason is that, if $\alpha < 0$ or $0 < \alpha < 1$, $q(R) \rightarrow R$ at large scales and the curve deviates from general relativity only at small scales $R < R_*$, quickly converging to Newtonian gravity when $R > R_*$. When $\alpha > 1$, then the rotation curve deviates from the standard case at large scales but the effect is of a suppression of velocity rather than the desired enhancement.

Contrary to the other two multi-fractional models of galaxy disks, in the theory T_q it is easy to consider the effect of logarithmic oscillations in the spacetime measure. We checked that the inclusion of a few harmonics of log oscillations does not improve the fit because the modulation of the log oscillations never generates a plateau, even for a minimum-frequency harmonic. An example is given in Fig. 9.

6.4 T_q : data-based rotation curve

The rotation curve of this theory for the actual matter density profile is easy to write down:

$$v_{\text{circ}}(R) = \frac{v_{\text{circ},0}[q(R)]}{v(R)}, \quad (6.29)$$

where $v_{\text{circ},0}[q(R)]$ is given by eqs. (2.48), (2.49) and (2.50) with R replaced by $q(R)$ everywhere.

We checked that the model does not fit any of the three galaxies' rotation curve. In the absence of log oscillations, varying α and R_* one obtains rotation curves always below the data at their maximum and decreasing as R increases. Log oscillations modulate these patterns or, if the amplitudes are large enough, they produce a strongly oscillatory pattern not matching data. In fact, while including only one harmonic does not improve the fit because the modulation of the log oscillations never generates a plateau, even for a minimum-frequency harmonic, adding several harmonics (we checked up to 10) creates a relatively well-known pattern of destructive and constructive interference [34, 35] resulting in spikes or sharp features across the whole range of scales, incompatible with the observed rotation curve. We do not show these plots here.

7 Conclusions

In this paper, we entertained the possibility to describe the observed rotation curve of galaxies in terms of geometric effects in spacetimes with varying dimension. In particular, we considered multi-fractional theories with integer-order derivatives.

The theory T_1 with ordinary derivatives does not easily lead to an analytic expression of the Newtonian potential and we could not fully determine the normalization constants. However, an inspection of the approximated potential led to fixing the fractional exponent α to the value (4.30). It would be interesting to make a more sophisticated analysis to see if this value eventually gives a good fit of data, as suggested by the results of [24].

In contrast, the theory T_q with q -derivatives is fully solvable but, unfortunately, it is unable to fit the SPARC data for NGC7814, NGC6503 and NGC3741. We checked this both in the absence and in the presence of log oscillations in the spatial measure. Therefore, we believe this negative result to be robust and we conclude that this theory does not offer an alternative to dark matter, just like it does not provide an alternative to dark energy [35].

The theory T_v with weighted derivatives fares better than the others and it can fit the SPARC data for the three galaxies at large radius, thus explaining the anomalous velocity profile of ordinary matter as an effect of geometry, more precisely, of a varying Hausdorff dimension of space. These results are promising but provisional because they do not hold for small radii, they are not based on a full profile of the potential valid at all scales and, finally, they have not been checked on a wider sample of galaxies. Still, we do not expect substantial changes in a more complete analysis because the terms we ignored are subdominant at the scales where the rotation curve is a plateau. For the theory T_v , the spatial Hausdorff dimension of the galaxy is

$$d_{\text{H}}^{\text{galaxy}} = 3\alpha \approx 4, \quad (7.1)$$

stating that, despite the static approximation in which the galaxy is described, its dynamics still “feels” four dimensions. This result is tantalizing because it matches the independent findings for the same theory in the context of dark energy [35]. In some yet poorly understood

way, dimensional flow in symmetry-reduced systems embedded in the theory T_v tends to recover four spacetime dimensions. In the homogenous, spatial-independent cosmological setting, which is one-dimensional, the late-time universe undergoes an accelerating phase with $d_H \approx 4$. In the static, time-independent setting of spherical or axisymmetric gravitational potentials, galaxy rotation curves behave as if the galaxy matter distribution had $d_H \approx 4$ dimensions. Just like in [35], to our regret we do not have an explanation of this phenomenon. It underscores a sort of conservation law for the dimension of spacetime, which is preserved asymptotically when some symmetry reduction is performed.

An explanation of rotation curves alone is not sufficient to claim that an alternative to dark matter has been found. Any theory beyond Einstein gravity should be tested against observations of the Bullet cluster [45], galaxy clusters [46], gravitational lensing [47, 48] and the cosmic microwave background [49], among others. To date, the theory T_v has not been applied to any of these physical systems and it would be important to do so in order to accumulate evidence, as it has been done in the case of Moffat’s scalar-tensor-vector modified gravity model [40–43]. As a preliminary result, we note that the theory T_v can explain in part, but perhaps not fully, the observations of the Bullet cluster, without however bridging the gap between baryonic-matter-based and dark-matter-based physics. We use the qualitative argument of [42] (updated with the values of [50]), which is orientative but not conclusive.

According to this argument, one crudely approximates the Bullet cluster as the linear superposition of two point sources, the main cluster with dynamical mass $M_{\text{main}} = 2 \times 10^{15} M_\odot$ and the “bullet” with dynamical mass $M_{\text{bullet}} = 5 \times 10^{14} M_\odot$ [50], where both masses are found from gravitational lensing observations. These masses include both baryonic and dark matter. In standard gravity, the escape velocity of the main and bullet clusters is found by setting to zero both the total (kinetic and potential) energy of the two clusters and the total momentum [42]:

$$\begin{aligned} \frac{1}{2} (M_{\text{main}} v_{\text{main}}^2 + M_{\text{bullet}} v_{\text{bullet}}^2) - \frac{GM_{\text{main}}M_{\text{bullet}}}{r} &= 0, \\ M_{\text{main}} v_{\text{main}} + M_{\text{bullet}} v_{\text{bullet}} &= 0. \end{aligned} \quad (7.2)$$

At a separation of $r = 2.5 \text{ Mpc}$ [50], one gets an infall velocity of $|v_{\text{main}} - v_{\text{bullet}}| \approx 2933 \text{ km s}^{-1}$. In contrast, baryonic matter amounts to about $M_{\text{baryon}}/M_{\text{tot}} = 0.14$ of the total, which would give an infall velocity three times smaller than (37% of) the observed one, $|v_{\text{main}} - v_{\text{bullet}}| \approx 1097 \text{ km s}^{-1}$. Repeating the estimate for the only multifractional theory that could partly explain the galaxy rotation curves, the theory T_v with potential (5.41), we have a system given by eq. (7.3) and

$$\frac{1}{2} (M_{\text{main}} v_{\text{main}}^2 + M_{\text{bullet}} v_{\text{bullet}}^2) - \frac{GM_{\text{main}}M_{\text{bullet}}}{r} + \frac{GM_{\text{main}}M_{\text{bullet}}}{r_*} \ln \frac{r}{r_*} = 0. \quad (7.4)$$

Taking the baryonic masses not including dark matter, the maximum of the infall velocity is obtained at $r_* = 6.8 \text{ Mpc}$ and is $|v_{\text{main}} - v_{\text{bullet}}| = 1283 \text{ km s}^{-1}$, slightly higher than the standard Newtonian value but, still, only 47% of the actual value. This mildly encouraging estimate should be refined by a much more rigorous calculation.

Other avenues to explore in the future may come across other multi-fractional theories, those with fractional operators [13, 44]. A phenomenological Newtonian model with fractional Laplacian seems able to fit galaxy rotation curves [19, 20] but it has not been embedded in a covariant theory. The multi-fractional theories T_γ offer an opportunity both to embed the model of [19, 20] and to further test the idea that a dynamics with fractional operators is a viable alternative to dark matter.

Acknowledgments

G.C. is supported by the I+D grant PID2020-118159GB-C41 of the Spanish Ministry of Science and Innovation. G.V. is supported by the Frank R. Seaver College of Science and Engineering, Loyola Marymount University.

A Circular velocity in the theory T_v

Recall that velocities in the theory T_v are defined through the weighted derivative $\mathcal{D}_t = v_0^{-1/2}(t) \partial_t [v_0^{1/2}(t) \cdot]$, where $v_0(t)$ is the time-dependent part of the factorizable measure. In particular, the angular velocity is $v_\omega := \mathcal{D}_t \theta$, where θ is an angle. In this theory, we can always transform to an “integer frame” where classical mechanics or field theory formally reduce to the standard ones with ordinary derivatives. Physical observables are calculated in the original frame with \mathcal{D} derivatives.

Therefore, we can define an (unphysical) angular velocity in the integer frame

$$\tilde{v}_\omega = \sqrt{v(t)} v_\omega = \frac{d\tilde{\theta}}{dt}, \quad (\text{A.1})$$

where $\tilde{\theta} = \sqrt{v_0(t)} \theta$. The circular velocity associated to a distance $r d\tilde{\theta}$ is

$$\tilde{v}_{\text{circ}} = r \frac{d\tilde{\theta}}{dt} = r \tilde{v}_\omega. \quad (\text{A.2})$$

In turn, the change in the circular velocity while changing the angle infinitesimally is equal to $\tilde{v}_{\text{circ}} d\tilde{\theta}$, so that the corresponding acceleration is

$$\tilde{g} = \tilde{v}_{\text{circ}} \frac{d\tilde{\theta}}{dt} = \tilde{v}_{\text{circ}} \tilde{v}_\omega = \frac{\tilde{v}_{\text{circ}}^2}{r}. \quad (\text{A.3})$$

At this point, we must convert velocities and accelerations in the integer frame to physical velocities and accelerations in the fractional frame. Regarding velocity, similarly to the expression linking v_ω and \tilde{v}_ω one has

$$\tilde{v}_{\text{circ}} = \sqrt{v_0(t)} v_{\text{circ}}, \quad (\text{A.4})$$

while

$$\tilde{g} = \tilde{v}_{\text{circ}} \tilde{v}_\omega = [\sqrt{v_0(t)} v_{\text{circ}}] [\sqrt{v_0(t)} v_\omega] = v_0(t) v_{\text{circ}} v_\omega = v_0(t) g, \quad (\text{A.5})$$

where we used $g = v_{\text{circ}} v_\omega = v_{\text{circ}} \mathcal{D}_t \theta$. However, we also have $\tilde{g} = v_0(t) v_{\text{circ}}^2 / r$, hence $g = v_{\text{circ}}^2 / r$ and eq. (5.45).

B Multipole expansion of inverse-power potentials

In this appendix, we recall some useful formulæ for the multipole expansion of inverse-power potentials

$$\frac{1}{|\mathbf{x} - \mathbf{x}'|^\lambda}, \quad \lambda \in \mathbb{R}, \quad (\text{B.1})$$

in terms of cylindrical coordinates in d spatial dimensions. Cylindrical coordinates are the axial radial distance $R = x_1^2 + x_2^2$, the elevation $Z_i = x_i$ with $i = 3, \dots, d$ and the azimuth ϕ , such that $x_1 = R \cos \phi$ and $x_2 = R \sin \phi$.

For $\lambda = 1$, one has [51–53]

$$\frac{1}{|\mathbf{x} - \mathbf{x}'|} = \frac{1}{\pi\sqrt{RR'}} \sum_{m=-\infty}^{+\infty} e^{im(\phi-\phi')} Q_{m-\frac{1}{2}} \left[\frac{R^2 + R'^2 + \sum_i (Z_i - Z'_i)^2}{2RR'} \right], \quad (\text{B.2})$$

where Q_s is the Legendre function of the second kind of order s . In terms of the hypergeometric functions [54, formula 8.820.2],

$$Q_s(z) = \frac{\sqrt{\pi}\Gamma(s+1)}{2^{s+1}\Gamma(s+\frac{3}{2})} \frac{1}{z^{s+1}} {}_2F_1 \left(\frac{s+2}{2}, \frac{s+1}{2}; \frac{2s+3}{2}; \frac{1}{z^2} \right). \quad (\text{B.3})$$

Formula (B.2) is equivalent to another one, popular from an exercise of Jackson's textbook on electrodynamics [55, exercise 3.16]:

$$\frac{1}{|\mathbf{x} - \mathbf{x}'|} = \sum_{m=-\infty}^{+\infty} \int_0^{+\infty} dy e^{im(\phi-\phi') - |Z-Z'|y} J_m(Ry) J_m(R'y), \quad (\text{B.4})$$

where $|Z - Z'| = \sqrt{\sum_i (Z_i - Z'_i)^2}$. In fact, eqs. (B.2) and (B.4) can be related to each other via the identity [54, formula 6.612.3]

$$\frac{1}{\pi\sqrt{RR'}} Q_{m-\frac{1}{2}} \left[\frac{R^2 + R'^2 + |Z - Z'|^2}{2RR'} \right] = \int_0^{+\infty} dy e^{-|Z-Z'|y} J_m(Ry) J_m(R'y), \quad (\text{B.5})$$

after continuing it analytically beyond its validity range $m > -1/2$.

When λ is real, one can make use of an expansion (which we derive below) in terms of Gegenbauer polynomials, valid for $\lambda > -1/2$ and $\lambda \neq 0$. Gegenbauer polynomials are the generating functionals of the expression [54, 56]

$$\frac{1}{(1 - 2za + a^2)^\lambda} = \sum_{n=0}^{+\infty} C_n^\lambda(z) a^n, \quad |a| < 1, \quad 0 \neq \lambda > -\frac{1}{2}. \quad (\text{B.6})$$

In terms of the hypergeometric functions [54, formula 8.932.1],

$$C_n^\lambda(z) = \frac{2^n \Gamma(\lambda + n)}{n! \Gamma(\lambda)} z^n {}_2F_1 \left(-\frac{n}{2}, -\frac{n-1}{2}; 1 - n - \lambda; \frac{1}{z^2} \right). \quad (\text{B.7})$$

Consider the distance in spherical coordinates

$$|\mathbf{x} - \mathbf{x}'| = \sqrt{r^2 + r'^2 - 2rr' \cos \gamma} = r_{>} \sqrt{1 + \left(\frac{r_{<}}{r_{>}} \right)^2 - 2 \frac{r_{<}}{r_{>}} \cos \gamma}, \quad (\text{B.8})$$

where $r = |\mathbf{x}|$, $r' = |\mathbf{x}'|$, γ is the angle between the vectors \mathbf{x} and \mathbf{x}' , $\cos \gamma = \mathbf{x} \cdot \mathbf{x}' / rr'$, and $r_{>}$ (respectively, $r_{<}$) is the largest (smallest) between r and r' . In $d = 3$ dimensions, $\cos \gamma = \cos \theta \cos \theta' + \sin \theta \sin \theta' \cos(\varphi - \varphi')$. Taking an arbitrary inverse power of (B.8) and identifying $a = r_{<}/r_{>}$ and $z = \cos \gamma$, one gets [56]

$$\frac{1}{|\mathbf{x} - \mathbf{x}'|^\lambda} = \sum_{n=0}^{+\infty} C_n^{\frac{\lambda}{2}}(\cos \gamma) \frac{r_{<}^n}{r_{>}^{n+\lambda}}, \quad 0 \neq \lambda > -\frac{1}{2}. \quad (\text{B.9})$$

When $\lambda = 1$, $C_n^{1/2} = P_n$ are the Legendre polynomials of the first kind and one recovers yet another formula for the inverse-power-law potential [52]:

$$\frac{1}{|\mathbf{x} - \mathbf{x}'|} = \sum_{n=0}^{+\infty} P_n(\cos \gamma) \frac{r_{<}^n}{r_{>}^{n+1}}. \quad (\text{B.10})$$

Finally, eq. (B.9) is transformed to a cylindrical coordinate system. In galaxy models in $d = 3$ dimensions, the discussion is limited to the $Z = 0$ plane and the $\theta = 0$ direction (so that $\cos \gamma = \cos \theta'$ in polar coordinates), in which case

$$r = R, \quad r' = \sqrt{R'^2 + Z'^2}, \quad \cos \gamma = \frac{R' \cos \phi'}{\sqrt{R'^2 + Z'^2}}. \quad (\text{B.11})$$

The thick-disk expression in cylindrical coordinates of (B.9) is obtained by replacing (B.11) therein:

$$\frac{1}{|\mathbf{x} - \mathbf{x}'|^\lambda} = \sum_{n=0}^{+\infty} C_n^{\frac{\lambda}{2}} \left(\frac{R'}{\sqrt{R'^2 + Z'^2}} \cos \phi' \right) \frac{R_{<}^n}{R_{>}^{n+\lambda}}, \quad 0 \neq \lambda > -\frac{1}{2}. \quad (\text{B.12})$$

In thin-disk models, the further constraint $Z' = 0$ is imposed, so that [22]

$$\frac{1}{|\mathbf{x} - \mathbf{x}'|^\lambda} = \sum_{n=0}^{+\infty} C_n^{\frac{\lambda}{2}}(\cos \phi') \frac{R_{<}^n}{R_{>}^{n+\lambda}}, \quad 0 \neq \lambda > -\frac{1}{2}, \quad (\text{B.13})$$

where $R_{>} = \max(R, \sqrt{R'^2 + Z'^2})$ and $R_{<} = \min(R, \sqrt{R'^2 + Z'^2})$.

When λ is complex-valued, other expansions exist [53, 57]. We do not show them here because eq. (B.13) already covers all the values of λ appearing in multi-fractional theories, except $\lambda = 0$. In this case, one can use the expansion in polar coordinates [56]

$$\ln |\mathbf{x} - \mathbf{x}'| = \ln r_{>} - \sum_{n=1}^{+\infty} \frac{\cos(n\gamma)}{n} \left(\frac{r_{<}}{r_{>}} \right)^n, \quad (\text{B.14})$$

or, as it is easy to convince oneself looking at eq. (B.8) in cylindrical coordinates and in the $Z = 0$ plane, the equivalent expression in cylindrical coordinates

$$\ln |\mathbf{x} - \mathbf{x}'| = \ln R_{>} - \sum_{n=1}^{+\infty} \frac{\cos(n\phi')}{n} \left(\frac{R_{<}}{R_{>}} \right)^n. \quad (\text{B.15})$$

C Useful formulæ

C.1 Angular integrals of Gegenbauer polynomials

Consider the integral

$$\mathcal{B}_{\frac{n}{2}}^\lambda(b) := \int_0^{2\pi} \frac{d\phi'}{2\pi} C_n^{\frac{\lambda}{2}}(b \cos \phi'), \quad (\text{C.1})$$

where $C_n^{\lambda/2}$ are Gegenbauer polynomials given by eq. (B.7) and $0 < b \leq 1$ is independent of ϕ' . With the change of variables $z = b \cos \phi'$, the integral is recast as

$$\mathcal{B}_{\frac{n}{2}}^\lambda(b) = \frac{1}{\pi} \int_{-b}^b dz \frac{C_n^{\frac{\lambda}{2}}(z)}{\sqrt{b^2 - z^2}}$$

$$= \frac{2^n \Gamma\left(\frac{\lambda}{2} + n\right)}{\pi n! \Gamma\left(\frac{\lambda}{2}\right)} \int_{-b}^b dz \frac{z^n}{\sqrt{b^2 - z^2}} {}_2F_1\left(-\frac{n}{2}, -\frac{n-1}{2}; 1 - n - \lambda; \frac{1}{z^2}\right). \quad (\text{C.2})$$

One can check that this integral is identically zero for odd n :

$$\mathcal{B}_{\frac{n}{2}}^\lambda(b) = 0, \quad n \text{ odd}, \quad (\text{C.3})$$

while for even $n \rightarrow 2n$ we find

$$\mathcal{B}_n^\lambda(b) = \frac{1}{n!} \frac{\Gamma\left(1 - \frac{\lambda}{2}\right)}{\Gamma\left(1 - \frac{\lambda}{2} - n\right)} {}_2F_1\left(-n, \frac{\lambda}{2} + n; 1; b^2\right), \quad \mathcal{B}_0^\lambda(b) = 1. \quad (\text{C.4})$$

In particular, for $b = 1$

$$\mathcal{B}_n^\lambda := \mathcal{B}_n^\lambda(1) = \left[\frac{\Gamma\left(1 - \frac{\lambda}{2}\right)}{n! \Gamma\left(1 - \frac{\lambda}{2} - n\right)} \right]^2 = \frac{1}{2^{2n} (n!)^2} \prod_{p=0}^{n-1} (\lambda + 2p)^2, \quad \mathcal{B}_0^\lambda = 1. \quad (\text{C.5})$$

Another integral of interest is

$$\mathcal{E}_{\frac{n}{2}}^\lambda := \int_0^\pi d\theta' \sin \theta' C_n^{\frac{\lambda}{2}}(\cos \theta'). \quad (\text{C.6})$$

Calling $z = \cos \theta'$,

$$\mathcal{E}_{\frac{n}{2}}^\lambda = \int_{-1}^1 dz C_n^{\frac{\lambda}{2}}(z) = \frac{1 + (-1)^n \Gamma(\lambda - 1 + n)}{\Gamma(2 + n) \Gamma(\lambda - 1)},$$

which vanishes for odd n . Therefore,

$$\mathcal{E}_n^\lambda = \frac{2}{(2n + 1)!} \frac{\Gamma(\lambda - 1 + 2n)}{\Gamma(\lambda - 1)}. \quad (\text{C.7})$$

C.2 Radial integrals

Consider the integral

$$\begin{aligned} \mathcal{C}_n^{\beta, \lambda}(R) &:= \frac{1}{R_0} \int_0^{+\infty} dR' e^{-\frac{R'}{R_0}} R'^\beta \frac{R_{>}^{2n}}{R_{>}^{\lambda+2n}} \\ &= \frac{1}{R_0} \frac{1}{R^{\lambda+2n}} \int_0^R dR' e^{-\frac{R'}{R_0}} R'^{\beta+2n} + R^{2n} \int_R^{+\infty} dR' e^{-\frac{R'}{R_0}} R'^{\beta-\lambda-2n} \\ &= R_0^{\beta-\lambda} \left\{ \left(\frac{R_0}{R} \right)^{\lambda+2n} \left[\Gamma(\beta + 1 + 2n) - \Gamma\left(\beta + 1 + 2n, \frac{R}{R_0}\right) \right] \right. \\ &\quad \left. + \left(\frac{R}{R_0} \right)^{2n} \Gamma\left(\beta - \lambda + 1 - 2n, \frac{R}{R_0}\right) \right\}. \end{aligned} \quad (\text{C.8})$$

Another integral of interest features a logarithm:

$$\begin{aligned} \mathcal{C}_{\log}^\beta(R) &:= \frac{1}{R_0} \int_0^{+\infty} dR' e^{-\frac{R'}{R_0}} R'^\beta \ln \frac{R_{>}}{R_*} \\ &= \frac{1}{R_0} \left(\ln \frac{R}{R_*} \int_0^R dR' e^{-\frac{R'}{R_0}} R'^\beta + \int_R^{+\infty} dR' e^{-\frac{R'}{R_0}} R'^\beta \ln \frac{R'}{R_*} \right) \\ &= R_0^\beta \left[\Gamma(1 + \beta) \ln \frac{R}{R_*} + G_{20}^{30} \left(\frac{R}{R_0} \middle| \begin{matrix} 1 & 1 \\ 0 & 0 & 1 + \beta \end{matrix} \right) \right], \end{aligned} \quad (\text{C.9})$$

where G is the Meijer function.

D Galaxy potential in the theory T_v with exponential matter density

D.1 Calculation of eqs. (5.46) and (5.47)

$$\begin{aligned}
\Phi^{\text{disk}}(R) &\stackrel{\text{(B.13)}}{=} -\frac{1}{3\alpha-2} \frac{MG}{R_0^2} \int_0^{+\infty} dR' R'^{3\alpha-2} \int_0^{2\pi} \frac{d\phi'}{2\pi} \int_{-\infty}^{+\infty} dZ' e^{-\frac{R'}{R_0}} \delta(Z') \\
&\quad \times \sum_{n=0}^{+\infty} C_n^{\frac{3\alpha-2}{2}}(\cos\phi') \frac{R_{<}^n}{R_{>}^{n+3\alpha-2}} \\
&= -\frac{1}{3\alpha-2} \frac{MG}{R_0^2} \sum_{n=0}^{+\infty} \int_0^{2\pi} \frac{d\phi'}{2\pi} C_n^{\frac{3\alpha-2}{2}}(\cos\phi') \int_0^{+\infty} dR' R'^{3\alpha-2} e^{-\frac{R'}{R_0}} \frac{R_{<}^n}{R_{>}^{n+3\alpha-2}} \\
&\stackrel{\text{(C.5)}}{\stackrel{\text{(C.8)}}{=}} -\frac{1}{3\alpha-2} \frac{MG}{R_0} \sum_{n=0}^{+\infty} \mathcal{B}_n^{3\alpha-2} \mathcal{C}_n^{3\alpha-2, 3\alpha-2}(R) \\
&= -\frac{1}{3\alpha-2} \frac{MG}{R_0} \sum_{n=0}^{+\infty} \mathcal{B}_n^{3\alpha-2} \left\{ \left(\frac{R}{R_0} \right)^{2n} \Gamma\left(1-2n, \frac{R}{R_0}\right) \right. \\
&\quad \left. + \left(\frac{R_0}{R} \right)^{2n+3\alpha-2} \left[\Gamma(2n+3\alpha-1) - \Gamma\left(2n+3\alpha-1, \frac{R}{R_0}\right) \right] \right\}. \tag{D.1}
\end{aligned}$$

For $\alpha > 0$, the series converges at all scales and, in particular, it converges to the $n = 0$ mode at large scales (modes with $n > 8 - 10$ do not contribute appreciably). Since our main interest is at large scales where general relativity deviates from observations, we take the zero mode as an approximation:

$$\Phi^{\text{disk}}(R) \simeq -\frac{1}{3\alpha-2} \frac{MG}{R_0} \left\{ \Gamma\left(1, \frac{R}{R_0}\right) + \left(\frac{R_0}{R} \right)^{3\alpha-2} \left[\Gamma(3\alpha-1) - \Gamma\left(3\alpha-1, \frac{R}{R_0}\right) \right] \right\}. \tag{D.2}$$

When $\alpha = 2/3$, the potential is eq. (5.47):

$$\begin{aligned}
\Phi^{\text{disk}}(R) &\stackrel{\text{(B.15)}}{=} \frac{G}{R_*} \int_{\mathcal{V}} d^3\mathbf{x}' \left| \frac{R'}{R_*} \right|^{-1} \rho(\mathbf{x}') \left[\ln \frac{R_{>}}{R_*} - \sum_{n=1}^{+\infty} \frac{\cos(n\phi')}{n} \left(\frac{R_{<}}{R_{>}} \right)^n \right] \\
&= \frac{MG}{R_0^2} \int_0^{+\infty} dR' e^{-\frac{R'}{R_0}} \int_0^{2\pi} \frac{d\phi'}{2\pi} \int_{-\infty}^{+\infty} dZ' \delta(Z') \\
&\quad \times \left[\ln \frac{R_{>}}{R_*} - \sum_{n=1}^{+\infty} \frac{\cos(n\phi')}{n} \left(\frac{R_{<}}{R_{>}} \right)^n \right] \\
&= \frac{MG}{R_0^2} \int_0^{+\infty} dR' e^{-\frac{R'}{R_0}} \left[\ln \frac{R_{>}}{R_*} - \sum_{n=1}^{+\infty} \left(\frac{R_{<}}{R_{>}} \right)^n \int_0^{2\pi} \frac{d\phi'}{2\pi} \frac{\cos(n\phi')}{n} \right] \\
&\stackrel{\text{(C.9)}}{=} \frac{MG}{R_0} \mathcal{C}_{\log}^0(R) \\
&= -\frac{MG}{R_0} \left[\ln \frac{R}{R_*} + \Gamma\left(0, \frac{R}{R_0}\right) \right], \tag{D.3}
\end{aligned}$$

where the angular integral is zero for all n .

D.2 Calculation of eqs. (5.49c) and (5.49d)

The term (5.49c) has a purely fractional measure and the ordinary Green's function (2.25). Using (2.29),

$$\begin{aligned}
\delta\Phi_1^{\text{disk}}(R) &= -\frac{MG}{R_0^2} \int_0^{+\infty} dR' R' \left| \frac{R'}{R_*} \right|^{3(\alpha-1)} \int_0^{2\pi} \frac{d\phi'}{2\pi} \int_{-\infty}^{+\infty} dZ' e^{-\frac{R'}{R_0}} \delta(Z') \\
&\quad \times \sum_{m=-\infty}^{+\infty} \int_0^{+\infty} dy e^{im(\phi-\phi')-|Z-Z'|y} J_m(Ry) J_m(R'y) \\
&= -\frac{MG}{R_0^2} \int_0^{+\infty} dy J_0(Ry) \int_0^{+\infty} dR' R' \left| \frac{R'}{R_*} \right|^{3(\alpha-1)} e^{-\frac{R'}{R_0}} J_0(R'y) \\
&= -MG \left| \frac{R_0}{R_*} \right|^{3(\alpha-1)} \Gamma(3\alpha-1) \int_0^{+\infty} dy J_0(Ry) {}_2F_1 \left(\frac{3\alpha}{2}, \frac{3\alpha-1}{2}; 1; -R_0^2 y^2 \right) \\
&= -\frac{MG}{R_0} \left| \frac{R}{R_*} \right|^{3(\alpha-1)} \Gamma(3\alpha-1) \\
&\quad \times \left[\frac{1}{3\alpha-2} \left| \frac{R}{R_0} \right|^{3(1-\alpha)} {}_2F_3 \left(\frac{1}{2}, \frac{1}{2}; 1, \frac{3-3\alpha}{2}, \frac{4-3\alpha}{2}; \frac{R^2}{4R_0^2} \right) \right. \\
&\quad - \frac{\sqrt{\pi}}{2^{3\alpha-1}} \frac{\Gamma\left(\frac{1-3\alpha}{2}\right)}{\Gamma\left(\frac{2-3\alpha}{2}\right) \Gamma\left(\frac{3\alpha-1}{2}\right) \Gamma\left(\frac{3\alpha+1}{2}\right)} \left(\frac{R}{R_0} \right)^2 \\
&\quad \times {}_2F_3 \left(\frac{3\alpha}{2}, \frac{3\alpha}{2}; \frac{3}{2}, \frac{3\alpha+1}{2}, \frac{3\alpha+1}{2}; \frac{R^2}{4R_0^2} \right) \\
&\quad \left. - \frac{3\alpha\sqrt{\pi}}{2^{3\alpha}} \frac{\Gamma\left(-\frac{3\alpha}{2}\right)}{\Gamma\left(\frac{3-3\alpha}{2}\right) \Gamma^2\left(\frac{3\alpha}{2}\right)} \frac{R}{R_0} {}_2F_3 \left(\frac{3\alpha-1}{2}, \frac{3\alpha-1}{2}; \frac{1}{2}, \frac{3\alpha}{2}, \frac{3\alpha}{2}; \frac{R^2}{4R_0^2} \right) \right], \quad (\text{D.4})
\end{aligned}$$

where ${}_2F_3$ is the generalized hypergeometric function. This expression is singular for $\alpha = 4/3$, in which case one has

$$\begin{aligned}
\delta\Phi_1^{\text{disk}}(R) &= -\frac{MG}{R_0^2 R_*} \int_0^{+\infty} dy J_0(Ry) \int_0^{+\infty} dR' R'^2 e^{-\frac{R'}{R_0}} J_0(R'y) \\
&= MG \frac{R_0}{R_*} \int_0^{+\infty} dy J_0(Ry) \frac{R_0^2 y^2 - 2}{(R_0^2 y^2 + 1)^{5/2}} \\
&= \frac{2}{3\sqrt{\pi}} \frac{MG}{R_*} \left[G_{13}^{21} \left(\frac{R^2}{4R_0^2} \middle| \begin{matrix} -\frac{1}{2} \\ 0 & 1 & 0 \end{matrix} \right) - 2G_{13}^{21} \left(\frac{R^2}{4R_0^2} \middle| \begin{matrix} \frac{1}{2} \\ 0 & 2 & 0 \end{matrix} \right) \right]. \quad (\text{D.5})
\end{aligned}$$

The term (5.49d) has an ordinary integration measure and a fractional Green's function. We can use the results reported in Appendix B about the expression of inverse powers in terms of Gegenbauer polynomials C_n^β . Plugging (2.33) and (B.13) into (5.49d), we obtain

$$\begin{aligned}
\delta\Phi_2^{\text{disk}}(R) &= \frac{MG}{R_0^2} \frac{7-6\alpha}{(4-3\alpha)R_*^{3(\alpha-1)}} \int_0^{+\infty} dR' R' \int_0^{2\pi} \frac{d\phi'}{2\pi} \int_{-\infty}^{+\infty} dZ' e^{-\frac{R'}{R_0}} \delta(Z') \\
&\quad \times \sum_{n=0}^{+\infty} C_n^{\frac{4-3\alpha}{2}}(\cos\phi') \frac{R_{<}^n}{R_{>}^{n+4-3\alpha}} \\
&= \frac{MG}{R_0^2} \frac{7-6\alpha}{(4-3\alpha)R_*^{3(\alpha-1)}} \sum_{n=0}^{+\infty} \int_0^{2\pi} \frac{d\phi'}{2\pi} C_n^{\frac{4-3\alpha}{2}}(\cos\phi') \int_0^{+\infty} dR' R' e^{-\frac{R'}{R_0}} \frac{R_{<}^n}{R_{>}^{n+4-3\alpha}}
\end{aligned}$$

$$\begin{aligned}
& \stackrel{\text{(C.5)}}{=} \frac{MG}{R_0} \frac{7-6\alpha}{(4-3\alpha)R_*^{3(\alpha-1)}} \sum_{n=0}^{+\infty} \mathcal{B}_n^{4-3\alpha} \mathcal{C}_n^{1,4-3\alpha}(R) \\
& \stackrel{\text{(C.8)}}{=} \frac{MG}{R_0} \frac{7-6\alpha}{4-3\alpha} \sum_{n=0}^{+\infty} \mathcal{B}_n^{4-3\alpha} \left\{ \left| \frac{R}{R_*} \right|^{3(\alpha-1)} \left(\frac{R_0}{R} \right)^{2n+1} \left[\Gamma(2+2n) - \Gamma\left(2+2n, \frac{R}{R_0}\right) \right] \right. \\
& \quad \left. + \left| \frac{R_0}{R_*} \right|^{3(\alpha-1)} \left(\frac{R}{R_0} \right)^{2n} \Gamma\left(3\alpha-2-2n, \frac{R}{R_0}\right) \right\}, \quad (\text{D.6})
\end{aligned}$$

where $\alpha \neq 4/3$, $r_* = R_*$ in the first line and $R_>$ and $R_<$ are, respectively, the largest and the smallest between R and R' . Although we were unable to resum the series (D.6), we checked that higher-order terms with $n \neq 1$ are subdominant at large scales for all $\alpha > 0$ with respect to the zero mode $n = 0$,

$$\delta\Phi_2^{\text{disk}}(R) \simeq \frac{MG}{R_0} \frac{7-6\alpha}{4-3\alpha} \left\{ \left| \frac{R}{R_*} \right|^{3(\alpha-1)} \frac{R_0}{R} \left[1 - \Gamma\left(2, \frac{R}{R_0}\right) \right] + \left| \frac{R_0}{R_*} \right|^{3(\alpha-1)} \Gamma\left(3\alpha-2, \frac{R}{R_0}\right) \right\}. \quad (\text{D.7})$$

At small scales the series does not converge but, as explained above in the case of the extreme fractional limit, we are mainly focus on the large-scale behaviour.

When $\alpha = 4/3$, we have to repeat the calculation of $\delta\Phi_2^{\text{disk}}$ with the logarithmic potential (5.41) with $r_* = R_*$. On the $Z = 0$ plane, using eq. (B.15) we get

$$\begin{aligned}
\delta\Phi_2^{\text{disk}}(R) &= \frac{G}{R_*} \int_{\mathcal{V}} d^3\mathbf{x}' \rho(\mathbf{x}') \ln \frac{|\mathbf{x} - \mathbf{x}'|}{R_*} \quad (\text{D.8}) \\
&= \frac{MG}{R_* R_0^2} \int_0^{+\infty} dR' R' \int_0^{2\pi} \frac{d\phi'}{2\pi} \int_{-\infty}^{+\infty} dZ' e^{-\frac{R'}{R_0}} \delta(Z') \\
&\quad \times \left[\ln \frac{R_>}{R_*} - \sum_{n=1}^{+\infty} \frac{\cos(n\phi')}{n} \left(\frac{R_<}{R_>} \right)^n \right] \\
&\stackrel{\text{(C.9)}}{=} \frac{MG}{R_* R_0} \mathcal{C}_{\log}^1(R) \\
&= \frac{MG}{R_*} \left[e^{-\frac{R}{R_0}} + \ln \frac{R}{R_*} - \text{Ei}\left(-\frac{R}{R_0}\right) \right], \quad (\text{D.9})
\end{aligned}$$

where Ei is the exponential integral function.

E Thick-disk data-based galaxy potential and gravitational field in T_v

E.1 Extreme fractional limit

E.1.1 $\alpha \neq 2/3$

Plugging the thick-disk profile (2.37) into eq. (5.43), for $\alpha \neq 2/3$ we get

$$\begin{aligned}
\Phi^{\text{disk+gas}}(R) &\stackrel{\text{(5.34)}}{=} -\frac{G}{(3\alpha-2)R_*} \int_{\mathcal{V}} d^3\mathbf{x}' \left| \frac{R'}{R_*} \right|^{3(\alpha-1)} \rho^{\text{disk+gas}}(\mathbf{x}') \left| \frac{R_*}{\mathbf{x} - \mathbf{x}'} \right|^{3\alpha-2} \\
&\stackrel{\text{(B.11)}}{=} -\frac{2G}{3\alpha-2} \sum_{n=0}^{+\infty} \int_0^{+\infty} dZ' \frac{e^{-\frac{Z'}{h_Z}}}{2h_Z} \int_0^{+\infty} dR' \Sigma(R') R'^{3\alpha-2} \\
&\stackrel{\text{(B.12)}}{=}
\end{aligned}$$

$$\begin{aligned}
& \times \frac{R_{<}^n}{R_{>}^{3\alpha-2+n}} \int_0^{2\pi} d\phi' C_n^{\frac{3\alpha-2}{2}} \left(\sqrt{\frac{R'^2}{R'^2 + Z'^2}} \cos \phi' \right) \\
\stackrel{(C.4)}{=} & -\frac{2\pi G}{3\alpha-2} \sum_{n=0}^{+\infty} \int_0^{+\infty} dZ' \frac{e^{-\frac{Z'}{h_Z}}}{h_Z} \int_0^{+\infty} dR' \Sigma(R') R'^{3\alpha-2} \\
& \times \frac{R_{<}^{2n}}{R_{>}^{3\alpha-2+2n}} \mathcal{B}_n^{3\alpha-2} \left(\sqrt{\frac{R'^2}{R'^2 + Z'^2}} \right) \\
= & -\frac{2\pi G}{3\alpha-2} \sum_{n=0}^{+\infty} \frac{1}{n!} \frac{\Gamma(2 - \frac{3\alpha}{2})}{\Gamma(2 - \frac{3\alpha}{2} - n)} \\
& \times \int_0^{+\infty} dZ' \frac{e^{-\frac{Z'}{h_Z}}}{h_Z} \int_0^{+\infty} dR' \Sigma(R') R'^{3\alpha-2} \frac{R_{<}^{2n}}{R_{>}^{3\alpha-2+2n}} \\
& \times {}_2F_1 \left(-n, \frac{3\alpha}{2} - 1 + n; 1; \frac{R'^2}{R'^2 + Z'^2} \right),
\end{aligned}$$

where $R_{<}$ ($R_{>}$) is the minimum (respectively, maximum) between R and $\sqrt{R'^2 + Z'^2}$. At this point, we split the integral in Z' on the two intervals $[0, R]$ and $[R, +\infty)$. Consider first $Z' \in [0, R]$. If $R_{>} = R$ and $R_{<} = \sqrt{R'^2 + Z'^2}$, then $R' \in [0, \sqrt{R^2 - Z'^2}]$, while if $R_{>} = \sqrt{R'^2 + Z'^2}$ and $R_{<} = R$, then $R' \in [\sqrt{R^2 - Z'^2}, +\infty)$. On the hand, when $Z' \in [R, +\infty)$, it is always true that $R < \sqrt{R'^2 + Z'^2}$, for any real value of R' . Therefore,

$$\begin{aligned}
\Phi^{\text{disk+gas}}(R) = & -\frac{2\pi G}{3\alpha-2} \sum_{n=0}^{+\infty} \frac{1}{n!} \frac{\Gamma(2 - \frac{3\alpha}{2})}{\Gamma(2 - \frac{3\alpha}{2} - n)} \left\{ \int_0^R dZ' \frac{e^{-\frac{Z'}{h_Z}}}{h_Z} \right. \\
& \times \left[\frac{1}{R^{3\alpha-2+2n}} \int_0^{\sqrt{R^2 - Z'^2}} dR' R'^{3\alpha-2} (R'^2 + Z'^2)^n \right. \\
& \quad \left. \left. + R^{2n} \int_{\sqrt{R^2 - Z'^2}}^{+\infty} dR' \frac{R'^{3\alpha-2}}{(R'^2 + Z'^2)^{\frac{3\alpha-2+2n}{2}}} \right] \right. \\
& \left. + \int_R^{+\infty} dZ' \frac{e^{-\frac{Z'}{h_Z}}}{h_Z} R^{2n} \int_0^{+\infty} dR' \frac{R'^{3\alpha-2}}{(R'^2 + Z'^2)^{\frac{3\alpha-2+2n}{2}}} \right\} \\
& \times \Sigma(R') {}_2F_1 \left(-n, \frac{3\alpha}{2} - 1 + n; 1; \frac{R'^2}{R'^2 + Z'^2} \right), \tag{E.1}
\end{aligned}$$

where

$${}_2F_1 \left(-n, \frac{3\alpha}{2} - 1 + n; 1; z \right) = \sum_{k=0}^n \binom{n}{k} \frac{\Gamma(\frac{3\alpha}{2} - 1 + n + k)}{\Gamma(\frac{3\alpha}{2} - 1 + n)} \frac{(-z)^k}{k!}. \tag{E.2}$$

Taking the first derivative in R of eq. (E.1), we get the disk-gas part of the gravitational field (5.44)

$$g^{\text{disk+gas}}(R) = -\frac{d\Phi^{\text{disk+gas}}(R)}{dR} - \frac{3(\alpha-1)}{2R} \Phi^{\text{disk+gas}}(R)$$

$$\begin{aligned}
&= \frac{2\pi G}{3\alpha - 2} \sum_{n=0}^{+\infty} \frac{1}{n!} \frac{\Gamma(2 - \frac{3\alpha}{2})}{\Gamma(2 - \frac{3\alpha}{2} - n)} \left\{ \int_0^R dZ' \frac{e^{-\frac{Z'}{h_Z}}}{h_Z} \right. \\
&\quad \times \left[-\frac{3\alpha - 2 + 2n}{R^{3\alpha-1+2n}} \int_0^{\sqrt{R^2-Z'^2}} dR' R'^{3\alpha-2} (R'^2 + Z'^2)^n \right. \\
&\quad \quad \left. \left. + 2n R^{2n-1} \int_{\sqrt{R^2-Z'^2}}^{+\infty} dR' \frac{R'^{3\alpha-2}}{(R'^2 + Z'^2)^{\frac{3\alpha-2+2n}{2}}} \right] \right. \\
&\quad \left. + \int_R^{+\infty} dZ' \frac{e^{-\frac{Z'}{h_Z}}}{h_Z} 2n R^{2n-1} \int_0^{+\infty} dR' \frac{R'^{3\alpha-2}}{(R'^2 + Z'^2)^{\frac{3\alpha-2+2n}{2}}} \right\} \\
&\quad \times \Sigma(R') {}_2F_1 \left(-n, \frac{3\alpha}{2} - 1 + n; 1; \frac{R'^2}{R'^2 + Z'^2} \right) - \frac{3(\alpha - 1)}{2R} \Phi^{\text{disk+gas}}(R) \\
&= \frac{\pi G}{3\alpha - 2} \sum_{n=0}^{+\infty} \frac{1}{n!} \frac{\Gamma(2 - \frac{3\alpha}{2})}{\Gamma(2 - \frac{3\alpha}{2} - n)} \left\{ \int_0^R dZ' \frac{e^{-\frac{Z'}{h_Z}}}{h_Z} \right. \\
&\quad \times \left[\frac{1 - 3\alpha - 4n}{R^{3\alpha-1+2n}} \int_0^{\sqrt{R^2-Z'^2}} dR' R'^{3\alpha-2} (R'^2 + Z'^2)^n \right. \\
&\quad \quad \left. \left. + (4n + 3\alpha - 3) R^{2n-1} \int_{\sqrt{R^2-Z'^2}}^{+\infty} dR' \frac{R'^{3\alpha-2}}{(R'^2 + Z'^2)^{\frac{3\alpha-2+2n}{2}}} \right] \right. \\
&\quad \left. + \int_R^{+\infty} dZ' \frac{e^{-\frac{Z'}{h_Z}}}{h_Z} (4n + 3\alpha - 3) R^{2n-1} \int_0^{+\infty} dR' \frac{R'^{3\alpha-2}}{(R'^2 + Z'^2)^{\frac{3\alpha-2+2n}{2}}} \right\} \\
&\quad \times \Sigma(R') {}_2F_1 \left(-n, \frac{3\alpha}{2} - 1 + n; 1; \frac{R'^2}{R'^2 + Z'^2} \right). \tag{E.3}
\end{aligned}$$

The bulge component of the potential is

$$\begin{aligned}
\Phi^{\text{bulge}}(r) &= -\frac{G}{(3\alpha - 2)r_*} \int_{\mathcal{V}} d^3\mathbf{x}' \left| \frac{r'}{r_*} \right|^{3(\alpha-1)} \rho^{\text{bulge}}(r') \left| \frac{r_*}{\mathbf{x} - \mathbf{x}'} \right|^{3\alpha-2} \\
&\stackrel{\text{(B.9)}}{=} -\frac{2\pi G}{3\alpha - 2} \sum_{n=0}^{+\infty} \int_0^\pi d\theta' \sin \theta' C_n^{\frac{3\alpha-2}{2}}(\cos \theta') \int_0^{+\infty} dr' \rho^{\text{bulge}}(r') r'^{3\alpha-1} \frac{r_{<}^n}{r_{>}^{2n+3\alpha-2}} \\
&\stackrel{\text{(C.7)}}{=} -\frac{4\pi G}{3\alpha - 2} \sum_{n=0}^{+\infty} \frac{1}{(2n+1)!} \frac{\Gamma(3\alpha - 3 + 2n)}{\Gamma(3\alpha - 3)} \int_0^{+\infty} dr' \rho^{\text{bulge}}(r') r'^{3\alpha-1} \frac{r_{<}^{2n}}{r_{>}^{2n+3\alpha-2}} \\
&= -\frac{2\pi G}{(3\alpha - 2)(3\alpha - 4)r} \int_0^{+\infty} dr' \rho^{\text{bulge}}(r') r'^{3\alpha-2} [(r_{>} - r_{<})^{4-3\alpha} - (r_{>} + r_{<})^{4-3\alpha}] \\
&= -\frac{2\pi G}{(3\alpha - 2)(3\alpha - 4)r} \int_0^r dr' \rho^{\text{bulge}}(r') r'^{3\alpha-2} [(r - r')^{4-3\alpha} - (r + r')^{4-3\alpha}] \\
&\quad - \frac{2\pi G}{(3\alpha - 2)(3\alpha - 4)r} \int_r^{+\infty} dr' \rho^{\text{bulge}}(r') r'^{3\alpha-2} [(r' - r)^{4-3\alpha} - (r' + r)^{4-3\alpha}].
\end{aligned}$$

(E.4)

The gravitational field is then

$$\begin{aligned}
g^{\text{bulge}}(R) &= - \left. \frac{d\Phi^{\text{bulge}}(r)}{dr} \right|_{r=R} - \frac{3(\alpha-1)}{2R} \Phi^{\text{bulge}}(R) \\
&= \frac{2\pi G}{(3\alpha-2)(3\alpha-4)R^2} \int_0^R dr' \rho^{\text{bulge}}(r') r'^{3\alpha-2} \left\{ [3(1-\alpha)R+r'](R-r')^{3(1-\alpha)} \right. \\
&\quad \left. - [3(1-\alpha)R-r'](R+r')^{3(1-\alpha)} \right\} \\
&\quad - \frac{2\pi G}{(3\alpha-2)(3\alpha-4)R^2} \int_R^{+\infty} dr' \rho^{\text{bulge}}(r') r'^{3\alpha-2} \\
&\quad \times \left\{ [3(1-\alpha)R+r'](r'-R)^{3(1-\alpha)} \right. \\
&\quad \left. + [3(1-\alpha)R-r'](r'+R)^{3(1-\alpha)} \right\} + \frac{3(1-\alpha)}{2R} \Phi^{\text{bulge}}(R) \\
&= \frac{\pi G}{(3\alpha-2)(3\alpha-4)R^2} \int_0^R dr' \rho^{\text{bulge}}(r') r'^{3\alpha-2} \\
&\quad \times \left\{ [3(1-\alpha)(R+r') + 2r'](R-r')^{3(1-\alpha)} \right. \\
&\quad \left. - [3(1-\alpha)(R-r') - 2r'](R+r')^{3(1-\alpha)} \right\} \\
&\quad - \frac{\pi G}{(3\alpha-2)(3\alpha-4)R^2} \int_R^{+\infty} dr' \rho^{\text{bulge}}(r') r'^{3\alpha-2} \\
&\quad \times \left\{ [3(1-\alpha)(R+r') + 2r'](r'-R)^{3(1-\alpha)} \right. \\
&\quad \left. + [3(1-\alpha)(R-r') - 2r'](r'+R)^{3(1-\alpha)} \right\} \\
&= \frac{\pi G}{(3\alpha-2)(3\alpha-4)R^2} \\
&\quad \times \left[\int_0^R dr' \rho^{\text{bulge}}(r') r'^{3\alpha-2} [3(1-\alpha)(R+r') + 2r'](R-r')^{3(1-\alpha)} \right. \\
&\quad - \int_R^{+\infty} dr' \rho^{\text{bulge}}(r') r'^{3\alpha-2} [3(1-\alpha)(R+r') + 2r'](r'-R)^{3(1-\alpha)} \\
&\quad \left. - \int_0^{+\infty} dr' \rho^{\text{bulge}}(r') r'^{3\alpha-2} [3(1-\alpha)(R-r') - 2r'](R+r')^{3(1-\alpha)} \right]. \quad (\text{E.5})
\end{aligned}$$

E.1.2 $\alpha = 2/3$

Plugging the thick-disk profile (2.37), the potential (5.35) with $r_* = R_*$ and the series representation (B.15) into eq. (5.43), for $\alpha = 2/3$ we get

$$\begin{aligned}
\Phi^{\text{disk+gas}}(R) &= \frac{G}{R_*} \int_{\mathcal{V}} d^3 \mathbf{x}' \left| \frac{R'}{R_*} \right|^{-1} \rho^{\text{disk+gas}}(\mathbf{x}') \ln \frac{|\mathbf{x} - \mathbf{x}'|}{R_*} \\
&= 2G \int_0^{+\infty} dZ' \frac{e^{-Z'/h_Z}}{2h_Z} \int_0^{+\infty} dR' \Sigma(R') \\
&\quad \times \left[2\pi \ln \frac{R_{>}}{R_*} - \sum_{n=1}^{+\infty} \int_0^{2\pi} d\phi' \frac{\cos(n\phi')}{n} \left(\frac{R_{<}}{R_{>}} \right)^n \right]
\end{aligned}$$

$$\begin{aligned}
&= 2\pi G \int_0^{+\infty} dZ' \frac{e^{-\frac{Z'}{h_Z}}}{h_Z} \int_0^{+\infty} dR' \Sigma(R') \ln \frac{R_{>}}{R_*} \\
&= \pi G \int_0^R dZ' \frac{e^{-\frac{Z'}{h_Z}}}{h_Z} \left[\ln \frac{R^2}{R_*^2} \int_0^{\sqrt{R^2-Z'^2}} dR' \Sigma(R') \right. \\
&\quad \left. + \int_{\sqrt{R^2-Z'^2}}^{+\infty} dR' \Sigma(R') \ln \frac{R'^2 + Z'^2}{R_*^2} \right] \\
&\quad + \pi G \int_R^{+\infty} dZ' \frac{e^{-\frac{Z'}{h_Z}}}{h_Z} \left[\int_0^{+\infty} dR' \Sigma(R') \ln \frac{R'^2 + Z'^2}{R_*^2} \right]. \tag{E.6}
\end{aligned}$$

The associated gravitational field is

$$\begin{aligned}
g^{\text{disk+gas}}(R) &= -\frac{d\Phi^{\text{disk+gas}}(R)}{dR} + \frac{1}{2R}\Phi^{\text{disk+gas}}(R) \\
&= -\frac{2\pi G}{R} \int_0^R dZ' \frac{e^{-\frac{Z'}{h_Z}}}{h_Z} \int_0^{\sqrt{R^2-Z'^2}} dR' \Sigma(R') + \frac{1}{2R}\Phi^{\text{disk+gas}}(R). \tag{E.7}
\end{aligned}$$

The bulge component of the galactic potential is

$$\begin{aligned}
\Phi^{\text{bulge}}(r) &= \frac{G}{r_*} \int_{\mathcal{V}} d^3\mathbf{x}' \left| \frac{r'}{r_*} \right|^{-1} \rho^{\text{bulge}}(r') \ln \frac{|\mathbf{x} - \mathbf{x}'|}{r_*} \\
&\stackrel{\text{(B.14)}}{=} 2\pi G \int_0^\pi d\theta' \sin \theta' \int_0^{+\infty} dr' \rho^{\text{bulge}}(r') r' \left[\ln \frac{r_{>}}{r_*} - \sum_{n=1}^{+\infty} \frac{\cos(n\theta')}{n} \left(\frac{r_{<}}{r_{>}} \right)^n \right] \\
&= 4\pi G \int_0^{+\infty} dr' \rho^{\text{bulge}}(r') r' \left[\ln \frac{r_{>}}{r_*} - \sum_{n=1}^{+\infty} \frac{1}{2n(1-4n^2)} \left(\frac{r_{<}}{r_{>}} \right)^{2n} \right] \\
&= 2\pi G \int_0^{+\infty} dr' \rho^{\text{bulge}}(r') r' \\
&\quad \times \left[-1 + 2 \ln \frac{r_{>}}{r_*} + \frac{r^2 + r'^2}{rr'} \operatorname{arctanh} \frac{r_{<}}{r_{>}} + \ln \left(1 - \frac{r_{<}^2}{r_{>}^2} \right) \right] \\
&= 2\pi G \int_0^r dr' \rho^{\text{bulge}}(r') r' \\
&\quad \times \left[-1 + 2 \ln \frac{r}{r_*} + \frac{r^2 + r'^2}{rr'} \operatorname{arctanh} \frac{r'}{r} + \ln \left(1 - \frac{r'^2}{r^2} \right) \right] \\
&\quad + 2\pi G \int_r^{+\infty} dr' \rho^{\text{bulge}}(r') r' \\
&\quad \times \left[-1 + 2 \ln \frac{r'}{r_*} + \frac{r^2 + r'^2}{rr'} \operatorname{arctanh} \frac{r}{r'} + \ln \left(1 - \frac{r^2}{r'^2} \right) \right]. \tag{E.8}
\end{aligned}$$

The gravitational potential reads

$$g^{\text{bulge}}(R) = -\left. \frac{d\Phi^{\text{bulge}}(r)}{dr} \right|_{r=R} + \frac{1}{2R}\Phi^{\text{bulge}}(R)$$

$$\begin{aligned}
&= -\frac{2\pi G}{R} \int_0^R dr' \rho^{\text{bulge}}(r') r' \left[1 + \frac{R^2 - r'^2}{Rr'} \operatorname{arctanh} \frac{r'}{R} \right] \\
&\quad - \frac{2\pi G}{R} \int_R^{+\infty} dr' \rho^{\text{bulge}}(r') r' \left[1 + \frac{R^2 - r'^2}{Rr'} \operatorname{arctanh} \frac{R}{r'} \right] + \frac{1}{2R} \Phi^{\text{bulge}}(R) \\
&= -\frac{\pi G}{R} \int_0^R dr' \rho^{\text{bulge}}(r') r' \left[3 - 2 \ln \frac{R}{R_*} - \ln \left(1 - \frac{r'^2}{R^2} \right) + \frac{R^2 - 3r'^2}{Rr'} \operatorname{arctanh} \frac{r'}{R} \right] \\
&\quad - \frac{\pi G}{R} \int_R^{+\infty} dr' \rho^{\text{bulge}}(r') r' \left[3 - 2 \ln \frac{r'}{R_*} - \ln \left(1 - \frac{R^2}{r'^2} \right) + \frac{R^2 - 3r'^2}{Rr'} \operatorname{arctanh} \frac{R}{r'} \right].
\end{aligned} \tag{E.9}$$

E.1.3 Comparison with data

Regarding NGC7814, the model has some overlap with the data curve at $\alpha = 0.84 - 0.86$, a range similar to the one found for NGC6503. As one can see in Fig. 10, as α decreases from 1 the curve is lifted and flattened, without, however, matching the data enough to warrant a more rigorous best-fit analysis. For NGC6503, as one varies α to values smaller than 1, the rotation curve is lifted up similarly to what depicted in Fig. 3, crossing the data at around $\alpha = 0.80 - 0.82$ (Fig. 11), but it does not change much its shape for $\alpha > 2/3$. For $\alpha < 2/3$, the theoretical rotation curve changes drastically and away from the data points, as in Fig. 3. Therefore, the plateau evidenced by the data is never reproduced. For NGC3741, the rotation curve is flat and low for $0.80 < \alpha < 1$ and reproduces the large- R behaviour of the data for $\alpha = 0.50 - 0.55$ (Fig. 12). However, the data points at small radii are never fitted, which may suggest to look at a more refined model away from the extreme fractional regime. Negative results for all the three galaxies are obtained also when $\alpha = 2/3$ and $R_* \gg R_0$ (i.e., for an R_* consistent with the extreme fractional limit).

E.2 Small fractional corrections

E.2.1 $\alpha \neq 4/3$

The contributions $\Phi_0^{\text{disk+gas}}(R) + \Phi_0^{\text{bulge}}(R)$ of the total potential (5.49a) have already been calculated in section (2.4) for general relativity or, alternatively, in Appendix E.1.1 for $\alpha = 1$:

$$\begin{aligned}
\Phi_0^{\text{disk+gas}}(R) &= -G \int_{\mathcal{V}} d^3 \mathbf{x}' \frac{\rho^{\text{disk+gas}}(\mathbf{x}')}{|\mathbf{x} - \mathbf{x}'|} \\
&= -2\pi G \sum_{n=0}^{+\infty} \frac{1}{n!} \frac{\sqrt{\pi}}{\Gamma(\frac{1}{2} - n)} \left\{ \int_0^R dZ' \frac{e^{-\frac{Z'}{h_Z}}}{h_Z} \right. \\
&\quad \times \left[\frac{1}{R^{1+2n}} \int_0^{\sqrt{R^2 - Z'^2}} dR' R' (R'^2 + Z'^2)^n \right. \\
&\quad \quad \left. \left. + R^{2n} \int_{\sqrt{R^2 - Z'^2}}^{+\infty} dR' \frac{R'}{(R'^2 + Z'^2)^{\frac{1+2n}{2}}} \right] \right. \\
&\quad \left. + \int_R^{+\infty} dZ' \frac{e^{-\frac{Z'}{h_Z}}}{h_Z} R^{2n} \int_0^{+\infty} dR' \frac{R'}{(R'^2 + Z'^2)^{\frac{1+2n}{2}}} \right\}
\end{aligned}$$

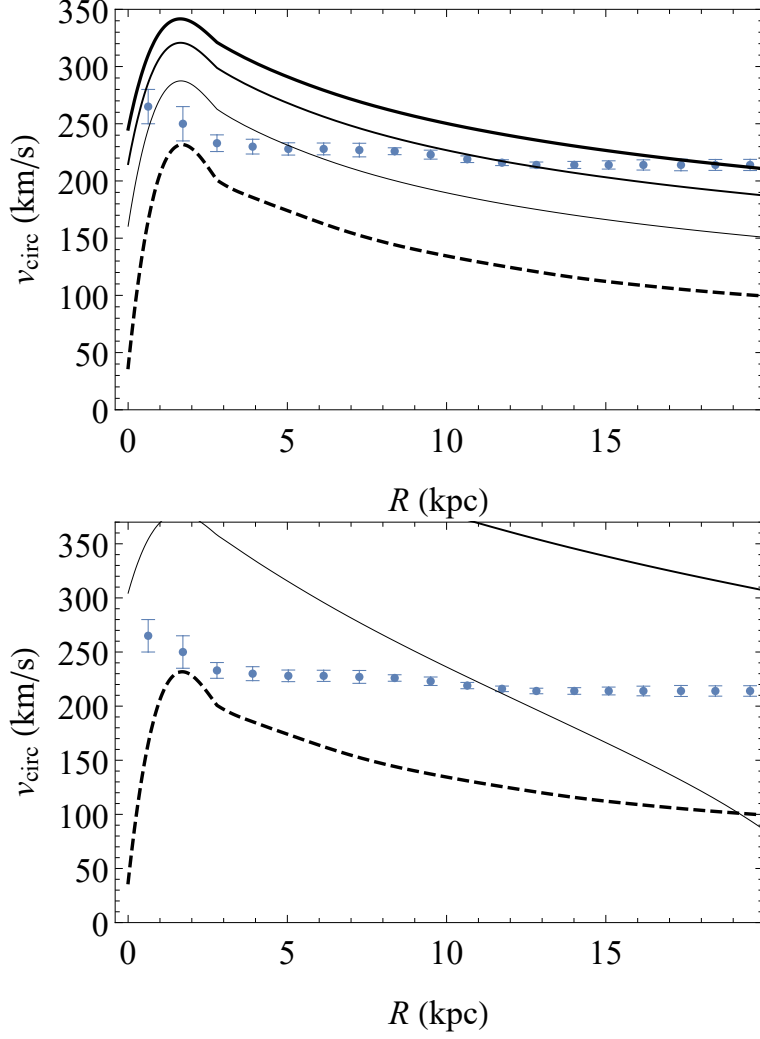


Figure 10. Comparison of the data points of NGC7814 with the $n = 0$ rotation curve of the theory T_v with weighted derivatives in the extreme fractional regime with a data-based matter density profile for $\alpha = 1$ (general relativity, dashed curve), $\alpha = 0.90, 0.86, 0.84$ (top panel, increasing thickness) or $\alpha = 2/3$ and $R_* = 3, 10$ kpc (bottom panel, increasing thickness).

$$\times \Sigma(R') {}_2F_1 \left(-n, \frac{1}{2} + n; 1; \frac{R'^2}{R'^2 + Z'^2} \right), \quad (\text{E.10})$$

and

$$\Phi_0^{\text{bulge}}(R) = -4\pi G \left[\frac{1}{R} \int_0^R dr' \rho^{\text{bulge}}(r') r'^2 + \int_R^{+\infty} dr' \rho^{\text{bulge}}(r') r' \right]. \quad (\text{E.11})$$

The gravitational fields associated to these potential components are

$$g_0^{\text{disk+gas}}(R) = -\frac{d\Phi_0^{\text{disk+gas}}(R)}{dR} - \frac{3(\alpha - 1)}{2R} \left| \frac{R}{R_*} \right|^{3(\alpha-1)} \Phi_0^{\text{disk+gas}}(R)$$

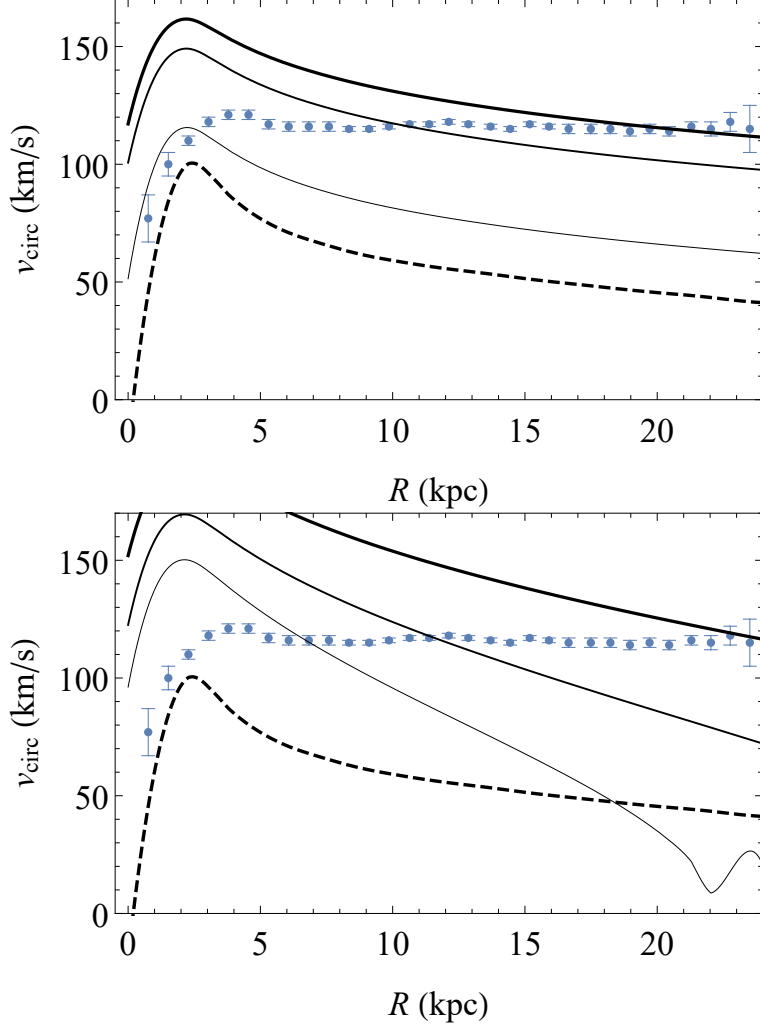


Figure 11. Comparison of the data points of NGC6503 with the $n = 0$ rotation curve of the theory T_v with weighted derivatives in the extreme fractional regime with a data-based matter density profile for $\alpha = 1$ (general relativity, dashed curve), $\alpha = 0.90, 0.82, 0.80$ (top panel, increasing thickness) or $\alpha = 2/3$ and $R_* = 3, 5, 10$ kpc (bottom panel, increasing thickness).

$$\begin{aligned}
&= 2\pi G \sum_{n=0}^{+\infty} \frac{1}{n!} \frac{\sqrt{\pi}}{\Gamma(\frac{1}{2} - n)} \left\{ \int_0^R dZ' \frac{e^{-\frac{Z'}{hZ}}}{hZ} \right. \\
&\quad \times \left[-\frac{1+2n}{R^{2(1+n)}} \int_0^{\sqrt{R^2-Z'^2}} dR' R' (R'^2 + Z'^2)^n \right. \\
&\quad \left. \left. + 2n R^{2n-1} \int_{\sqrt{R^2-Z'^2}}^{+\infty} dR' \frac{R'}{(R'^2 + Z'^2)^{\frac{1+2n}{2}}} \right] \right\}
\end{aligned}$$

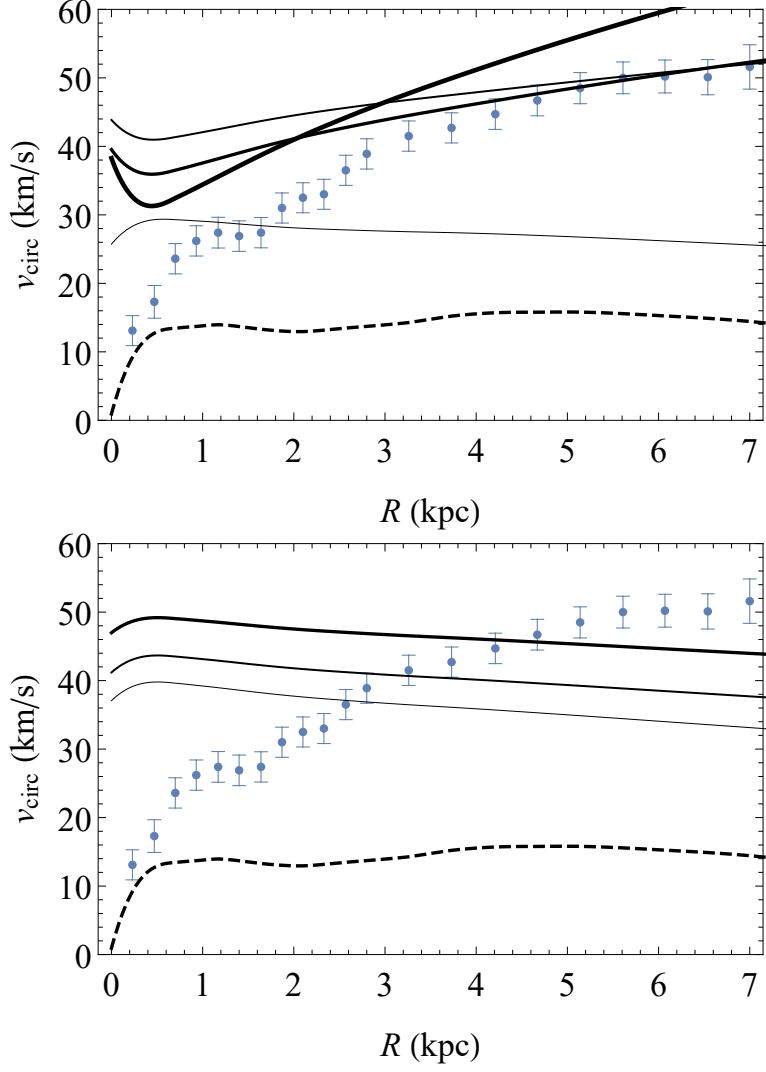


Figure 12. Comparison of the data points of NGC3741 with the $n = 0$ rotation curve of the theory T_v with weighted derivatives in the extreme fractional regime with a data-based matter density profile for $\alpha = 1$ (general relativity, dashed curve), $\alpha = 0.80, 0.55, 0.50, 0.40$ (top panel, increasing thickness) or $\alpha = 2/3$ and $R_* = 10, 20, 60$ kpc (bottom panel, increasing thickness).

$$\begin{aligned}
& \left. + \int_R^{+\infty} dZ' \frac{e^{-\frac{Z'}{hZ}}}{hZ} 2n R^{2n-1} \int_0^{+\infty} dR' \frac{R'}{(R'^2 + Z'^2)^{\frac{1+2n}{2}}} \right\} \\
& \times \Sigma(R') {}_2F_1 \left(-n, \frac{1}{2} + n; 1; \frac{R'^2}{R'^2 + Z'^2} \right) - \frac{3(\alpha - 1)}{2R} \Phi_0^{\text{disk+gas}}(R), \quad (\text{E.12})
\end{aligned}$$

and

$$\begin{aligned}
g_0^{\text{bulge}}(R) &= -\frac{d\Phi_0^{\text{bulge}}(R)}{dR} - \frac{3(\alpha - 1)}{2R} \Phi_0^{\text{bulge}}(R) \\
&= -\frac{4\pi G}{R^2} \int_0^R dr' \rho^{\text{bulge}}(r') r'^2 - \frac{3(\alpha - 1)}{2R} \Phi^{\text{bulge}}(R). \quad (\text{E.13})
\end{aligned}$$

The potential term (5.49c) is simply given by eqs. (E.10) and (E.11) with a measure factor inserted in the radial integral,

$$\begin{aligned}
\delta\Phi_1^{\text{disk+gas}}(R) &= -G \int_{\mathcal{V}} d^3\mathbf{x}' \left| \frac{R'}{R_*} \right|^{3(\alpha-1)} \frac{\rho^{\text{disk+gas}}(\mathbf{x}')}{|\mathbf{x} - \mathbf{x}'|} \\
&= -2\pi GR_* \sum_{n=0}^{+\infty} \frac{1}{n!} \frac{\sqrt{\pi}}{\Gamma(\frac{1}{2} - n)} \left\{ \int_0^R dZ' \frac{e^{-\frac{Z'}{hZ}}}{hZ} \right. \\
&\quad \times \left[\frac{1}{R^{1+2n}} \int_0^{\sqrt{R^2 - Z'^2}} dR' \left| \frac{R'}{R_*} \right|^{3\alpha-2} (R'^2 + Z'^2)^n \right. \\
&\quad \left. \left. + R^{2n} \int_{\sqrt{R^2 - Z'^2}}^{+\infty} dR' \left| \frac{R'}{R_*} \right|^{3\alpha-2} \frac{1}{(R'^2 + Z'^2)^{\frac{1+2n}{2}}} \right] \right. \\
&\quad \left. + \int_R^{+\infty} dZ' \frac{e^{-\frac{Z'}{hZ}}}{hZ} R^{2n} \int_0^{+\infty} dR' \left| \frac{R'}{R_*} \right|^{3\alpha-2} \frac{1}{(R'^2 + Z'^2)^{\frac{1+2n}{2}}} \right\} \\
&\quad \times \Sigma(R') {}_2F_1 \left(-n, \frac{1}{2} + n; 1; \frac{R'^2}{R'^2 + Z'^2} \right), \tag{E.14}
\end{aligned}$$

$$\delta\Phi_1^{\text{bulge}}(R) = -4\pi GR_* \left[\frac{R_*}{R} \int_0^R dr' \left| \frac{r'}{R_*} \right|^{3\alpha-1} \rho^{\text{bulge}}(r') + \int_R^{+\infty} dr' \left| \frac{r'}{R_*} \right|^{3\alpha-2} \rho^{\text{bulge}}(r') \right], \tag{E.15}$$

where $r_* = R_*$, while the gravitational fields are

$$\begin{aligned}
g_1^{\text{disk+gas}}(R) &= -\frac{d\delta\Phi_1^{\text{disk+gas}}(R)}{dR} \\
&= 2\pi GR_* \sum_{n=0}^{+\infty} \frac{1}{n!} \frac{\sqrt{\pi}}{\Gamma(\frac{1}{2} - n)} \left\{ \int_0^R dZ' \frac{e^{-\frac{Z'}{hZ}}}{hZ} \right. \\
&\quad \times \left[-\frac{1+2n}{R^{2(1+n)}} \int_0^{\sqrt{R^2 - Z'^2}} dR' \left| \frac{R'}{R_*} \right|^{3\alpha-2} (R'^2 + Z'^2)^n \right. \\
&\quad \left. \left. + 2n R^{2n-1} \int_{\sqrt{R^2 - Z'^2}}^{+\infty} dR' \left| \frac{R'}{R_*} \right|^{3\alpha-2} \frac{1}{(R'^2 + Z'^2)^{\frac{1+2n}{2}}} \right] \right. \\
&\quad \left. + \int_R^{+\infty} dZ' \frac{e^{-\frac{Z'}{hZ}}}{hZ} 2n R^{2n-1} \int_0^{+\infty} dR' \left| \frac{R'}{R_*} \right|^{3\alpha-2} \frac{1}{(R'^2 + Z'^2)^{\frac{1+2n}{2}}} \right\} \\
&\quad \times \Sigma(R') {}_2F_1 \left(-n, \frac{1}{2} + n; 1; \frac{R'^2}{R'^2 + Z'^2} \right), \tag{E.16}
\end{aligned}$$

$$g_1^{\text{bulge}}(R) = -\frac{d\delta\Phi_1^{\text{bulge}}(R)}{dR} = -4\pi G \frac{R_*^2}{R^2} \int_0^R dr' \left| \frac{r'}{R_*} \right|^{3\alpha-1} \rho^{\text{bulge}}(r'). \tag{E.17}$$

Finally, the potential term (5.49d) is

$$\begin{aligned}
\delta\Phi_2^{\text{disk+gas}}(R) &= -G \frac{7-6\alpha}{(3\alpha-4)R_*^{3(\alpha-1)}} \int_{\mathcal{V}} d^3\mathbf{x}' \frac{\rho^{\text{disk+gas}}(\mathbf{x}')}{|\mathbf{x}-\mathbf{x}'|^{4-3\alpha}} \\
&\stackrel{\text{(B.12)}}{=} -G \frac{7-6\alpha}{(3\alpha-4)R_*^{3(\alpha-1)}} \sum_{n=0}^{+\infty} \int_0^{+\infty} dZ' \frac{e^{-\frac{Z'}{h_Z}}}{h_Z} \int_0^{+\infty} dR' \Sigma(R') \\
&\quad \times \frac{R_{<}^{2n}}{R_{>}^{3\alpha-2+2n}} \int_0^{2\pi} d\phi' C_n^{\frac{3\alpha-2}{2}} \left(\sqrt{\frac{R'^2}{R'^2+Z'^2}} \cos \phi' \right) \\
&\stackrel{\text{(C.4)}}{=} -2\pi G \frac{7-6\alpha}{(3\alpha-4)R_*^{3(\alpha-1)}} \sum_{n=0}^{+\infty} \frac{1}{n!} \frac{\Gamma(2-\frac{3\alpha}{2})}{\Gamma(2-\frac{3\alpha}{2}-n)} \\
&\quad \times \int_0^{+\infty} dZ' \frac{e^{-\frac{Z'}{h_Z}}}{h_Z} \int_0^{+\infty} dR' \Sigma(R') \frac{R_{<}^{2n}}{R_{>}^{3\alpha-2+2n}} \\
&\quad \times {}_2F_1 \left(-n, \frac{3\alpha}{2} - 1 + n; 1; \frac{R'^2}{R'^2+Z'^2} \right) \\
&= -2\pi G \frac{7-6\alpha}{(3\alpha-4)R_*^{3(\alpha-1)}} \sum_{n=0}^{+\infty} \frac{1}{n!} \frac{\Gamma(2-\frac{3\alpha}{2})}{\Gamma(2-\frac{3\alpha}{2}-n)} \left\{ \int_0^R dZ' \frac{e^{-\frac{Z'}{h_Z}}}{h_Z} \right. \\
&\quad \left[\frac{1}{R^{3\alpha-2+2n}} \int_0^{\sqrt{R^2-Z'^2}} dR' (R'^2+Z'^2)^n \right. \\
&\quad \left. \left. + R^{2n} \int_{\sqrt{R^2-Z'^2}}^{+\infty} \frac{dR'}{(R'^2+Z'^2)^{\frac{3\alpha-2+2n}{2}}} \right] \right. \\
&\quad \left. + \int_R^{+\infty} dZ' \frac{e^{-\frac{Z'}{h_Z}}}{h_Z} R^{2n} \int_0^{+\infty} \frac{dR'}{(R'^2+Z'^2)^{\frac{3\alpha-2+2n}{2}}} \right\} \\
&\quad \times \Sigma(R') {}_2F_1 \left(-n, \frac{3\alpha}{2} - 1 + n; 1; \frac{R'^2}{R'^2+Z'^2} \right), \tag{E.18}
\end{aligned}$$

with bulge component

$$\begin{aligned}
\delta\Phi_2^{\text{bulge}}(R) &\stackrel{\text{(B.9)}}{=} -2\pi G \frac{7-6\alpha}{(3\alpha-4)R_*^{3(\alpha-1)}} \sum_{n=0}^{+\infty} \int_0^\pi d\theta' \sin \theta' C_n^{\frac{4-3\alpha}{2}}(\cos \theta') \\
&\quad \times \int_0^{+\infty} dr' \rho^{\text{bulge}}(r') r'^2 \frac{r_{<}^n}{r_{>}^{n+4-3\alpha}} \\
&\stackrel{\text{(C.7)}}{=} -2\pi G \frac{7-6\alpha}{(3\alpha-4)R_*^{3(\alpha-1)}} \int_0^{+\infty} dr' \rho^{\text{bulge}}(r') \frac{r'^2}{r_{>}^{4-3\alpha}} \\
&\quad \times \sum_{n=0}^{+\infty} \frac{2}{(2n+1)!} \frac{\Gamma(3-3\alpha+2n)}{\Gamma(3-3\alpha)} \left(\frac{r_{<}}{r_{>}} \right)^{2n}
\end{aligned}$$

$$\begin{aligned}
&= -2\pi G \frac{7-6\alpha}{(3\alpha-4)(3\alpha-2)R_*^{3(\alpha-1)}} \int_0^{+\infty} dr' \rho^{\text{bulge}}(r') \frac{r'^2}{r_{>}^{4-3\alpha}} \\
&\quad \times \frac{r_{>}^{3-3\alpha}}{r_{<}} [(r_{>} + r_{<})^{3\alpha-2} - (r_{>} - r_{<})^{3\alpha-2}] \\
&= -2\pi G \frac{7-6\alpha}{(3\alpha-4)(3\alpha-2)R_*^{3(\alpha-1)}} \frac{1}{R} \int_0^{+\infty} dr' \rho^{\text{bulge}}(r') r' \\
&\quad \times [(R+r')^{3\alpha-2} - (r_{>} - r_{<})^{3\alpha-2}] \\
&= -2\pi G \frac{7-6\alpha}{(3\alpha-4)(3\alpha-2)R_*^{3(\alpha-1)}} \frac{1}{R} \left[\int_0^{+\infty} dr' \rho^{\text{bulge}}(r') r' (R+r')^{3\alpha-2} \right. \\
&\quad \left. - \int_0^R dr' \rho^{\text{bulge}}(r') r' (R-r')^{3\alpha-2} - \int_R^{+\infty} dr' \rho^{\text{bulge}}(r') r' (r'-R)^{3\alpha-2} \right]. \tag{E.19}
\end{aligned}$$

The gravitational fields are

$$\begin{aligned}
g_2^{\text{disk+gas}}(R) &= -\frac{d\delta\Phi_2^{\text{disk+gas}}(R)}{dR} \\
&= 2\pi G \frac{7-6\alpha}{(3\alpha-4)R_*^{3(\alpha-1)}} \sum_{n=0}^{+\infty} \frac{1}{n!} \frac{\Gamma(2-\frac{3\alpha}{2})}{\Gamma(2-\frac{3\alpha}{2}-n)} \left\{ \int_0^R dZ' \frac{e^{-\frac{Z'}{hZ}}}{hZ} \right. \\
&\quad \left[\frac{2-3\alpha-2n}{R^{3\alpha-1+2n}} \int_0^{\sqrt{R^2-Z'^2}} dR' (R'^2+Z'^2)^n \right. \\
&\quad \left. \left. + 2n R^{2n-1} \int_{\sqrt{R^2-Z'^2}}^{+\infty} \frac{dR'}{(R'^2+Z'^2)^{\frac{3\alpha-2+2n}{2}}} \right] \right. \\
&\quad \left. + \int_R^{+\infty} dZ' \frac{e^{-\frac{Z'}{hZ}}}{hZ} 2n R^{2n-1} \int_0^{+\infty} \frac{dR'}{(R'^2+Z'^2)^{\frac{3\alpha-2+2n}{2}}} \right\} \\
&\quad \times \Sigma(R') {}_2F_1 \left(-n, \frac{3\alpha}{2} - 1 + n; 1; \frac{R'^2}{R'^2+Z'^2} \right), \tag{E.20}
\end{aligned}$$

$$\begin{aligned}
g_2^{\text{bulge}}(R) &= -\frac{d\delta\Phi_2^{\text{bulge}}(R)}{dR} \\
&= 2\pi G \frac{7-6\alpha}{(3\alpha-4)(3\alpha-2)R_*^{3(\alpha-1)}} \frac{1}{R^2} \\
&\quad \times \left\{ \int_0^{+\infty} dr' \rho^{\text{bulge}}(r') r' [3(\alpha-1)R-r'] (R+r')^{3(\alpha-1)} \right. \\
&\quad \left. - \int_0^R dr' \rho^{\text{bulge}}(r') r' [3(\alpha-1)R+r'] (R-r')^{3(\alpha-1)} \right. \\
&\quad \left. + \int_R^{+\infty} dr' \rho^{\text{bulge}}(r') r' [3(\alpha-1)R+r'] (r'-R)^{3(\alpha-1)} \right\}. \tag{E.21}
\end{aligned}$$

E.2.2 $\alpha = 4/3$

At lowest order, the potential is given by eqs. (E.10) and (E.11), while the gravitational field is eqs. (E.12) and (E.13) with $\alpha = 4/3$:

$$\begin{aligned}
g_0^{\text{disk+gas}}(R) &= 2\pi G \sum_{n=0}^{+\infty} \frac{1}{n!} \frac{\sqrt{\pi}}{\Gamma(\frac{1}{2} - n)} \left\{ \int_0^R dZ' \frac{e^{-\frac{Z'}{h_Z}}}{h_Z} \right. \\
&\quad \times \left[-\frac{1+2n}{R^{2(1+n)}} \int_0^{\sqrt{R^2-Z'^2}} dR' R' (R'^2 + Z'^2)^n \right. \\
&\quad \quad \left. \left. + 2n R^{2n-1} \int_{\sqrt{R^2-Z'^2}}^{+\infty} dR' \frac{R'}{(R'^2 + Z'^2)^{\frac{1+2n}{2}}} \right] \right. \\
&\quad \left. + \int_R^{+\infty} dZ' \frac{e^{-\frac{Z'}{h_Z}}}{h_Z} 2n R^{2n-1} \int_0^{+\infty} dR' \frac{R'}{(R'^2 + Z'^2)^{\frac{1+2n}{2}}} \right\} \\
&\quad \times \Sigma(R') {}_2F_1 \left(-n, \frac{1}{2} + n; 1; \frac{R'^2}{R'^2 + Z'^2} \right) - \frac{1}{2R} \Phi_0^{\text{disk+gas}}(R), \quad (\text{E.22})
\end{aligned}$$

$$g_0^{\text{bulge}}(R) = -\frac{4\pi G}{R^2} \int_0^R dr' \rho^{\text{bulge}}(r') r'^2 - \frac{1}{2R} \Phi^{\text{bulge}}(R). \quad (\text{E.23})$$

The next terms in the expansion are (E.14) and (E.15) with $\alpha = 4/3$:

$$\begin{aligned}
\delta\Phi_1^{\text{disk+gas}}(R) &= -G \int_{\mathcal{V}} d^3\mathbf{x}' \frac{R'}{R_*} \frac{\rho^{\text{disk+gas}}(\mathbf{x}')}{|\mathbf{x} - \mathbf{x}'|} \\
&= -2\pi G R_* \sum_{n=0}^{+\infty} \frac{1}{n!} \frac{\sqrt{\pi}}{\Gamma(\frac{1}{2} - n)} \left\{ \int_0^R dZ' \frac{e^{-\frac{Z'}{h_Z}}}{h_Z} \right. \\
&\quad \times \left[\frac{1}{R^{1+2n}} \int_0^{\sqrt{R^2-Z'^2}} dR' \frac{R'^2}{R_*^2} (R'^2 + Z'^2)^n \right. \\
&\quad \quad \left. \left. + R^{2n} \int_{\sqrt{R^2-Z'^2}}^{+\infty} dR' \frac{R'^2}{R_*^2} \frac{1}{(R'^2 + Z'^2)^{\frac{1+2n}{2}}} \right] \right. \\
&\quad \left. + \int_R^{+\infty} dZ' \frac{e^{-\frac{Z'}{h_Z}}}{h_Z} R^{2n} \int_0^{+\infty} dR' \frac{R'^2}{R_*^2} \frac{1}{(R'^2 + Z'^2)^{\frac{1+2n}{2}}} \right\} \\
&\quad \times \Sigma(R') {}_2F_1 \left(-n, \frac{1}{2} + n; 1; \frac{R'^2}{R'^2 + Z'^2} \right), \quad (\text{E.24})
\end{aligned}$$

$$\delta\Phi_1^{\text{bulge}}(R) = -4\pi G R_* \left[\frac{R_*}{R} \int_0^R dr' \frac{r'^3}{R_*^3} \rho^{\text{bulge}}(r') + \int_R^{+\infty} dr' \frac{r'^2}{R_*^2} \rho^{\text{bulge}}(r') \right], \quad (\text{E.25})$$

leading to

$$\begin{aligned}
g_1^{\text{disk+gas}}(R) &= 2\pi G R_* \sum_{n=0}^{+\infty} \frac{1}{n!} \frac{\sqrt{\pi}}{\Gamma\left(\frac{1}{2} - n\right)} \left\{ \int_0^R dZ' \frac{e^{-\frac{Z'}{h_Z}}}{h_Z} \right. \\
&\quad \times \left[-\frac{1+2n}{R^{2(1+n)}} \int_0^{\sqrt{R^2-Z'^2}} dR' \frac{R'^2}{R_*^2} (R'^2 + Z'^2)^n \right. \\
&\quad \quad \left. + 2n R^{2n-1} \int_{\sqrt{R^2-Z'^2}}^{+\infty} dR' \frac{R'^2}{R_*^2} \frac{1}{(R'^2 + Z'^2)^{\frac{1+2n}{2}}} \right] \\
&\quad \left. + \int_R^{+\infty} dZ' \frac{e^{-\frac{Z'}{h_Z}}}{h_Z} 2n R^{2n-1} \int_0^{+\infty} dR' \frac{R'^2}{R_*^2} \frac{1}{(R'^2 + Z'^2)^{\frac{1+2n}{2}}} \right\} \\
&\quad \times \Sigma(R') {}_2F_1\left(-n, \frac{1}{2} + n; 1; \frac{R'^2}{R'^2 + Z'^2}\right), \tag{E.26}
\end{aligned}$$

$$g_1^{\text{bulge}}(R) = -4\pi G \frac{R_*^2}{R^2} \int_0^R dr' \frac{r'^3}{R_*^3} \rho^{\text{bulge}}(r'). \tag{E.27}$$

Next, eq. (D.8) is

$$\begin{aligned}
\delta\Phi_2^{\text{disk+gas}}(R) &= \frac{G}{R_*} \int_{\mathcal{V}} d^3\mathbf{x}' \rho(\mathbf{x}') \ln \frac{|\mathbf{x} - \mathbf{x}'|}{R_*} \\
&\stackrel{\text{(B.15)}}{=} \frac{G}{R_*} \int_0^{+\infty} dZ' \frac{e^{-\frac{Z'}{h_Z}}}{h_Z} \int_0^{+\infty} dR' \Sigma(R') R' \\
&\quad \times \left[2\pi \ln \frac{R_{>}}{R_*} - \sum_{n=1}^{+\infty} \int_0^{2\pi} d\phi' \frac{\cos(n\phi')}{n} \left(\frac{R_{<}}{R_{>}}\right)^n \right] \\
&= \frac{2\pi G}{R_*} \int_0^{+\infty} dZ' \frac{e^{-\frac{Z'}{h_Z}}}{h_Z} \int_0^{+\infty} dR' \Sigma(R') R' \ln \frac{R_{>}}{R_*} \\
&= \frac{2\pi G}{R_*} \int_0^R dZ' \frac{e^{-\frac{Z'}{h_Z}}}{h_Z} \left[\ln \frac{R}{R_*} \int_0^{\sqrt{R^2-Z'^2}} dR' \Sigma(R') R' \right. \\
&\quad \left. + \int_{\sqrt{R^2-Z'^2}}^{+\infty} dR' \Sigma(R') \ln \frac{\sqrt{R'^2 + Z'^2}}{R_*} \right] \\
&\quad + \frac{2\pi G}{R_*} \int_R^{+\infty} dZ' \frac{e^{-\frac{Z'}{h_Z}}}{h_Z} \int_0^{+\infty} dR' \Sigma(R') R' \ln \frac{\sqrt{R'^2 + Z'^2}}{R_*}, \tag{E.28} \\
\delta\Phi_2^{\text{bulge}}(R) &\stackrel{\text{(B.14)}}{=} \frac{2\pi G}{R_*} \int_0^{+\infty} dr' \rho^{\text{bulge}}(r') r'^2 \left[2 \ln \frac{r_{>}}{R_*} - \sum_{n=1}^{+\infty} \int_0^{\pi} d\theta' \sin \theta' \frac{\cos(n\theta')}{n} \left(\frac{r_{<}}{r_{>}}\right)^n \right] \\
&= \frac{2\pi G}{R_*} \int_0^{+\infty} dr' \rho^{\text{bulge}}(r') r'^2 \left[2 \ln \frac{r_{>}}{R_*} - \sum_{n=1}^{+\infty} \frac{1}{n(1-4n^2)} \left(\frac{r_{<}}{r_{>}}\right)^{2n} \right] \\
&= \frac{2\pi G}{R_*} \int_0^{+\infty} dr' \rho^{\text{bulge}}(r') r'^2 \left[2 \ln \frac{r_{>}}{R_*} - 1 + \ln \left(1 - \frac{r_{<}^2}{r_{>}^2}\right) \right]
\end{aligned}$$

$$\begin{aligned}
& + \left(\frac{r_{<}}{r_{>}} + \frac{r_{>}}{r_{<}} \right) \operatorname{arctanh} \frac{r_{<}}{r_{>}} \Big] \\
= & \frac{2\pi G}{R_*} \int_0^R dr' \rho^{\text{bulge}}(r') r'^2 \left[2 \ln \frac{R}{R_*} - 1 + \ln \left(1 - \frac{r'^2}{R^2} \right) \right. \\
& \left. + \frac{R^2 + r'^2}{r' R} \operatorname{arctanh} \frac{r'}{R} \right] \\
& + \frac{2\pi G}{R_*} \int_R^{+\infty} dr' \rho^{\text{bulge}}(r') r'^2 \left[2 \ln \frac{r'}{R_*} - 1 + \ln \left(1 - \frac{R^2}{r'^2} \right) \right. \\
& \left. + \frac{R^2 + r'^2}{r' R} \operatorname{arctanh} \frac{R}{r'} \right], \tag{E.29}
\end{aligned}$$

with corresponding gravitational fields

$$g_2^{\text{disk+gas}}(R) = -\frac{2\pi G}{R_* R} \int_0^R dZ' \frac{e^{-\frac{Z'}{h_Z}}}{h_Z} \int_0^{\sqrt{R^2 - Z'^2}} dR' \Sigma(R') R', \tag{E.30}$$

$$\begin{aligned}
g_2^{\text{bulge}}(R) = & -\frac{2\pi G}{R_* R} \left[\int_0^{+\infty} dr' \rho^{\text{bulge}}(r') r'^2 + \frac{1}{R} \int_0^R dr' \rho^{\text{bulge}}(r') r' (R^2 - r'^2) \operatorname{arctanh} \frac{r'}{R} \right. \\
& \left. + \frac{1}{R} \int_R^{+\infty} dr' \rho^{\text{bulge}}(r') r' (R^2 - r'^2) \operatorname{arctanh} \frac{R}{r'} \right]. \tag{E.31}
\end{aligned}$$

References

- [1] D. Oriti (ed.), *Approaches to Quantum Gravity*, Cambridge University Press, Cambridge, UK (2009).
- [2] G.F.R. Ellis, J. Murugan and A. Weltman (eds.), *Foundations of Space and Time*, Cambridge University Press, Cambridge, UK (2012).
- [3] L. Modesto and L. Rachwał, *Nonlocal quantum gravity: a review*, *Int. J. Mod. Phys. D* **26** (2017) 1730020.
- [4] G. Calcagni, *Next step in gravity and cosmology: fundamental theory or data-driven models?*, *Front. Astron. Space Sci.* **7** (2020) 52 [[arXiv:2009.00846](#)].
- [5] G. 't Hooft, *Dimensional reduction in quantum gravity*, in *Salamfestschrift*, A. Ali, J. Ellis, S. Randjbar-Daemi eds., World Scientific, Singapore (1993) [[arXiv:gr-qc/9310026](#)].
- [6] S. Carlip, *Spontaneous dimensional reduction in short-distance quantum gravity?*, *AIP Conf. Proc.* **1196** (2009) 72 [[arXiv:0909.3329](#)].
- [7] G. Calcagni, *Fractal universe and quantum gravity*, *Phys. Rev. Lett.* **104** (2010) 251301 [[arXiv:0912.3142](#)].
- [8] G. Calcagni, *Multiscale spacetimes from first principles*, *Phys. Rev. D* **95** (2017) 064057 [[arXiv:1609.02776](#)].
- [9] S. Carlip, *Dimension and dimensional reduction in quantum gravity*, *Class. Quantum Grav.* **34** (2017) 193001 [[arXiv:1705.05417](#)].
- [10] J. Mielczarek and T. Trześniewski, *Towards the map of quantum gravity*, *Gen. Relativ. Grav.* **50** (2018) 68 [[arXiv:1708.07445](#)].
- [11] G. Calcagni, *ABC of multi-fractal spacetimes and fractional sea turtles*, *Eur. Phys. J. C* **76** (2016) 181 [[arXiv:1602.01470](#)].

- [12] G. Calcagni, *Multifractional theories: an unconventional review*, *JHEP* **03** (2017) 138 [[arXiv:1612.05632](#)].
- [13] G. Calcagni, *Multifractional theories: an updated review*, *Mod. Phys. Lett. A* **36** (2021) 2140006 [[arXiv:2103.06557](#)].
- [14] P.D. Mannheim, *Alternatives to dark matter and dark energy*, *Prog. Part. Nucl. Phys.* **56** (2006) 340 [[arXiv:astro-ph/0505266](#)].
- [15] S. Capozziello and M. De Laurentis, *The dark matter problem from $f(R)$ gravity viewpoint*, *Annalen Phys.* **524** (2012) 545.
- [16] R.H. Sanders and S.S. McGaugh, *Modified Newtonian dynamics as an alternative to dark matter*, *Ann. Rev. Astron. Astrophys.* **40** (2002) 263 [[arXiv:astro-ph/0204521](#)].
- [17] J.D. Bekenstein, *Relativistic gravitation theory for the MOND paradigm*, *Phys. Rev. D* **70** (2004) 083509; *Erratum-ibid.* **71** (2005) 069901 [[arXiv:astro-ph/0403694](#)].
- [18] B. Famaey and S. McGaugh, *Modified Newtonian Dynamics (MOND): observational phenomenology and relativistic extensions*, *Living Rev. Rel.* **15** (2012) 10 [[arXiv:1112.3960](#)].
- [19] A. Giusti, *MOND-like fractional Laplacian theory*, *Phys. Rev. D* **101** (2020) 124029 [[arXiv:2002.07133](#)].
- [20] A. Giusti, R. Garrappa and G. Vachon, *On the Kuzmin model in fractional Newtonian gravity*, *Eur. Phys. J. Plus* **135** (2020) 798 [[arXiv:2009.04335](#)].
- [21] G.U. Variaschi, *Newtonian fractional-dimension gravity and MOND*, *Found. Phys.* **50** (2020) 1608 [[arXiv:2003.05784](#)].
- [22] G.U. Variaschi, *Newtonian fractional-dimension gravity and disk galaxies*, *Eur. Phys. J. Plus* **136** (2021) 183 [[arXiv:2008.04737](#)].
- [23] G.U. Variaschi, *Newtonian fractional-dimension gravity and rotationally supported galaxies*, *Newtonian fractional-dimension gravity and rotationally supported galaxies*, *Mon. Not. R. Astron. Soc.* **503** (2021) 1915 [[arXiv:2011.04911](#)].
- [24] G.U. Variaschi, *Relativistic fractional-dimension gravity*, *Universe* **7** (2021) 387 [[arXiv:2109.02855](#)].
- [25] S.S. McGaugh, F. Lelli and J.M. Schombert, *Radial acceleration relation in rotationally supported galaxies*, *Phys. Rev. Lett.* **117** (2016) 201101 [[arXiv:1609.05917](#)].
- [26] F. Lelli, S.S. McGaugh and J.M. Schombert, *SPARC: mass models for 175 disk galaxies with Spitzer Photometry and Accurate Rotation Curves*, *Astron. J.* **152** (2016) 157 [[arXiv:1606.09251](#)].
- [27] C.W. Misner, K.S. Thorne and J.A. Wheeler, *Gravitation*, Freeman, New York, NY (1973).
- [28] P.C. van der Kruit, *The three-dimensional distribution of light and mass in disks of spiral galaxies*, *Astron. Astrophys.* **192** (1988) 117.
- [29] M.A. Bershadsky, M.A.W. Verheijen, K.B. Westfall, D.R. Andersen, R.A. Swaters and T. Martinsson, *The DiskMass Survey. II. Error budget*, *Astrophys. J.* **716** (2010) 234 [[arXiv:1004.5043](#)].
- [30] J. Binney and S. Tremaine *Galactic Dynamics (2nd ed.)*, Princeton University Press, Princeton, NJ (2008).
- [31] G. Calcagni, *Geometry and field theory in multi-fractional spacetime*, *JHEP* **01** (2012) 065 [[arXiv:1107.5041](#)].
- [32] G. Calcagni and G. Nardelli, *Momentum transforms and Laplacians in fractional spaces*, *Adv. Theor. Math. Phys.* **16** (2012) 1315 [[arXiv:1202.5383](#)].

- [33] G. Calcagni, *Quantum field theory, gravity and cosmology in a fractal universe*, *JHEP* **03** (2010) 120 [[arXiv:1001.0571](#)].
- [34] G. Calcagni, *Complex dimensions and their observability*, *Phys. Rev. D* **96** (2017) 046001 [[arXiv:1705.01619](#)].
- [35] G. Calcagni and A. De Felice, *Dark energy in multifractional spacetimes*, *Phys. Rev. D* **102** (2020) 103529 [[arXiv:2004.02896](#)].
- [36] G. Calcagni, *Multi-scale gravity and cosmology*, *JCAP* **12** (2013) 041 [[arXiv:1307.6382](#)].
- [37] G. Calcagni, D. Rodríguez-Fernández and M. Ronco, *Black holes in multi-fractional and Lorentz-violating models*, *Eur. Phys. J. C* **77** (2017) 335 [[arXiv:1703.07811](#)].
- [38] G. Calcagni and M. Ronco, *Dimensional flow and fuzziness in quantum gravity: emergence of stochastic spacetime*, *Nucl. Phys. B* **923** (2017) 144 [[arXiv:1706.02159](#)].
- [39] G. Calcagni, G. Nardelli and D. Rodríguez-Fernández, *Standard Model in multiscale theories and observational constraints*, *Phys. Rev. D* **94** (2016) 045018 [[arXiv:1512.06858](#)].
- [40] J.W. Moffat, *Scalar-tensor-vector gravity theory*, *JCAP* **0603** (2006) 004 [[arXiv:gr-qc/0506021](#)].
- [41] J.R. Brownstein and J.W. Moffat, *The Bullet Cluster 1E0657-558 evidence shows modified gravity in the absence of dark matter*, *Mon. Not. R. Astron. Soc.* **382** (2007) 29 [[arXiv:astro-ph/0702146](#)].
- [42] J.W. Moffat and V.T. Toth, *Can modified gravity (MOG) explain the speeding Bullet (Cluster)?*, [arXiv:1005.2685](#).
- [43] N.S. Israel and J.W. Moffat, *The Train Wreck Cluster Abell 520 and the Bullet Cluster 1E0657-558 in a generalized theory of gravitation*, *Galaxies* **6** (2018) 41 [[arXiv:1606.09128](#)].
- [44] G. Calcagni *Classical and quantum gravity with fractional operators*, *Class. Quantum Grav.* **38** (2021) 165005; *Erratum-ibid.* **38** (2021) 169601 [[arXiv:2106.15430](#)].
- [45] D. Clowe, M. Bradač, A.H. Gonzalez, M. Markevitch, S.W. Randall, C. Jones and D. Zaritsky, *A direct empirical proof of the existence of dark matter*, *Astrophys. J. Lett.* **648** (2006) L109 [[arXiv:astro-ph/0608407](#)].
- [46] S.W. Allen, A.E. Evrard and A.B. Mantz, *Cosmological parameters from observations of galaxy clusters*, *Ann. Rev. Astron. Astrophys.* **49** (2011) 409 [[arXiv:1103.4829](#)].
- [47] R. Massey, T. Kitching and J. Richard, *The dark matter of gravitational lensing*, *Rept. Prog. Phys.* **73** (2010) 086901 [[arXiv:1001.1739](#)].
- [48] N. Jeffrey et al. [DES Collaboration], *Dark Energy Survey Year 3 results: curved-sky weak lensing mass map reconstruction*, *Mon. Not. R. Astron. Soc.* **505** (2021) 4626 [[arXiv:2105.13539](#)].
- [49] N. Aghanim et al. [PLANCK Collaboration], *Planck 2018 results. VI. Cosmological parameters*, *Astron. Astrophys.* **641** (2020) A6 [[arXiv:1807.06209](#)].
- [50] C. Lage and G.R. Farrar, *The Bullet cluster is not a cosmological anomaly*, *JCAP* **1502** (2015) 038 [[arXiv:1406.6703](#)].
- [51] H.S. Cohl and J.E. Tohline, *A compact cylindrical Green's function expansion for the solution of potential problems*, *Astrophys. J.* **527** (1999) 86.
- [52] H.S. Cohl, A.R.P. Rau, J.E. Tohline, D.A. Browne, J.E. Cazes and E.I. Barnes *Useful alternative to the multipole expansion of 1/r potentials*, *Phys. Rev. A* **64** (2001) 052509 [[arXiv:physics/0101086](#)].

- [53] H.S. Cohl, *Fourier, Gegenbauer and Jacobi expansions for a power-law fundamental solution of the polyharmonic equation and polyspherical addition theorems*, *SIGMA* **9** (2013) 042 [[arXiv:1209.6047](#)].
- [54] I.S. Gradshteyn and I.M. Ryzhik, *Table of Integrals, Series, and Products (7th edition)*, Academic Press, London, UK (2007).
- [55] J.D. Jackson, *Classical Electrodynamics (3rd ed.)*, Wiley, New York, NY (1998).
- [56] H.S. Cohl and E.G. Kalnins, *Fourier and Gegenbauer expansions for a fundamental solution of the Laplacian in the hyperboloid model of hyperbolic geometry*, *J. Phys. A: Math. Theor.* **45** (2012) 145206 [[arXiv:1105.0386](#)].
- [57] H.S. Cohl, *On a generalization of the generating function for Gegenbauer polynomials*, *Integr. Transf. Special Func.* **24** (2013) 807 [[arXiv:1105.2735](#)].